Low-silver Electrically Conductive Adhesives for Shingled Solar Cell Interconnection

Zur Erlangung des akademischen Grades einer
DOKTORIN DER INGENIEURWISSENSCHAFTEN (DR.-ING.)

von der KIT-Fakultät für Chemieingenieurwesen und Verfahrenstechnik des
Karlsruher Instituts für Technologie (KIT)
genehmigte

DISSERTATION

von
Marianne Woll geb. Kronsbein
aus Karlsruhe

Tag der mündlichen Prüfung: 26.10.2026

Erstgutachter: Prof. Dr. Norbert Willenbacher

Zweitgutachter: Prof. Dr. Stefan Glunz

Preface

This publication-based dissertation consists of three peer-reviewed scientific journal articles. They include the main results of my experimental work at Karlsruhe Institute of Technology (KIT), Institute of Mechanical Process Engineering and Mechanics (MVM) in the group of Applied Mechanics (AME) during February 2023 until March 2026.

This thesis comprises a short introduction on the topic, a more detailed background on electrically conductive adhesives and their utilization in the shingled PV module design, followed by the motivation behind this work's aim. The main part of this dissertation consists of the following publications:

- Less is more: Enabling low-filled electrically conductive adhesives for shingled solar cell interconnection using the capillary suspension concept
- Polyethylene glycol-assisted stabilization of low-silver electrically conductive adhesives for solar cell interconnection
- Low-filled electrically conductive adhesives based on silver-coated glass and copper particles

The dissertation closes with an overall conclusion and outlook as well as a bibliography. The bibliography includes all references of the publications. Hereby, the publications are slightly changed. Some diagrams and images are modified in size and color, taking into account the format of this dissertation and the spelling was adjusted to ensure consistency with American English conventions.

Acknowledgements

First of all, I would like to thank my supervisor Prof. Dr. Norbert Willenbacher for the opportunity to do my doctorate in his working group Applied Mechanics (AME) at the Institute of Mechanical Process Engineering and Mechanics at Karlsruhe Institute of Technology (KIT), including fruitful discussions and his general support.

Furthermore, I am very grateful to have been part of the “Mod30+” consortium. My special thanks go to Leonhard Böck and Torsten Rößler from Fraunhofer ISE and Simon Malandain, Vincent Charlot and Frederic Durand from Protavic Int. for the wonderful and supportive collaboration. It was a pleasure working with you!

My deep gratitude also to Bernhard Hochstein, Karsten Sasso and Claude Oelschlaeger (AME) and Klara Urbschat from Institute for Chemical Technology and Polymer Chemistry (ITCP) for their professional and technical support.

I further would like to thank my colleagues at AME: Tillman, Fabian, Kevin, Lucas, Mona and Katrin, which whom I shared an office. Thank you for all we shared. David, Moritz, Christoph, Johannes and Jonas, for diverting lunch breaks; as well as Anna, Max, Katrin, Karim, Kasia, Felipe and Bruna. Thank you all for your support and the fruitful discussions we had.

This work would have not been possible without the work of my students Yasin, Max, Lorenz, Charlotte, Lucas, Sofia, Julia, Irem, Nishant, Adrian, Bogdan, Boyko and Jannis. It was a pleasure for me to work with you.

Thank you to my parents Christina and Sven, my siblings Maren and Mark and my grandparents Eli, Karin, Mike and Rudolf for their never-ending support and interest in my work, even though they come from a totally different professional background. You taught me what really matters in life.

Last but not least, I thank my partner Simon – for everything.

Abstract

The 2030 Agenda for Sustainable Development established by the United Nations defines 17 Sustainable Development Goals aimed at ensuring peace and prosperity for both the planet and its people. One of these goals is taking action against climate change (Goal 13) which implies Goal 7: affordable and clean energy. A transition of the energy production to renewable solutions is therefore of utmost importance. Photovoltaics (PV), which converts solar radiation into electrical energy, is one of the cornerstones of a renewable energy supply system.
Building-integrated PV where visual appearance and limited installation space play an important role gain increasing relevance in decentralized energy supply. The shingled PV module design with a gapless interconnection of solar cells provides both visual uniformity and efficient area utilization. In the shingling approach, overlapping solar cells are interconnected using electrically conductive adhesives (ECAs). ECAs consist of a polymer matrix filled with a conductive filler, usually silver at high volume fractions. In this context, Goal 12: responsible consumption and production becomes particularly relevant as silver is costly and may face supply shortages in the near future. Consequently, the PV industry aims to significantly reduce its silver consumption in order to remain competitive to other energy production technologies and to be consistent with the UN Sustainable Development Goals.

The aim of this thesis was the formulation of low-filled, low-silver ECAs based on commercially available materials for application in shingled PV. A reduced filler content improves the mechanical properties of the ECA by providing lower shear and elastic moduli and high shear strength, which is required for the shingled cell interconnection. However, a simple reduction in filler content deteriorates paste stability and electrical conductivity. Therefore, suitable stabilization concepts must be applied to ensure both processability of the ECA by screen printing or dispensing and electrical properties which do not compromise module performance.
In this thesis, the capillary suspension concept was explored for utilization with ECAs. In capillary suspensions, the addition of a small volume fraction of an immiscible secondary liquid induces a strong particle network which stabilizes the suspension against sedimentation and also provides rheological properties required for screen printing and dispensing. In case conductive particles are used, as in ECAs, this percolating network can also provide electrical conductivity as demanded for solar cell interconnection. The starting point of this work was a so-called snap-cure epoxy resin, which is well established in die-attach applications and meets the curing kinetics requirements of the PV industry, in combination with a specific grade of silver flakes that has also been proven in commercial applications. A suitable secondary liquid was identified which reduced the required silver flake volume fraction for the formation of a yield stress from 15 to 5 vol%. In both cases, application by screen printing required slightly higher yield stresses and therefore slightly higher filler contents. The secondary liquid was chosen not to alter the curing kinetics of the ECA, thereby preserving the advantage of rapid curing within seconds at low temperatures (120-200°C) of the chosen epoxy system. Furthermore, the percolation threshold for electrical conductivity decreased from 15 vol% to below 5 vol% silver flakes when the capillary suspension concept was applied. Due to silver alignment on the contacts, the contact resistivity remained generally low and was unaffected by either filler content or formulation concept. As expected, a lower filler content improved mechanical properties, as demonstrated by a linear increase in lap-shear strength with decreasing filler volume fraction. For all investigated ECAs, long-term stability under heat exposure and cyclic shear loading was demonstrated. At module level, a low-filled ECA containing between 5 and 10 vol% silver exhibited performance comparable to that of a highly-filled (20 vol% silver) reference ECA. Overall, the feasibility of the

capillary suspension concept for significant reduction of silver consumption in ECAs was successfully demonstrated.

However, the maximum volume resistivity of 1 x10^{-2} Ω cm, required for solar cell shingling, could be achieved even below 5 vol% provided that appropriate particle stabilization was employed to increase the yield stress. Polyethylene glycol (PEG) was found to improve both yield stress and lap-shear strength in the investigated particle-polymer system without compromising the electrical properties. This effect was attributed to altered interfacial properties, as PEG dissolved into both the polymer matrix and the polar secondary liquid present in the system. As a result, the three-phase contact angle of a secondary phase droplet on the silver flakes in the presence of the main fluid decreased, which enabled the formation of a "capillary" state capillary suspension. This led to the transformation of the well-dispersed particle system into a micro-phase separated particle network. However, further increasing PEG content led to a decrease in yield stress and lap-shear strength due to reduced interfacial tension between the main and secondary phases and increasing replacement of polymer matrix by PEG. Nevertheless, an ECA containing only 4 vol% (28 wt%) silver was successfully formulated that fulfilled all requirements for the shingled cell interconnection.

Further reduction in silver content was pursued by replacing the silver flakes with silver-coated glass particles and silver-coated copper particles. Even though the silver-reduced particles were selected to exhibit size distribution and surface chemistry similar to those of the silver flakes, a direct one-by-one replacement was not feasible.
Using silver-coated glass particles, partial substitution of silver particles was possible and a halogen-based additive was additionally introduced. However, the glass particles could be used to adjust the yield stress without altering the superior lap-shear strength and volume resistivity, provided that the silver content remained at 3.5 vol% and the total filler content between 5 and 8 vol%. A similar halogen-stabilized formulation was developed using silver-coated copper particles. In this case, 10 vol% of total filler, corresponding to 1.3 vol% silver or 7 wt% silver, was necessary to meet the requirements for solar cell shingling. However, the presence of copper appeared to affect the curing kinetics of the polymer matrix used here, resulting in a drastically reduced Young's Modulus of (34 ± 13) MPa instead of approximately 1000 MPa. This reduction in stiffness is believed to have caused failure during the accelerated thermal cycling test at module level, as the resulting higher strains might have disrupted the conductive pathways. Nevertheless, stability against oxidation was demonstrated in damp heat tests, and the ECA containing silver-coated glass particles achieved overall promising results at module level.

In summary, this thesis demonstrates the formulation of ECAs containing only 1.7-4 vol% silver (7-28 wt%), which is significantly lower than in conventional ECAs which typically contain 20-30 vol% silver (70-80 wt%), while still meeting the requirements for the shingled solar cell interconnection. This enables more sustainable material usage in photovoltaic module manufacturing, and thereby contributes to more sustainable energy production in line with the Sustainable Development Goals defined by the United Nations.

Zusammenfassung

Die von den Vereinten Nationen verabschiedete Agenda 2030 für nachhaltige Entwicklung definiert 17 Ziele, die Frieden und Wohlstand für Mensch und Umwelt sichern sollen. Zu diesen zählt insbesondere der Klimaschutz (Ziel 13), der eng mit dem Ziel einer bezahlbaren und sauberen Energieversorgung (Ziel 7) verknüpft ist. Eine Umstellung der Energieerzeugung auf erneuerbare Quellen ist daher von zentraler Bedeutung. Die Photovoltaik (PV), die Sonnenstrahlung direkt in elektrische Energie umwandelt, stellt einen wesentlichen Baustein eines nachhaltigen Energiesystems dar.
Gebäudeintegrierte Photovoltaiksysteme gewinnen zunehmend an Bedeutung für die dezentrale Energieversorgung, dabei spielen insbesondere ästhetische Anforderungen und begrenzte Installationsflächen eine Rolle. Das sogenannte geschindelte Moduldesign mit lückenloser Verschaltung der Solarzellen ermöglicht sowohl ein einheitliches Erscheinungsbild als auch eine effiziente Flächennutzung. Bei diesem Konzept werden überlappende Solarzellen mithilfe elektrisch leitfähiger Klebstoffe (engl. electrically conductive adhesives, ECAs) kontaktiert. Diese bestehen aus einer Polymermatrix mit einem leitfähigen Füllstoff, in der Regel Silber in hohen Volumenanteilen. Vor diesem Hintergrund gewinnt Ziel 12 (nachhaltige/r Konsum- und Produktion) besondere Relevanz, da Silber teuer ist und künftig Versorgungsengpässe nicht ausgeschlossen werden können. Die Photovoltaikindustrie ist daher bestrebt, den Silberverbrauch deutlich zu reduzieren, um wettbewerbsfähig zu bleiben und den Nachhaltigkeitszielen gerecht zu werden.

Ziel der vorliegenden Arbeit war die Entwicklung niedrig gefüllter, silberreduzierter ECAs auf Basis kommerziell etablierter Materialien für den Einsatz in geschindelten PV-Modulen. Ein reduzierter Füllstoffgehalt führt zu verbesserten mechanischen Eigenschaften, insbesondere zu geringeren Schub- und Elastizitätsmoduli bei gleichzeitig hoher Scherfestigkeit, die für die Zellverschaltung erforderlich sind. Eine bloße Reduktion des Füllstoffanteils verschlechtert jedoch die Pastenstabilität und elektrische Leitfähigkeit. Daher ist die Anwendung geeigneter Stabilisierungskonzepte erforderlich, um sowohl eine gute Verarbeitbarkeit (z. B. im Siebdruck oder durch Dispensieren) als auch ausreichende elektrische Eigenschaften sicherzustellen.
Im Rahmen dieser Arbeit wurde das Konzept der Kapillarsuspensionen auf ECAs angewandt. Dabei führt die Zugabe geringer Mengen einer nicht mischbaren Zweitflüssigkeit zur Ausbildung eines ausgeprägten Partikelnetzwerks, das die Suspension stabilisiert und geeignete rheologische Eigenschaften für den Verarbeitungsprozess bereitstellt. Im Fall leitfähiger Partikel kann dieses Netzwerk zugleich elektrische Ladung transportieren. Als Ausgangssystem diente ein schnellaushärtendes Epoxidharz, welches in der Elektronikindustrie etabliert ist und die Anforderungen an die Aushärtekinetik erfüllt, kombiniert mit kommerziell bewährten Silberpartikeln. Durch die Auswahl einer geeigneten Zweitflüssigkeit konnte der erforderliche Silberanteil zur Ausbildung einer Fließgrenze von 15 auf 5 Vol.-% reduziert werden. Für die Anwendung im Siebdruck waren jeweils geringfügig höhere Silberanteile erforderlich. Die gewählte Zweitflüssigkeit beeinflusste die Aushärtungskinetik nicht, sodass die schnelle Aushärtung bei vergleichsweise niedrigen Temperaturen (120–200 °C) erhalten blieb. Gleichzeitig verringerte sich die Perkolationsschwelle für die elektrische Leitfähigkeit von 15 Vol.-% auf unter 5 Vol.-% Silber. Der Kontaktwiderstand blieb dabei niedrig und unabhängig von Füllstoffgehalt und Formulierung. Wie erwartet, führte der reduzierte Füllstoffgehalt zu verbesserten mechanischen Eigenschaften, was sich in einer steigenden Scherfestigkeit zeigte. Für alle untersuchten Systeme konnte zudem eine gute Langzeitstabilität nachgewiesen werden. Auf Modulebene wies ein niedrig gefüllter ECA mit 5–10 Vol.-% Silber eine vergleichbare Leistung wie ein Referenzsystem

mit 20 Vol.-% Silber auf. Insgesamt konnte somit die Eignung des Kapillarsuspensionskonzepts zur deutlichen Reduktion des Silberverbrauchs nachgewiesen werden.

Der für die Zellverschaltung maximal zulässige Volumenwiderstand von 1 x 10^{-2} Ω cm konnte bereits bei Silbergehalten unterhalb von 5 Vol.-% erreicht werden, sofern eine geeignete Partikelstabilisierung vorlag. Dabei erwies sich Polyethylenglykol (PEG) als vorteilhaft, da es sowohl die Fließgrenze als auch die Scherfestigkeit erhöhte, ohne die elektrischen Eigenschaften zu beeinträchtigen. Dies wird auf veränderte Grenzflächeneigenschaften zurückgeführt, da PEG sowohl in der Polymermatrix als auch in der polaren Zweitflüssigkeit löslich ist. Infolgedessen verringerte sich der Dreiphasenkontaktwinkel, wodurch die Ausbildung einer Kapillarsuspension begünstigt wurde und ein mikrophasenseparierte Partikelnetzwerk entstand. Eine weitere Erhöhung des PEG-Gehalts führte jedoch aufgrund verringerter Grenzflächenspannung zwischen den flüssigen Phasen und Verdrängung des Polymers zu einer Abnahme von Fließgrenze und Scherfestigkeit. Dennoch konnte ein ECA mit lediglich 4 Vol.-% Silber erfolgreich formuliert werden, der alle Anforderungen für die Zellverschaltung erfüllt.

Zur weiteren Reduktion des Silberanteils wurden Silberpartikel durch versilberte Glas- bzw. Kupferpartikel ersetzt. Diese Partikel wurden so gewählt, dass sie den Silberpartikeln in Größenordnung und Oberflächeneigenschaften ähnelten. Dennoch war ein eins-zu-eins-Austausch der Partikel nicht möglich. Mit versilberten Glaspartikeln konnte eine partielle Substitution unter Einsatz eines halogenhaltigen Additivs erreicht werden. Dabei konnte der Glasgehalt zur Einstellung der Fließgrenze genutzt werden ohne die elektrischen Eigenschaften zu beeinflussen, solange der Silbergehalt bei 3,5 Vol.-% und der Gesamtpartikelanteil zwischen 5 und 8 Vol.-% lag. Eine vergleichbare halogenbasierte Formulierung mit versilberten Kupferpartikeln erforderte höhere Füllstoffgehalte von 10 Vol.-%. Dies entspricht einem Silberanteil von 1,3 Vol.% bzw. 7 Gew.-%. Allerdings beeinflusste das Kupfer offenbar die Aushärtung der Polymermatrix, was zu einem deutlich reduzierten Elastizitätsmodul von nur (34 ± 13) MPa anstelle von ca. 1000 MPa führte. Diese reduzierte Steifigkeit führte vermutlich zu den Ausfällen in den thermischen Belastungstests auf Modulebene, da die höhere Dehnung zu einer Unterbrechung der leitfähigen Pfade geführt haben könnte. Dennoch wiesen die ECAs eine gute Oxidationsbeständigkeit auf. Insbesondere die Systeme mit Glaspartikeln lieferten vielversprechende Ergebnisse auf Modulebene.

Zusammenfassend beweist die vorliegende Arbeit, dass ECAs mit einem Silbergehalt von lediglich 1,7–4 Vol.-% (7–28 Gew.-%) formuliert werden können. Dies ist deutlich weniger als bei konventionellen Systemen mit typischerweise 20–30 Vol.-%. Trotz dieser erheblichen Reduktion erfüllen die entwickelten ECAs die Anforderungen der geschindelten Zellverschaltung. Damit leisten sie einen Beitrag zu einem nachhaltigeren Materialeinsatz in der Photovoltaik und unterstützen eine ressourcenschonende Energieerzeugung im Sinne der Ziele der Vereinten Nationen.

Notations

Latin symbols

A	area	[cm^2]
a_T	temperature dependent shift factors	[-]
d	diameter	[mm]
F	force	[N]
G'	storage modulus	[MPa]
G''	loss modulus	[MPa]
g	gravitational constant	[m/s^2]
h	distance	[µm]
I	current	[A]
i	counting number	[-]
l	length	[cm]
N	number of bridges	[-]
n	number	[-]
P	power	[W]
p	percentage	[-]
R	resistance	[Ω]
r	radius	[mm]
T	temperature	[°C]
t	thickness	[cm]
V	voltage	[V]
V	volume	[$µm^3$]
v	velocity	[m/s]
w	width	[cm]
x	value	
$\bar{x}$	mean value	
$x_{50,3}$	mass-weighted median equivalent particle diameter	[µm]
y	gap height	[mm]

Greek symbols

Γ	interfacial tension	[mN/m]
γ	deformation	[-]
$\dot{\gamma}$	shear rate	[1/s]
η	viscosity	[Pa s]
θ	three-phase contact angle	[°]
ρ	density	[g/ml]
ρ_c	contact resistivity	[Ω cm^2]
ρ_v	volume resistivity	[Ω cm]

Σ	standard deviation	
σ_y	yield stress	[Pa]
T	shear stress	[Pa]
Φ	volume fraction	[-]

Indices

b, B	bulk
C	contact
Cap	capillary
F	finger
G	glass transition
J	joint
Max	maximum
Oc	open-circuit
P	particle
S	series
Sc	short-circuit
Sec	secondary
Sed	sedimentation

Abbreviations

ACA	Anisotropically Conductive Adhesives
Ag	Silver
AgI	Silver Iodide
Al	Aluminum
aTC	Accelerated Thermal Cycling
BMWE	German Federal Ministry of Economic Affairs and Energy
BMWK	German Federal Ministry of Economics and Climate Action
CapS	Capillary Suspension
CIGS	Copper Indium Gallium Selenide
CTE	Coefficient of Thermal Expansion
Cu	Copper
DH	Damp Heat
DMA	Dynamical Mechanical Analysis
DSC	Differential Scanning Calorimetry
ECA	Electrically Conductive Adhesive
EL	Electroluminescence
FF	Fill Factor
h	Halogen
HF	Humidity Freeze
HJT	Heterojunction Technology

I	Iodine
ICA	Isotropically Conductive Adhesives
IL	Ionic Liquid
ITRPV	International Roadmap of Photovoltaics
IV	Current-Voltage (Curve)
LSMC	Laser Scribe and Mechanical Cleaving
ML	Mechanical Load
MPP	Maximum Power Point
Ni	Nickel
PEG	Polyethylene Glycol
PERC	Passivated Emitter and Rear Cell
POE	Polyolefin Elastomer
PSQ	Pseudo-Square
PV	Photovoltaic
RoHS	Restriction of Hazardous Substances
SEM	Scanning Electron Microscopy
SHJ	Silicon Heterojunction
TC	Thermal Cycling
TGA	Thermogravimetric Analysis
TLM	Transfer Length Method
TOPCon	Tunnel Oxide Passivated Contact
TPO	Thermoplastic Polyolefins
TPTA	Terephthalaldehyde
TPU	Thermoplastic Polyurethane
TTSP	Time-Temperature Superposition Principle
vol	Volume
wt	Weight
xBC	Back Contact Cell Concepts

Table of Contents

Preface iii
Acknowledgements iv
Abstract v
Zusammenfassung vii
Notations ix
1 General Introduction 1
2 Theoretical background and State of the Art 3
2.1 Electrically Conductive Adhesives 3
2.1.1 Components and fields of application 3
2.1.2 Percolation in ECAs 4
2.2 PV interconnection 14
2.2.1 Solar Cell Shingling and resulting requirements for ECAs 15
2.2.2 Performance of ECAs in shingled PV modules 20
3 Motivation and Outline 22
4 Capillary suspension-based ECAs 24
4.1 Introduction 25
4.2 Material and Methods 26
4.3 Theory 28
4.3.1 Capillary Suspensions 28
4.3.2 Requirements for ECAs in shingled solar cell interconnections 30
4.4 Results and Discussion 31
4.4.1 Uncured ECA 31
4.4.2 Curing 32
4.4.3 Cured ECA 34
4.4.4 Module performance 37
4.5 Conclusion 39
5 Influence of polyethylene glycol on ECAs 40
5.1 Introduction 41
5.2 Experimental 42
5.3 Results and Discussion 44
5.3.1 PEG 200 enhances the mechanical properties of ECAs 44
5.3.2 PEG 200 potentially promotes the formation of a capillary suspension 48
5.4 Conclusion and Outlook 52
5.5 Supplementary Materials 53
6 ECAs with silver-coated glass and copper particles 57
6.1 Introduction 58
6.2 Material and Methods 61
6.3 Results and Discussion 62

6.3.1 Particle Characterization....62
6.3.2 ECAs based on silver-coated glass particles....64
6.3.3 ECAs based on silver-coated copper particles....66
6.3.4 Application in shingled solar modules....68
6.4 Conclusion and Outlook....70
6.5 Supplementary information....71
7 Conclusion....75
8 Outlook....79
References....81

1 General Introduction

Considering the major challenges of the 21st century, climate change is frequently named in first position. Driven by the extensive emission of CO_2 since the beginning of industrialization and its accumulation in atmosphere, the global average temperature has increased by 1 °C over the last 30 years. This rise in temperature leads to an increased frequency of extreme weather events and reduced ice coverage, thereby affecting ecosystems, wildlife and human society alike [1]. In response to these developments, the European Commission introduced the "European Green Deal" in 2019 which aims to achieve a net carbon neutral European Union by 2050 [2]. A central component of this strategy is the transition of energy production towards renewable energy sources. Among these, photovoltaic (PV) is projected to experience the most significant growth by 2050 [3]. The International Roadmap for Photovoltaic [4] forecasts an increase in cumulative PV installations to app. 8.9 TWp in Europe and 63.4 TWp globally, compared to app. 3.6 TWp globally in 2025. Such an expansion in PV capacity will inevitably lead to a substantial increase in material demand.

At the solar cell level, crystalline silicon is the dominant material. Efforts to reduce silicon consumption per cell is primarily achieved by decreasing the thickness of the silicon wafer. Additionally, alternative photovoltaic technologies are explored. However, established thin film technologies, such as cadmium telluride or copper indium gallium selenide (CIGS) solar cells, have a decreasing market share accounting for 2-3% in 2024 [5]. Emerging cell concepts are so far only relevant for space application (III/V-semiconductors) [6] or on lab-scale (perovskites) [7]. In cell interconnection, lead-based solder is dominant [4]. However, the use of lead is regulated under the Restriction of Hazardous Substances (RoHS) directive [8] and is generally prohibited. The photovoltaic industry currently benefits from a temporary exemption, which requires regular extension. The use of lead can be avoided by employing lead-free solder. However, lead-free solder typically requires higher processing temperatures. Such temperatures are often incompatible with thin wafers or some of the emerging photovoltaic materials. Therefore, electrically conductive adhesives (ECA) have been introduced as an alternative interconnection material in PV interconnection.

Work on ECAs, which are composite materials consisting of non-conductive polymer matrices and conductive fillers, dates back to the early 20th century [9]. The U.S. patent by Wolfson and Elliot [10], filed in 1956 on electrically conductive cements, is widely regarded as the first documented application of ECAs in electronic technology. Over the years, ECAs have developed into established interconnection materials in the electronics industry, particular for flip-chip and die-attach applications [11]. Their widespread use can be attributed not only to their role as lead-free, low-temperature alternatives to solder, but also because of their lower mechanical stiffness compared to solder materials. These properties make ECAs particularly attractive for PV applications, where they enable innovative module concepts such as shingled solar modules [12].

In comparison to conventional PV modules, where metallic ribbons are bonded onto the cell surface to establish electrical interconnection between adjacent cells, in the shingling approach cells are directly interconnected overlapping like roof-tiles. This design increases area utilization, as gaps between the cells are omitted. However, the overlapping structure requires that thermo-mechanical stresses must be accommodated within the adhesive bond [13]. Consequently, the requirements for interconnection materials remain an active topic of research. These requirements include rheological properties in the uncured state, processability during application and electrical and mechanical performance after curing. The work presented in this

thesis aims to define material specifications for ECAs used in shingled solar cell interconnection and to investigate how these properties can be tailored through optimized ECA formulations.
Despite their technological advantages, ECAs face material-related challenges as well. Especially their typically high silver content makes them economically less competitive compared to solder-based interconnection technologies. Silver is a relatively expensive material and may face supply shortage in the future, which further increases cost pressure. Consequently, reducing the silver consumption has become a key objective for ECA manufacturers, especially in the rapidly growing PV sector [4].
In the present work, this challenge is addressed through two complimentary approaches. First, the capillary suspension concept is introduced to stabilize low-filled ECAs, enabling reliable formulations with significantly reduced silver content. Second, the pure silver filler is replaced by silver-reduced fillers, namely silver-coated glass particles and silver-coated copper particles, in order to further decrease the overall silver usage in ECA formulations.

2 Theoretical background and State of the Art

The following section gives an overview on electrically conductive adhesives and their use in solar cell interconnection. Special attention is paid to stabilization mechanisms as well as material specifications for the shingled interconnection approach.

2.1 Electrically Conductive Adhesives

Electrically conductive adhesives (ECAs) are composite materials consisting of a conductive filler dispersed in a polymer matrix [9]. They serve the dual function of mechanically and electrically interconnecting two substrates. While the electrical conductivity is primarily governed by the type, volume fraction, and spatial distribution of conductive filler, the mechanical properties are determined by both the polymer matrix and the filler. In general, increasing the filler volume fraction improves electrical conductivity but deteriorates adhesion and shear strength [14–16]. This section provides an overview of ECA composition, conduction mechanism and rheological properties, as well as strategies to tune and improve these characteristics.

2.1.1 Components and fields of application

The polymer matrix provides the mechanical interconnection by forming covalent and secondary bonds with the substrate [17]. It therefore primarily determines the mechanical properties like adhesion, mechanical strength and impact resistance of the composite material [16]. The electrical resistivity of common polymers typically ranges between 10^{12} and 10^{15} Ω cm [18].
Thermosetting polymers are most commonly used in ECAs, typically as solvent-free one-component systems, such as epoxy resins, cyanate esters, silicones or polyurethanes [9,11,19]. Thermosets are preferred because of their higher crosslink density [20] and their ability to form strong covalent bonds with the substrate increasing adhesion strength [17]. Among these, epoxies are the most widely used. Epoxy adhesive systems generally consist of a resin and a hardener. In some cases accelerators are added to control the curing reaction [14]. Epoxy resins cure through an exothermic crosslinking reaction. The curing kinetics as well as resulting crosslink density depends on curing time, curing temperature, hardener type (e.g. catalysts (Lewis acids and bases), amines, anhydrides [14] or imidazoles), reactivity and number of functional groups as well as filler loading, as fillers can act as catalysts [9]. Epoxy systems offer several advantages, including high chemical and thermal resistance, good adhesion and compatibility to various substrates as well as high mechanical strength and toughness [9,21].
Alternatively, thermoplastic polymers may be used as the polymer matrix. These materials offer advantages such as repairability and recyclability but often exhibit lower adhesive strength particularly at elevated temperatures [9]. Common thermoplastic adhesives include polyvinyl acetate, chlorate or ether as well as polyimides and polyacrylates [9,11,19,22].

To achieve electrical conductivity, conductive particles are dispersed within the polymer matrix. In terms of mechanical properties, these particles act as defects within the polymer network, deteriorating the strength of the composite [14]. Consequently, the filler volume fraction must be balanced to ensure sufficient electrical conductivity while maintaining adequate mechanical properties.
Conductive fillers are available from various materials, including metals such as silver, gold, nickel, aluminum or copper, as well as carbon-based fillers and metal-coated fillers. In the latter case, the conductive shell may surround either a conductive metal core, e.g. silver-coated copper particles, or a non-conductive core, such as glass, ceramics, or polymers. The geometry of the filler particles ranges from fibers and needles over spheres to flakes and platelets. Filler

dimensions vary widely from nanometer-scale fillers such as carbon nanotubes or fibers to micrometer-scale particles up to app. 20 µm, as in the case of flakes [9,11,14,17,22,23].
Among the conductive fillers, silver is the most widely used owing to its high electrical and thermal conductivity, chemical stability and ease of processing [21,24]. Importantly, even silver oxides retain relatively high electrical conductivity [17]. Silver particles are commercially available in various sizes and shapes, with silver flakes being the most commonly used form in ECAs [9]. Silver flakes are fabricated by ball-milling silver powders. During this processing step, lubricants are added to prevent cold-welding and agglomeration of the particles. These lubricants are usually fatty acids, which remain on the flake surface as chemically bound silver salts and free fatty acids. This organic surface layer improves the dispersibility of the particles in the polymer matrix but it is generally electrically insulating and therefore impedes electron transport. The organic surface can be thermally decomposed within a temperature range of app. 150 and 250 °C [25–27]. One of the major drawbacks of silver as filler material is its high and fluctuating cost. Therefore, recent research efforts have focused on the (partial) substitution of silver with copper. Copper is significantly less expensive and exhibits high electrical conductivity. However, copper is prone to oxidation, which results in the formation of non-conductive copper oxides. Hence, copper is often used in the form of silver-coated copper particles, aiming to combine the cost advantage of copper with the chemical stability of silver [11].
Another approach to achieving electrical conductivity involves doping the non-conductive polymer matrix with inherently conductive polymers. These materials offer good processability and mechanical flexibility, comparable to the polymer matrix. However, their electrical conductivity is generally at least eight orders of magnitude lower than that achieved using conventional metallic fillers. Examples of inherently conductive polymers are polypyrrole, polyaniline, polythiophene, polyacetylene and Poly(3,4-ethylenedioxy thiophene):Poly(styrene sulfonate) [9,28].

ECAs provide not only electrical and mechanical interconnection but also contribute to thermal management within electronic assemblies [24]. Therefore, they are widely applied as replacement for solder [29]. ECAs offer low processing temperatures below 200 °C, are environmentally friendly due to the absence of lead, offer higher flexibility than solder and can bond non-solderable materials as well [9,24]. Hence, ECAs are applied in electronic packaging, die attachment, surface mount technology, flip-chip assembly, liquid-crystal displays and conductive coatings, etc. [22,30]. Recently, the photovoltaic industry has gained interest in ECAs as an alternative interconnection material [31]. Still, challenges remain in the application of ECAs. These include their lower conductivity compared to solder, moisture uptake and associated corrosion, limited reworkability as well as unstable contacts against non-noble materials and relatively high material costs [14,30,32].

2.1.2 Percolation in ECAs

ECAs can be classified into anisotropically conductive adhesives (ACA) and isotropically conductive adhesives (ICA). ACAs are typically low-filled systems in which electrical interconnection between the substrates is established by individual conductive particles, as illustrated in Figure 1a. As a result, electrical conduction occurs only along the z-axis but not in the x-y-plane. To ensure reliable electrical contact, pressure must be applied during curing to bring particles and substrates into contact. In contrast, ICAs rely on the formation of a continuous conductive particle network with redundant electrical pathways providing conductivity in all spatial directions, see Figure 1b. Consequently, ICAs are highly filled and do not require external pressure during curing [33]. Therefore, ICAs are more widely used than ACAs in practical

application [17]. Hence, the following considerations on electrical conductivity as well as paste stability focus primarily on ICAs.

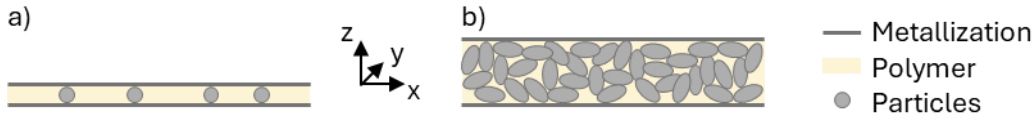


Figure 1. a) anisotropically conductive adhesive, b) isotropically conductive adhesives

Electrical Conduction Mechanism in ECAs

Electrical conduction in ECAs requires close proximity between the particles as well as between particles and the bonding surface. The overall resistance of an ECA bonded joint consists of the contact resistance between the ECA and the substrate and the intrinsic resistance of the ECA itself. The latter can be further divided into the intrinsic resistance of the filler particles and the contact resistance between neighboring filler particles. When conductive particles approach each other within a gap distance smaller than approximately 10 nm, electrons may overcome the potential barrier between particles, which is referred to as electron tunnelling. This mechanism is highly sensitive to the gap width as well as applied voltage and temperature. When particles come in direct physical contact, a conductive network forms in which electron transport occurs via band conduction. In ECAs, electron tunnelling is believed to dominate over band conduction due to the presence of the organic surface layer on the particles and residual polymer separating neighboring particles. Nevertheless, it is likely that both mechanisms, direct particle contact and electron tunnelling, coexist within the conductive network. Therefore, the contact resistance between particles consists of two contributions: constriction resistance, arising from the limited contact area through which electrons pass, and tunnelling resistance associated with the nanoscale separation between particles [9,14,16,23].

In the uncured state, most ICAs are electrical insulating. It is widely assumed that polymer shrinkage during curing reduces the distance between neighboring particles, enabling the formation of continuous conductive pathways [18,34]. Other studies suggest that the fillers rearrange into a conductive network during the initial viscosity decrease upon heating the adhesives for curing [21,35]. Additionally, evaporation of the organic surface layer during curing may further enhance electrical conductivity of the ECAs [29].

Percolation theory

At low filler volume fractions, particles are well dispersed within the polymer matrix and remain isolated from each other. In this regime, the electrical resistivity of the composite is dominated by that of the polymer. With increasing filler content, particles begin to form clusters which eventually connect to a sample-spanning conductive network. The critical volume fraction at which this transition occurs is referred to as the percolation threshold. At the percolation threshold, the composite undergoes a transition from an electrical insulator to a conductor and resistivity decreases by several orders of magnitude. Further increases in filler content primarily result in the formation of additional network branches and redundant conductive pathways, which reduce the resistivity only gradually [9,14,18,22]. The critical volume fraction can be described by percolation theory, which is derived from graph theory. Graph theory considers a lattice structure, in which the knots are randomly occupied by particles. Neighboring occupied sites form a bond. The percolation threshold is defined as the particle volume fraction at which a continuous chain of such bonds extends from one side of the lattice to the other [14,18]. However, in truly random distributions the assumption of a lattice fails. Furthermore, thermodynamic effects such as surface energies of polymer and particles and polymer melt viscosity, the

preparation technique as well as geometrical parameters including particle size, shape, orientation or size distribution cannot be accounted for in this basic model [14,18,23]. To account for conduction mechanisms that do not rely on direct particle–particle contact, Zhang et al. [22] recommend incorporating tunnelling effect theory and field emission theory into the theoretical description.

Assuming spherical metallic particles, the percolation threshold for ECAs has been theoretically predicted to lie between 15 and 20 vol%. However, in practice, filler volume fractions of 30-35 vol% are typically required to achieve sufficient electrical conductivity and stability [14,18,21]. Generally, the percolation threshold decreases with increasing particle aspect ratio [23] and when mixtures of fillers with different shapes and sizes are used [15]. In practice, flake-shaped particles are most widely employed as they provide more contact points than spheres and are commercially available from a broad spectrum of materials [17]. The percolation threshold is well suited for experimentally comparing different ECA material systems as well as describing the conductivity on a macroscopic scale. However, for its theoretical prediction other theories have to be included into the model [36].

Volume and contact resistivity and their measurement

To compare and quantify the electrical properties of ECAs, the volume resistivity is commonly determined. This parameter is typically measured using a four-point probe method, in which four electrodes are arranged linearly on the ECA sample. As illustrated in Figure 2a, a current I is applied between the two outer electrodes and the drop in voltage V is measured between the two inner electrodes. In this setup, the bulk resistance R_b as the ratio of V/I is a measure of the sample only [37]. The volume resistivity ρ_v is then calculated from the resistance and the sample geometry according to [38]:

$$\rho_v = R_b \cdot \frac{wt}{l} \tag{1}$$

with width w, thickness t of the ECA and distance between the inner electrodes l. The measured resistance R depends not only on the material properties but also on sample geometry and electrode position. To obtain R_b, correction factors have to be applied for samples with finite thickness and lateral dimension as well as when electrodes are positioned close to the sample edge. In case of thickness, this correction factor is 1, when the ratio of thickness to electrode spacing is below 0.2. To ensure reliable comparisons, it is essential to use similar sample geometries and measurement configurations. Additionally, the four-point method is applicable only to isotropic materials [37].

In a bonded joint, the total electrical resistance consists of the bulk resistance of the ECA as well as the contact resistance at the interface between adhesive and substrate. The contact resistance R_c refers to the total resistance at the interface and depends on the contact geometry. In contrast, contact resistivity ρ_c represents an intrinsic property of the interface that is independent of the contact geometry. For ideal, homogeneous contacts with uniform current density, contact resistivity is calculated according to [39]:

$$\rho_c = R_c \cdot A \tag{2}$$

with contact area A. In practice, however, most contacts are non-ideal due to current crowding effects or defects [39]. To account for these effects, the transfer length method (TLM) is commonly employed to determine a parameter known as the current transfer length. In this approach, the contact resistance is assumed to be equivalent to the resistance that would occur if the current travelled an additional distance, referred to as the transfer length, within the host layer before transferring abruptly into the contacting material [40]. Devoto et al. [36,41–43] performed

extensive research on measurement set-ups to gain reliable and comparable results for contact resistivity measurements of ECAs. They proposed a measurement configuration consisting of metallic fingers which are interconnected by the ECA sample, see Figure 2b. Two electrodes for current application and two for voltage measurement are placed on the fingers. When the current electrodes are placed on finger *i* and *i+1* and the voltage electrodes on fingers *i+1* and *i+2*, , the end-contact resistance can be measurement directly [43]. To obtain a joint resistance, current and voltage electrodes are placed on the same fingers, e.g. *i* and *i+1* [42]. This joint resistance consists of the finger resistance, the bulk resistance of the ECA and the contact resistance. By subtracting bulk and finger resistance from the joint resistance, the contact resistance is obtained. However, contact resistance is typically very small and may be obscured when bulk or finger resistance are relatively high [43]. Furthermore, contact resistivity is only defined for ohmic contacts. Achieving ohmic behavior requires a sufficiently large contact area, which reduces the influence of local inhomogeneities. In general, larger contact areas are recommended for ECAs containing small particles or low filler content [36]. Finally, to obtain meaningful results, the test configuration should suitably resemble the actual contact geometry in the intended application.

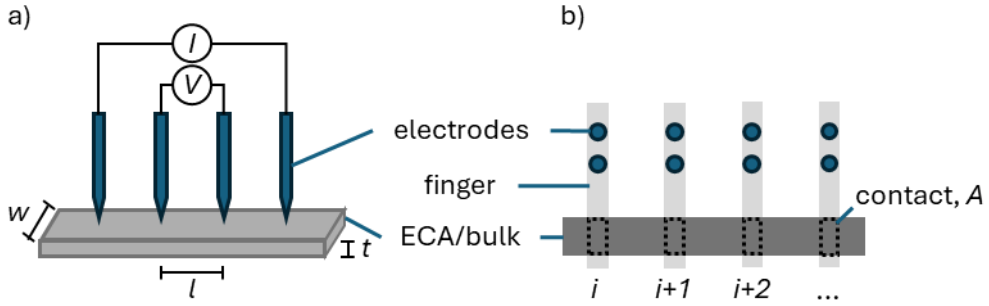


Figure 2. measurement set-up for a) volume resistivity and b) contact resistivity based on [43]

Strategies for electrical improvement

Although silver exhibits the lowest intrinsic volume resistivity of 1.6 x 10^{-6} Ω cm, ECAs typically achieve a resistivity only in the order of 10^{-3} – 10^{-4} Ω cm which is high compared to solder with 2 x 10^{-5} Ω cm [44]. Therefore, much effort has been devoted to improve the volume resistivity of ECAs. Two main strategies have been pursued: replacement or removal of the organic surface layer on silver particles and low-temperature sintering of silver nanoparticles.

The silver salt layer on the particles improves dispersibility and influences rheological properties such as viscosity of the ECA [25,27]. Li et al. [45] observed a decrease in volume resistivity accompanied by an increase in viscosity, when malonic or adipic acid was added to their ECA. However, several studies have reported significant reductions in volume resistivity ranging from 30 to 75% for highly-filled ECAs containing more than 67 wt% silver without substantially affecting viscosity. Such improvements were achieved using additives such as salicylaldehyde and trans-cinnamaldehyde [46], palmitic acid [47], acetic or adipic acid [48], DGBE or polyethylene glycol (PEG) [25] or diluted sulfuric acid and coupling agents [49,50]. Furthermore, Li et al. [51] proposed that the organic surface layer as well as silver oxides could be reduced by thermal pre-treatment of the particles at 700 °C, thereby improving electrical conductivity.

Another strategy for improving electrical conductivity involves the introduction of silver nanoparticles into the adhesive formulation. The addition of nanoparticles significantly increases the number of potential contact points within the conductive network and therefore, increases volume resistivity. Thus, sintering of the nanoparticles is required to obtain material bridges instead of particle-particle contacts. Thereby, the melting point depression effect of nanoparticles is exploited, allowing sintering to occur below or at the curing temperature of the

ECA [16,44,52]. Nanoparticles were mostly generated in-situ in the ECA. Gao et al. [53] employed a silver-imidazole complex as precursor, while Cheng et al. [54] generated nanoparticles during photo-polymerization from Ag-2-ethylhexanoate. Most commonly, silver nitrate has been used as precursor and reduced to silver nanoparticles through thermal treatment while curing [55], in presence of non-ionic Triton X-100 or PEG 600 [56], redox reaction with N,N-dimethyl-4-aminobenzaldehyde [57] or in different reducing agents such as polyethylene glycol [58,59] or triethanolamine [60]. In systems containing 70–80 wt% silver filler, decreases in resistivity between 30 and 75% have been reported. Chee and Lee [61] anchored nanoparticles onto the Ag flakes before ECA preparation by mixing $AgNO_3$, Ethanol and bimodal flakes. The nanoparticles mainly attached on the edges of the flakes. This method improved resistivity just below the percolation threshold with a small number of nanoparticles. Namely they achieved app. 1 Ω cm by utilization of 1 wt% Ag NP in a 12 vol% filled ECA. Another approach is to exclusively use nanoparticles. Tee et al. [62] decreased the volume resistivity of a system filled with 5 wt% silver nanoparticles from 4 x 10^2 Ω cm to 0.25 Ω cm through the addition of the silane-based coupling agent 3APTES. Yang et al. [63] sintered nanorods and nanoparticles at 160 °C for 20 min and achieved a resistivity of (3-4) x 10^{-5} Ω cm at a filler weight fraction of app. 50%. Chen et al. [64] further demonstrated that the combination of nanowires and nanoparticles yields superior conductivity compared to systems containing nanoparticles only. In their work, silver nanoparticles were synthesized from $AgNO_3$ using ethylene glycol, silver chloride and polyvinylpyrrolidone. By addition of NaCl, the particle morphology could be adjusted from spherical particles to nanowires, thereby improving network formation.

In general, it is advisable to use particles with high aspect-ratio or a mixture of particles of different size [15] but smaller than 20 µm [65]. For thermosets, polymer shrinkage during curing contributes to the formation of conductive pathways. Therefore, systems with higher curing shrinkage tend to exhibit improved conductivity [34]. To ensure long-term stability, the incorporation of corrosion inhibitors, reducing agents, oxygen scavengers or sacrificial metals has been recommended [16,44,52]. So far, research focused mainly on improving volume resistivity. In contrast, contact resistivity has received comparatively less attention, partly because it is more difficult to measure accurately. Devoto et al. [36] demonstrated recently that particle shape and orientation at the interface can significantly influence contact resistivity.

Rheology and Rheometry

Many studies have focused on the conductivity improvement of highly-filled ECAs in order to approach the electrical performance of solder. Applications with lower conductivity requirements offer the possibility to reduce the filler content as especially relevant for silver [66]. However, reducing the filler content often leads to stability issues in the adhesive paste, such as sedimentation of the particles, or to processing deficits, particularly in screen printing or dispensing. This can be overcome by a high low-shear viscosity and/or introduction of a yield stress into the system.

Viscosity is the resistance of a fluid against flow. The simplest representation of fluid deformation under shear stress is given by the parallel-plate model, as depicted in Figure 3. In this model, a fluid is confined between two plates, one stationary and the other subjected to a shear stress τ. As a result, a linear velocity profile is established within the fluid, with a velocity v = 0 m/s at the stationary plate and v_{max} at the moving plate. For a gap height y, the shear rate $\dot{\gamma}$ is defined according to [67]:

$$\dot{\gamma} = \frac{dv}{dy} \tag{3}$$

Viscosity η is then the proportionality constant between shear rate and shear stress:

$$\tau = \eta \cdot \dot{\gamma} \tag{4}$$

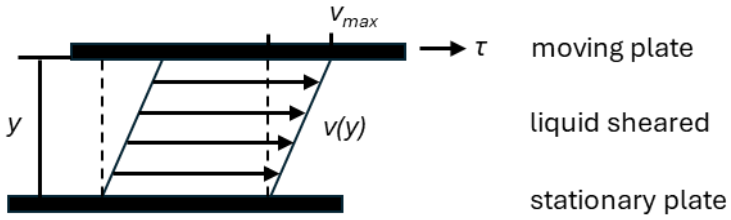


Figure 3. parallel-plate model with a liquid under shear between one stationary and one moving plate

For Newtonian fluids, the viscosity is a constant, which depends only on temperature and pressure. In non-Newtonian fluids, viscosity is a function of shear rate, shear time and electrical or magnetic field (if present). ECAs exhibit typically shear-thinning behavior, meaning their viscosity decreases with increasing shear rate. Additionally, many ECAs show thixotropic behavior, where the flow curve depends on the shear history. For example, particle alignment under increasing shear may lead to hysteresis in the flow curve when the shear rate is subsequently decreased. The viscosity of ECAs is therefore also time dependent.
To prevent sedimentation of filler particles, a high low-shear viscosity is required. For spherical particles in Newtonian fluids under laminar flow conditions, Stokes' law describes the sedimentation velocity v_{sed}, which is inversely proportional to viscosity:

$$v_{sed} = \frac{d^2 \cdot \Delta\rho \cdot g}{18 \cdot \eta} \tag{5}$$

with particle diameter d, density difference $\Delta\rho$ between particle and fluid and gravitational constant g. Alternatively, a yield stress can be introduced into the system. The yield stress represents the minimum applied stress required to initiate flow. Below the yield stress, the material behaves like an elastic solid.
Generally, rotational rheometers are used to determine viscosity and yield stress of suspensions [67]. For yield stress determination, usually a shear stress ramp is applied and the resulting deformation γ of the sample is recorded. For materials with a yield stress, two distinct regions are observed, when data are plotted in a double-logarithmic deformation vs. shear stress diagram: one regime with a slope of one, corresponding to the elastic behavior of the sample and a subsequent region with a much steeper slope, corresponding to flow regime. According to the tangent-intersect method, the intersect of these two lines is taken as the yield stress. Often, a vane geometry is employed to determine the yield stress in order to avoid slip phenomena at the sample/fixture interface prior to the breakup of the sample structure. Compared to plate-plate geometries, the vane rotor has the additional advantage of minimizing disturbance of the sample structure during insertion [67]. Various other methods, such as shear stress amplitude sweeps in oscillatory shear or fitting e.g. a Herschel-Bulkley model to stress vs. shear rate data can be employed to determine the yield stress [67,68]. However, absolute values should only be compared when the same measurement protocol is applied [68].
For suspensions with a yield stress, viscosity determination is preferentially done in controlled stress mode and stresses beyond the yield stress are applied. The shear stress is increased in logarithmic steps over the relevant range, while the resulting shear rate is recorded. The measurement requires laminar, uniform steady state flow in the gap as well as the absence of wall-slip, sample spillage, shear banding or elastic instabilities [67]. These aspects have to be addressed in preliminary experiments in order to define an appropriate experimental protocol and to select an appropriate fixture (e.g. sufficient roughness to avoid slip, appropriate dimensions to

meet the rotational speed specification range of the rheometer). Typically plate-plate or concentric cylinder geometries with gap width at least 10 times larger than the particle size are used. Detailed measurement protocols for viscosity and yield stress determination of silver pastes for solar cell metallization have been reported by Yüce and Willenbacher in [69].

Iodide-induced percolation in ECAs

Diluted suspensions of sterically or electrostatically stabilized particles not trapped in a percolating network controlled by dominating attractive colloidal forces usually do not exhibit a yield stress and when the viscosity of the continuous liquid is low, particle sedimentation occurs rapidly. In 2010, Yang et al. [70] demonstrated that iodide ions can improve the electrical conductivity and decrease the percolation threshold of silver flake-epoxy ECAs. More recently, Marten et al. [71] demonstrated that a similar treatment also induces a yield stress in silver-filled thermoplastic polyurethane (TPU) adhesives.

Yang et al. [70] reported that silver oxide on the particle surface is converted to silver iodide upon addition of iodide. This resulted in the formation of Ag/AgI nano-islands on the surface of the flake-shaped silver particles. The silver iodide successfully prevents re-oxidation of the particles during curing. Additionally, the observed decrease in percolation threshold indicated increased agglomeration of the particles. These findings were later confirmed by Wu et al. [72] in a study aimed at improving the thermal conductivity of silver-filled epoxy systems and Li et al. [73], who additionally stated that iodide may reduce the organic surface layer on the silver particles. In a subsequent study, Li et al. [74] demonstrated that exposure to sunlight reduces the silver iodide to iodine and silver nanoparticles, which remain attached to the silver flake surface. Consequently, the silver nanoparticles sinter during curing, thereby decreasing the volume resistivity of the composites by two orders of magnitude compared to untreated ECAs. Zheng et al. [75] demonstrated the same mechanism for silver-filled composites based on silicone.

Sun et al. [76–78] observed a transition from a well-dispersed particle distribution to a sample-spanning particle network upon addition of a ionic liquid (IL) containing iodide as the counter ion (1-Butyl-3methylimidazolium iodide). Because the IL was immiscible with their polymer matrix, the authors proposed the formation of a capillary suspension (see next section). However, the adhesive paste changed color from silver to brownish upon addition of the IL [77], indicating a chemical reaction of the silver particles presumably with iodide. Furthermore, the iodide distribution observed by energy-dispersive X-ray imaging [76] matches well with the nano-island structure reported by Yang and others, suggesting a similar mechanism. In 2025, Marten et al. [71] observed a similar change in spatial particle distribution in a silver-filled TPU system as previously reported by Sun et al. [76–78]. However, in their case the IL was miscible with the polymer rendering the proposed explanation based on the formation of a capillary suspension unlikely. Moreover, Marten et al. [71] obtained similar results using simple iodide salts, namely potassium iodide and natrium iodide. They proposed that the replacement of the long-chain fatty acids on the particle surface by the much smaller iodide decreases steric repulsion between the particles. This allows for closer particle spacing, which enhances electron tunnelling, thereby increasing electrical conductivity, and simultaneously promotes van-der-Waals attraction between particles. As a result, the particles aggregate to form a sample-spanning network, which prevents sedimentation and induces a yield stress. However, further addition of iodide caused the formation of more compact aggregates separated from each other, thus leading to increased resistivity in the dried films [71,79].

The capillary suspension phenomenon

Capillary suspensions were first described by Koos and Willenbacher in 2011 [80]. Capillary suspensions are ternary solid-liquid-liquid systems in which a small amount of a secondary

liquid, immiscible with the bulk liquid, is added to a binary suspension. Two states of capillary suspensions can be distinguished, named in analogy to granular wet matter. In the “pendular” state, the secondary liquid preferentially wets the particles, forming pendular bridges of secondary liquid between the particles. In the “capillary” state, the bulk fluid preferentially wets the particles and particle clusters form around secondary liquid droplets shielding them from the surrounding bulk liquid, thus reducing the free energy of the system [81]. In both states, the secondary liquid droplets are typically smaller than the particles and interfacial forces are responsible for the formation of a particle network. Additionally, the volume fraction and number of secondary liquid droplets strongly influence structure and strength of a capillary suspension [82]. The formation of a sample-spanning network transforms the system from a liquid to a gel-like state, thereby inducing or reinforcing a yield stress. Thus, even low-filled capillary suspensions are stable against particle sedimentation [83].
Most scientific publications deal with the “pendular” state, as the theory of capillary bridges is well understood. It is generally accepted that the capillary force dominates the network formation exceeding other interactions like gravitational or van-der-Waals forces by orders of magnitude [80,84]. The capillary force F_{cap} between two equally sized spheres connected by a liquid bridge is:

$$F_{cap} = f(V,h) \cdot 2\pi\, r\, \Gamma \cos\theta \tag{6}$$

where $f(V,h)$ is a function of droplet volume V and particle surface separation h, r is the particle radius, Γ the interfacial tension between bulk and secondary fluid and θ the three-phase contact angle. As the force in a single bridge should correlate to the macroscopic mechanical strength of the suspension represented by the rheological properties of the composite [85], the yield stress σ_y of a capillary suspension is commonly approximated by [86]:

$$\sigma_y = f(\phi_P, N) \cdot \frac{F_{cap}}{r^2} = f(\phi_P, N)\; g(V) \cdot \frac{F_{cap}}{r} \tag{7}$$

where $f(\phi_P, N)$ is a function of particle volume fraction ϕ_P and number N of capillary bridges per unit volume and $g(V)$ a function of the droplet volume V. For dilute suspension ($\phi_P << 1$), $f(\phi_P)$ is estimated to be ϕ_P^2 [87]. When a small amount of secondary liquid is added, the yield stress initially increases sharply, which is attributed to the formation of a particle network in which single particles are connected to each other by capillary bridges. Once all particles contribute to the network, the yield stress reaches a maximum. Further addition of secondary liquid increases the bridge volume, causing neighboring bridges to merge without significantly affecting the yield stress. The configuration, where three particles are connected by a liquid droplet is often referred to as the “funicular” state. With further increasing secondary liquid volume, more particles and bridges join into so called spherical agglomerates which disrupt the network structure and cause the yield stress to decrease again, eventually approaching the value of the original binary suspension. [82,88,89] The different structural states are illustrated schematically in Figure 4a.

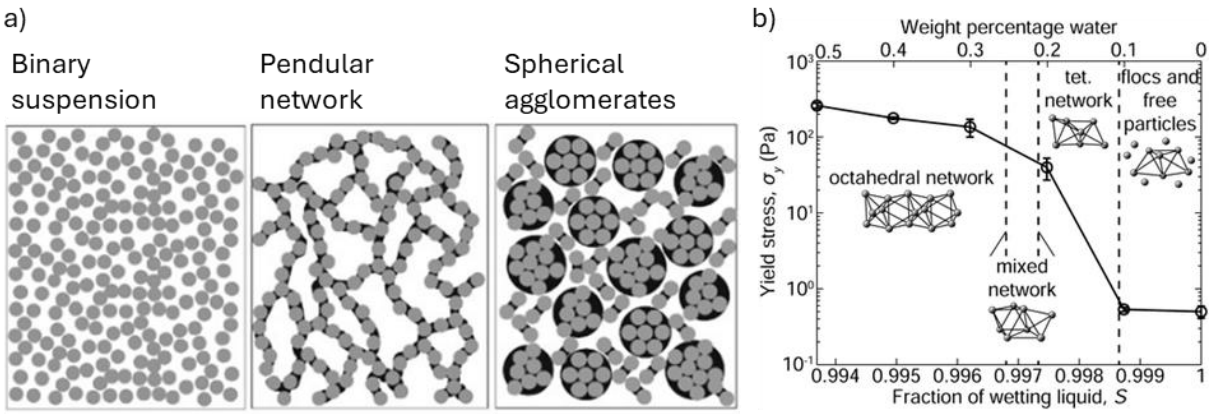


Figure 4. a) transition from a binary suspension to a pendular network in a "pendular" state capillary suspension into spherical agglomerates with increasing secondary liquid volume fraction, based on [88]; b) cluster formation in "capillary" state capillary suspensions and resulting yield stress in a model system with water as secondary phase, reproduced with permission from [81]

The secondary liquid volume fraction at which the maximum yield stress occurs increases with increasing particle volume fraction. However, when the secondary liquid fraction is normalized by the particle volume fraction, the resulting curves collapse onto a master curve [90]. A broad distribution of particle and bridge size shifts the maximum to lower secondary volume fractions [87]. Koos et al. [91] experimentally confirmed the dependence of yield stress on inverse particle radius (r^{-1}) and Jarray et al. [92] among others, confirmed an increase in gel strength when interfacial tension increased and three-phase contact angle decreased.

When the three-phase contact angle exceeds 90°, the bridge geometry would be convex, resulting in repulsive forces between particles [82]. Therefore, in the "capillary" state, particles rather form clusters around single secondary liquid droplets shielding them from the bulk fluid. These clusters reduce the energy state of the system, thereby generating an effective attractive interaction. While the dependence of interfacial tension and reciprocal radius remains valid on the macroscopic scale, $\sigma_y \sim \cos\theta$ must be replaced by a still unknown term [91]. The "capillary" state was first theoretically described by Koos and Willenbacher in 2012 [81] and demonstrated experimentally by Bossler and Koos in 2016 [82].

Upon addition of secondary fluid, initially isolated tetrahedral clusters form. When these basic building blocks connect to form a sample-spanning network, the yield stress increases, see Figure 4b. The geometry and energetical state of these basic building blocks depend on three-phase contact angle and droplet volume. An increasing fraction of secondary liquid leads to the formation of clusters of higher order. Structures formed from larger secondary liquid droplets are more stable as they use a greater number of particles and consequently, yield stress increases further. However, not all cluster configurations are equally probable due to entropic restrictions [93]. Particularly, a maximum three-phase contact angle exists beyond which cluster formation becomes energetically unfavorable. For spherical particles, maximum contact angles of 151° for tetrahedral and 165° for octahedral clusters were calculated [81,82]. The network structure represents only a local energy minimum and is therefore highly dependent on mixing conditions during preparation. According to Hauf and Koos [94], droplets must be completely surrounded by particles to allow clusters to relax into the lowest energetically favored state. Under low shear conditions, the network structure may also rearrange [81]. Additionally, as a capillary suspension requires droplets smaller or equal in size to the particles, droplet breakup during mixing is important. The formation of a Pickering emulsion in which particles accumulate on the liquid phase interface of larger droplets, competes with the formation of a "capillary" state network.

However, Pickering emulsions are typically formed at higher fractions of secondary liquid to particle volume. The presence of other attractive interactions between particles may favor the formation of a capillary suspension [95].

The solid like behavior of capillary suspensions not only shows up in the occurrence of a yield stress, but is also reflected in small amplitude oscillatory measurements. Capillary suspensions exhibit typical gel-like behavior, i.e. the storage modulus *G'* exceeds the loss modulus *G''* and remains nearly frequency-independent over a broad frequency range. Besides introducing or reinforcing a yield stress, capillary suspensions exhibit shear-thinning behavior. Their low-shear viscosity is higher than that of the corresponding binary suspension, but with increasing shear rate the viscosity decreases as the particle network progressively breaks down. This decrease is dependent on particle size. At sufficiently high shear rates, the viscosity approaches that of the binary suspension [91,96].
Over the years, numerous factors have been reported that influence both the state and strength of a capillary suspension. Among these, mixing history seems most important, since droplet breakup determines the number of bridges and thus the strength of the network. Important parameters include mixing time, mixing speed and viscosity ratio of bulk and secondary liquid [86,95,96]. Diffusive processes are also important in generating very small droplets that may not be accessible through droplet breakup by mechanical energy input. This is also evident from the observation that capillary suspensions can form spontaneously when particles are uniformly covered by a thin layer of secondary fluid, e.g. through water uptake from humidity, prior to dispersion [97,98]. Additionally, mixing order can influence particle wettability, depending on which phase the particles were initially dispersed in [99]. In practice, it is likely that a contact angle distribution occurs in the capillary suspension due to contact angle hysteresis, wetting and de-wetting during mixing [85], particle surface roughness [100], chemical surface inhomogeneities or particle porosity [82]. Polymer layers absorbed on the particle surface may introduce steric hindrance, preventing the formation of a capillary suspension [83]. If the secondary liquid displaces these polymers, a capillary suspension can still form. Alternatively, surfactants, other polymers or salts may be added to modify the particle surface properties and promote network formation [91,101,102]. The theoretical considerations described above are based primarily on spherical particles. In practice, however, particles with various shapes and aspect ratios are commonly used. Plate-shaped particles favor the pendular state due to the plane interfaces with large area which allow the formation of large liquid bridges [103]. Cube-shaped particles further increase the possible number for bridge attachment sites [104]. In contrast, needle-shaped particles tend to form spherical agglomerates without surpassing the “pendular” state [84]. Due to the afore mentioned factors, each material combination tends to have a state which is easier to prepare than the other [85].
A key advantage of the capillary suspension phenomenon is its broad applicability across different material systems, provided that the necessary wetting and interfacial conditions are fulfilled. Therefore, the capillary suspension phenomenon is applied in the formulation of food products [97], slurries for battery electrodes [105,106], structured ceramic materials [107,108], glass filters [109,110] or materials for bone tissue engineering [111] among others. Recently, capillary suspensions were formulated with conductive particles improving electrical and thermal conductivity as well as printability of thermal interface materials [77], conductive elastomers [78] or pastes for printed electronics [112], as well as 3D- and 4D-printing [113]. One of the most recent application areas is metallization of solar cells, where pastes formulated as capillary suspensions can reduce or even eliminate the need for polymeric additives. Thereby, the residual carbon in the sintered metallization is reduced and accordingly the conductivity

increases. This allows for the reduction of silver consumption in this important technology field [114,115].

2.2 PV interconnection

Photovoltaics (PV) refers to the direct conversion of sunlight into electrical energy. This process is enabled by semiconductor materials such as silicon or germanium. A schematic illustration of the working principle of a solar cell is shown in Figure 5a. Conventional PV cells consist of a p-n junction comprising two differently doped semiconductor layers. The n-type layer, typically phosphorus-doped silicon, contains an excess of free electrons, while the p-type layer, usually boron-doped silicon, provides electron vacancies referred to as “holes”. Once both layers are combined, an internal electric field arises at the p-n junction. When a photon is absorbed by the material, electron-hole pairs are generated. In case the electric filed is weak, the electron-hole pair immediately recombines. Once the photon energy exceeds the bandgap energy of the material, the electron moves through the n-type layer and the holes through the p-type layer. When an external circuit is connected to the cell, the electron exits the cell through the front-side electrode, passes through the external circuit and recombines with a hole at the back-side electrode in the p-type layer [116–118]. To reduce recombination, optical and resistive losses, state-of-the-art solar cells contain additional layers. For some time, the Passivated Emitter and Rear Cell (PERC) Technology has dominated the solar cell market [119]. PERC comprises additional oxide layers between silicon wafer and electrodes to passivate the surface of the cells and reduce recombination losses [116]. Nowadays, Tunnel Oxide Passivated Contact (TOPCon) cells are the market leader, which are expected to force PERC out of the market by 2029 [4]. TOPCon cells are an evolution of PERC comprising a thin tunnel oxide layer at the semiconductor-electrode interface which allows only electrons to pass but not holes. Thereby, recombination losses are further reduced [120]. Another emerging cell technology is the Heterojunction Technology (HJT), which comprises different semiconductor materials. Namely, the crystalline silicon wafer is surrounded by thin layers of amorphous silicon, which provides an excellent surface passivation [116]. Finally, in back contacted solar cells (xBC), both positive and negative electrodes are placed on the rear-side of the cell to eliminate shading of the front-side. This technology is compatible with a broad range of solar cell types, including TOPCon and HJT [4]. Next to crystalline silicon solar cells, several new cell concepts have emerged over the last years, including thin-film or amorphous cells, organic PV cells and perovskite solar cells, e.g. [117].

To increase the voltage output to a usable level, individual solar cells are electrically connected in series. This is usually achieved by soldering metallic ribbons to the cells, thereby connecting the front-side of one cell to the rear-side of the next cell, see Figure 5b. The resulting cell strings are subsequently placed between a front glass and a polymeric backsheet with encapsulant material between all layers. The encapsulant material is then cured in a vacuum laminator, thus forming a tightly bonded laminate, which protects the solar cells from environmental influences. Finally, electrical connectors are attached and the module is framed [117,118].

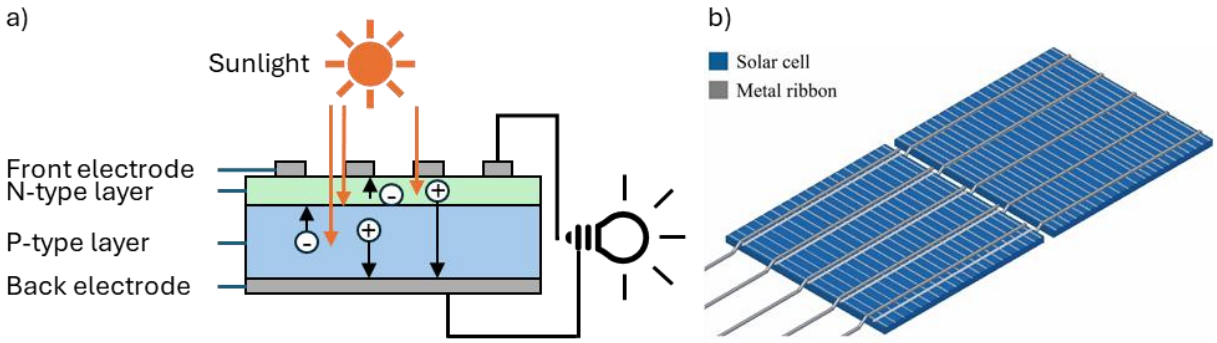


Figure 5. a) schematic of a standard silicon solar cell; b) traditional ribbon interconnection of solar cells, reproduced with permission from [121]

Electrically conductive adhesives were first introduced into PV technology in 2001. Their low curing temperature and therefore reduced thermomechanical stresses compared to solder, make them particular attractive for interconnecting very thin cells as well as temperature-sensitive cell concepts [12]. Additionally, ECAs enable new interconnection concepts such as interconnection by conductive backsheets or the shingling approach [122]. This section provides an overview on solar cell interconnection through the shingling approach and highlights material specifications for ECAs used as interconnection material.

2.2.1 Solar Cell Shingling and resulting requirements for ECAs

Even though the first patent on solar cell shingling was filed in 1956 [123] and shingled modules have been popular in vehicle-integrated PV since the 1990s especially for solar powered racing cars, setting several module efficiency records [124], the concept only reached commercial availability in the early 2000er. Shingling can therefore be regarded as a relatively new module concept with ongoing scientific interest. In the work of Tonini et al. [125] and Rößler et al. [13] the process of solar cell shingling has been well described.

In the first step, host wafers are separated into three to six rectangular stripes, the so-called shingles. These shingles retain the width of the initial cell and have a reduced length of a few centimeters. In principle, any cell concept can be used for shingling. The separation is typically performed by laser processing, which induces defects at the cell edges. Edge passivation can be applied to reduce efficiency losses. The front-side cell metallization usually consists of a larger number of shorter fingers compared to half or full cells and a busbar located along one long edge, onto which ECA is applied in a second step. On the rear-side of the cell, an additional busbar is required on the opposite edge. In the third step, the shingles are placed adjacent to each other with a small overlap, in a way that the front-side busbar of one shingle aligns with the rear-side busbar of the next shingle, analogous to roof-tiles, see Figure 7. This is referred to as linear shingling. Alternatively, every second row of shingles can be shifted by one half-cut shingle (half in width) in a way that every shingle is connected to four cells instead of two. This results in the so-called “shingle matrix” layout [126]. The ECA is then cured to form a series-interconnected solar cell string. The strings are subsequently connected in series and partially in parallel to match the power output of standard modules. After positioning the strings onto the glass/encapsulant stack and attaching terminal connectors, the solar module is laminated. A 3D-model of a module is shown in Figure 9. The completed module is then subjected to extensive reliability testing or field operation [13,125].

The main advantage of the shingling approach is the improved area utilization as gaps between the cells are omitted. The busbars are overlapped by active cell area and ribbons and wires are no longer required, thereby reducing shading losses. Furthermore, the smaller cell size reduces

ohmic losses, resulting in lower operating temperatures. However, the shingled module design is not yet standardized and requires adjustment to the existing stringing equipment.
Each processing step comes with specific requirements on the interconnection material. These requirements are described step by step in the following sections:

ECA preparation/formulation

One-component ECAs are usually delivered and stored frozen to ensure a shelf-life beyond six month, inhibiting premature curing or phase separation [127,128]. Prior to application, the adhesives are thawed and should exhibit an open time (pot-life) beyond eight hours, while maintaining stable properties throughout the application process.
One of the major advantages of ECAs compared to solder is the absence of lead or other materials restricted by the RoHS directive [8]. However, the typical high silver content in ECAs raises economical and supply concerns. In 2024, the PV industry accounted for 17% of the global silver demand [129]. Cattaneo et al. [130] projected that this demand could exceed 40% of the global silver supply by 2030 in case of fast increasing expansion of PV. Due to the impending shortage of silver in addition with its high and volatile price, the PV industry aims to reduce its silver consumption significantly [4]. Therefore, ECAs should ideally contain as little silver as possible while maintaining performance.

ECA application

In PV manufacturing, dispensing and screen printing are the most common ECA application methods [42]. In other application fields, doctor-blade coating/stencil printing and flexographic or lithographic methods are reported [131,132]. During application, parameters such as accuracy, precision as well as laydown must be carefully controlled [125]. Printing parameters, including temperature, printing speed, applied pressure and snap-off in the case of screen printing or valve opening and closing during dispensing, must be determined specifically for the ECA formulation used, particularly with respect to its rheological behavior [12,36]. For ECAs with low viscosity, undesired bleeding or spreading may occur after deposition [32]. Commonly, ECAs are shear-thinning and exhibit a viscosity that is three to six times larger at a given shear rate compared to the viscosity at a shear rate which is ten times higher to avoid slumping or sagging [18]. However, the dispensing speed can influence spreading behavior as well [133]. Viscosity and degree of shear-thinning can be adjusted through the amount and type of filler. Additionally, a yield stress between 10 and 100 Pa is beneficial to avoid flow through the screen or particle sedimentation in the syringe. The choice of application technique depends on the available equipment but primarily on the achievable throughput. For dispensing, maximum application speeds have been reported where ECA could still be applied in a homogeneous line [122,134]. Screen printing has the advantage of printing several lines simultaneously [135]. Regardless of the method used, it is essential that no ECA is smudged around the shingle edge, as this may lead to shunting of the shingle [136].
The thickness of ECAs in shingled interconnection is approximately 50 µm [137]. ECA is typically deposited as a continuous line on the front-side busbar. To reduce silver consumption, alternative approaches involving discrete adhesive pads with spacing between them have been proposed [135,138]. This results in an ECA consumption of only a few milligrams (1-5 mg) per shingle [13,139,140] compared to app. 10 mg in continuous lines [122], which adds up to a few grams of ECA per module [141]. To further reduce silver consumption, the busbars on the cells might even be omitted [121]. As ECAs often contain flake-shaped particles with high anisotropy, particle alignment in the direction of shear flow or in parallel to the wafer surface should be considered when designing the deposition process [18,142].

String assembly (Shingling)

In the next step, the shingles are positioned with a controlled overlap, such that the front-side busbar aligns with the back-side busbar of the adjacent cell. Depending on the busbar width and its distance from the shingle edges, overlap lengths of 1.2 mm or less are realized. A wider overlap would improve mechanical stability, but increases shaded area. Too narrow gaps increase the risk of ECA smearing around the shingle edge, which may cause electrical short circuits [13,125]. A high accuracy in shingle-to-shingle alignment as well as in total string length is required to achieve optimal module output and performance as different shading results in current mismatch between shingles [136,143], but also for aesthetic reasons. During assembly, the ECA should provide sufficient tack in the uncured state to hold the shingles in place until curing. Additionally, air entrapment within the ECA during shingle placement must be avoided [144].

Curing of ECA

Subsequently, the assembled shingle string is submitted to curing, where the electrical and mechanical bonds are established. Curing can be done in a furnace, with a hot bar bonder, on a heat plate [145] or with infrared lamp heaters [128]. Alternatively, the ECA can be cured during lamination after assembly of front glass, encapsulant and backsheet. However, curing during lamination increases the risk of air bubble entrapment in the adhesive layer [131,144]. Usually, strings are cured without mechanical fixation but holding down the shingles can improve module performance [13]. To compete with conventional soldering processes, high production throughput is required, which is realized by a short curing time, ideally below 30 s [146–148]. So-called snap-curable ECAs cure within a few seconds at curing temperatures between 110 and 200 °C [13]. Such curing temperatures are particularly advantageous for temperature-sensitive cell technologies, such as perovskite solar cells, which typically should not be exposed to temperature exceeding 150 °C during processing [146]. The required curing time and temperature depends on the polymer system, curing method as well as the substrate [142,149]. Especially, heat-up and cool-down periods of the equipment have to be taken into account [145]. Generally, to achieve similar ECA properties, a lower curing temperature requires longer curing time and vice versa [150]. Curing kinetics can be assessed by differential scanning calorimetry (DSC). DSC measurements provide information about curing energy in dependence of time or temperature. From the results, the minimum required curing temperature as well as the degree of curing at given process conditions can be calculated [145].

The ECA joint introduces an additional electrical resistance into the solar cell string. A basic equation to estimate the resistance R_{Joint} is given by:

$$R_{Joint} = \frac{\rho_v \cdot t_{ECA}}{A} + 2 \cdot \frac{\rho_c}{A} \tag{8}$$

where ρ_v and ρ_c are the volume and contact resistivity of the ECA, t_{ECA} is the thickness of the ECA and A the contact area. However, all of the parameters are difficult to determine experimentally. The equation is valid only for shingles with two rectangular busbars connected by a continuous ECA line [151] and especially, the actual contact resistivity ρ_c within the joint is reported to differ significantly from values obtained using simplified test structures [152]. According to equation (8), the electrical losses caused by the ECA joint are relatively small, affecting module output only above a threshold value [32]. These thresholds have been estimated to be app. $10^{-3}\,\Omega\,\mathrm{cm}$ for volume resistivity [136] and $10^{-2}\,\Omega\,\mathrm{cm}^2$ for contact resistivity [126], assuming a large, i.e. continuous ECA line. It should be taken into account, that resistivity may change during life-time. Especially, contacts against non-noble metals like copper, tin or aluminum are reported to degrade due to electrochemical corrosion under high temperature or moisture ingress. The addition of corrosion inhibitors may prevent contact degradation [136,153].

During curing, the ECA not only develops electrical conductivity but also mechanical strength. The ECA transits from a viscous liquid to an elastic gel, and finally arrests in a glass state (vitrification) before being fully cured [21]. As the crosslink density increases with increasing curing time, the glass transition temperature T_g of the polymer network increases, which can be used as an indicator for the degree of curing [154].

Transport and module assembly

After curing, the shingle strings may be transported for string characterization or assembly of front glass, encapsulant, interconnectors and backsheet prior to lamination. After lamination, the module is typically mounted in a frame. During all processing steps, the shingles must remain securely fixed by the ECA joints. Especially after cooling down from lamination, stresses arise in the joints due to the mismatches in the coefficients of thermal expansion (CTE) of the different materials involved.

Differences in CTE cause relative movement between materials, which results in shear stresses within the interconnection joints [155]. As silicon is rather brittle, solar cells tend to break under mechanical stress [156]. Therefore, these stresses must be mitigated by the interconnection material. ECAs are regarded for their higher flexibility, especially compared to solder [137]. Tune et al. [12] reported maximum shear strains of app. 6.5% and shear stresses of app. 25 MPa in shingled ECA-based joints, values that are of the same order of magnitude as the material strength limit. Beaucarne [138] therefore recommends using interconnection materials with a low shear modulus-to-shear strength ratio. However, maximum strains and stresses depend on the module design parameters such as module width, joint thickness, joint width as well as cell overlap and the materials used [157]. Especially thicker joints reduce maximum stresses, but require more material which increases cost [138]. A suitable experimental method to determine shear properties of the ECA is the lap-shear test, as defined in [158]. To assess the ECA's flexibility, Young's Modulus can be determined through tensile testing, with standardized procedures described in [159,160].

The general mechanical response of ECA materials is described using viscoelastic material models [161]. The relevant material parameters are commonly obtained through dynamic mechanical analysis (DMA) in combination with the time-temperature superposition principle (TTSP). In DMA experiments, a sinusoidal dynamic load is applied to a test specimen at different temperatures and frequencies. Depending on the test configuration, this load may be tensile stress [31,33] or shear stress [162]. Then, the resulting time-dependent strain response is determined. From the measured stress and strain amplitudes as well as the phase delay between them, the storage modulus G' and the loss modulus G'' can be calculated as functions of frequency as long as the material response is in the linear viscoelastic response regime, i.e. the response is also sinusoidal and varies linearly with the applied load. As measurements at very low frequencies require long measurement times, the time-temperature superposition principle is commonly applied. TTSP is based on the kinetic theory of polymers which states that all polymer relaxation processes exhibit the same temperature dependence. The mechanical response function of a polymer is thus independent of temperature, but shifted on the time or frequency scale when temperature is varied. The same processes contributing to the response function at a selected reference temperature and frequency range take place faster at higher temperatures (or slower at lower temperatures). Therefore, frequency-dependent data obtained at different temperatures can be shifted along the frequency axis by means of temperature dependent shift factors a_T to construct a master curve at a chosen reference temperature, as exemplarily shown in Figure 6 [31,67]. Strictly speaking, TTSP is only valid above the glass transition temperature. However, most organic ECAs undergo glass transition within the relevant application temperature range [138]. In practice, TTSP is therefore often applied even below T_g, provided that the

experimental data can be successfully combined into a continuous master curve. The obtained material parameters can subsequently be used in finite element simulations to predict stress development in PV module interconnection [31,33,162].
Lamination not only induces shear stresses in the joints. As lamination is performed under vacuum, the solar cells are pressed tightly onto each other. This can result in a reduced interconnection resistance [151]. Especially in strings in which the ECA is applied in discrete pads with gaps in between, a pressure-based electrical contact can form between the busbars [163].

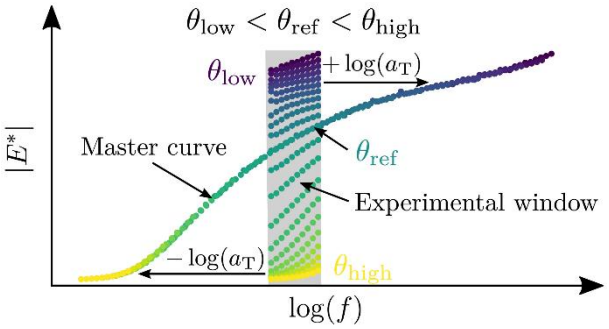


Figure 6. The principle of time-temperature superposition exemplarily applied on data obtained at a given frequency *f*-window at different temperatures θ and shifted along the *f*-axis by means of temperature dependent shift factors a_T to obtain a master curve at a reference temperature θ_{ref}, E^* represents the storage, loss or complex modulus, reproduced with permission from [31]

Module and interconnection characterization

Once the modules are completed, they are commercialized and installed in field, where they are exposed to environmental stress factors, such as fluctuating temperature generating thermomechanical stresses in the assembly and mechanical loads caused by wind or snow [161]. Generally, thermally induced stresses are more critical than mechanical loads [156]. The nominal operating cell temperature of PV modules is typically (45 ± 3) °C [164], although temperatures may occasionally exceed 80 °C [147]. Springer and Bosco [31] identified temperature cycles lasting a few hours caused by cloud shading up to seasonal temperature variations over the course of a year. Because solar modules are expected to operate for several decades, their reliability is evaluated using accelerated aging tests. These tests are specified in the IEC 61730 and IEC 61215 standards [165,166]. Among the various testing methods, Geipel [147] reports that most failure occurs during thermal cycling (TC), damp heat (DH) and humidity freeze (HF) tests. In TC 200 tests, modules undergo 200 temperature cycles between -40 and 85 °C under current flow. During the DH 1000 test, modules are exposed to 85 °C and 85% relative humidity for 1000 h. In the HF 10 test, modules are cycled 10-times between -40 and 85 °C at 85% relative humidity. All tests are considered passed, when performance degradation remains below 5%.
Common failure modes in ECA-bonded interconnections include chemical changes, i.e. oxide formation or corrosion, mechanical cracking and debonding. In chemical degradation, moisture ingress is considered the primary driver [147]. Defects in the joint can be investigated by imaging techniques, such as X-Ray imaging, electroluminescence (EL) imaging [167], scanning acoustic microscopy [168] or magnetic field imaging [136]. Alternatively, electrical measurements can be used. In such measurements, the current-voltage (*IV*) characteristics of a module are determined, which are plotted as an *IV*-curve. From the curve, the short-circuit current I_{sc} as the maximum current at zero voltage and the open-circuit voltage V_{oc} as the maximum voltage at zero current can be obtained. Additionally, the maximum power point P_{max} or MPP is calculated as the point where the product of *I* and *V* is maximal. The fill factor FF is defined as:

$$\mathrm{FF} = \frac{P_{max}}{I_{sc} \cdot V_{oc}} \tag{9}$$

indicating better module quality the closer it is to one [169]. Furthermore, the series resistance R_s can be calculated from *IV*-measurements. This parameter reflects the accumulated internal resistances of the emitter, substrate, contacts and interconnections [170]. While interconnection losses influence both FF and P_{max}, the best representation is given by R_s, especially when the *IV*-measurements are performed in the dark [151,171]. A statistical analysis of module data from twelve years conducted by Gebhardt et al. [172] showed that the shingle module concept yields comparable or even superior long-term stability compared to conventional module designs.

2.2.2 Performance of ECAs in shingled PV modules

The shingled module design increases the power output for a given module area compared to conventional module designs, as demonstrated in several studies [125,173,174]. Abdel Latif et al. [175] reported that long-term stability of shingled modules depends primarily on the laser separation method used for the cells, the dispensing parameters of ECA as well as the precision of shingle placement. Weber et al. [171] investigated the influence of edge passivation and showed that it does not negatively affect the interconnection as long as the applied aluminum oxide layer does not cover the busbar, therefore, making it beneficial at module level. Harmful interactions between ECA and common encapsulants were excluded by Oreski et al. [19]. Therefore, the stability of the interconnection itself remains of high interest. Mittag et al. [143] calculated that the power loss due to ECA interconnection is negligible in its initial state. However, cohesive or adhesive cracks, delamination, bubbles or structural changes, which are common defect mechanisms in ECAs [12], may increase interconnection resistance upon aging.

Many researchers showed that the mechanical strength of ECAs, such as peel and shear strength or flexibility, does not affect the module performance as long as the bond persists [32,128,176,177]. Nevertheless, the mechanical response of the ECA may change during aging [31]. If cracks develop, they often occur at the rear-side of the solar cell due to thermal z-contraction of the encapsulant [155]. Such existing cracks can also grow under subcritical stress conditions [178]. However, due to the tight packing within the laminated module, electrical contact may even persist in the presence of cracks [179].

There appears to be a certain threshold value below which the interconnection resistance does not affect the module performance [32,150]. As conductivity develops during curing, incomplete curing may result in reduced module output. Increasing curing temperatures or curing time then improves the module performance [148,150]. To reduce contact resistance, contacting area could be increased. However, an increasing overlap causes shading, counteracting the gains from reduced contact resistance [180]. Additionally, performance must always be balanced against material cost.

Under accelerated stress tests, humid conditions were found to cause the most degradation in ECA-bonded joints, likely due to oxidation or galvanic corrosion [128,153]. Encapsulants can delay moisture ingress and protect the cells. At low humidity, ECAs are rather stable [32]. Interestingly, a water-based ECA is reported, where water is used as the solvent that evaporates during curing. Modules produced with this ECA exhibited comparable initial and aging performance to conventional ECAs [181]. However, most commonly, solvent-free one-component ECAs are used in PV interconnection. Studies have further demonstrated that ECA-based interconnections can achieve performance comparable to soldered joints [122].

Despite promising performance, the high silver content of ECAs remains their main economic drawback. Consequently, current efforts in ECA development for PV focus on reducing the silver content. Two concepts are mainly pursued: replacing silver with alternative conductive materials and reducing the amount of applied ECA per module.

Abdel Latif et al. [174] reported on ECAs with decreasing silver content from 70 to 50 wt% based on the same raw materials. Both initial and performance after aging decreased with decreasing silver content, highlighting the need for new formulation concepts. A common approach is the use of silver-coated copper particles. However, copper oxidation rises concerns regarding long-term stability [182]. Devoto et al. [183] replaced silver with carbon nanotubes and obtained ECAs which showed promising long-term stability at module level. Hacke et al. [184] investigated electrically conductive double-sided tape containing nickel instead of silver and demonstrated PV modules with good initial and aging performance. Attempts to replace silver with the intrinsically conductive polymer PEDOT:PSS have so far been unsuccessful. Although similar initial performance was achieved, degradation under TC testing occurred [127].
In terms of ECA reduction, research ranges from printing discrete pads instead of continuous lines to omitting the use of ECA at all. Many studies confirm that from the electrical perspective, the amount of ECA per joint can be significantly reduced. However, mechanical stability often becomes the limiting factor [122,125,135,185]. Weber et al. [152,163] demonstrated ECA-free shingled modules, in which the electrical interconnection was achieved solely through a pressure contact after lamination. The interconnection resistance was three times higher compared to an ECA-based joint and much more variable between single joints. Under DH testing the ECA-free joints were stable. However, significant degradation occurred after TC testing. Alternatively to reducing the ECA content, Oh et al. [121] omitted the silver busbar on the cells and achieved good stability during DH testing.

Despite the promising performance of ECA-based interconnections, their market share is predicted to grow only moderately over the next ten years. According to the International Technology Roadmap for Photovoltaic 2024 [4], ECAs currently account for only a few percent of the interconnection market, with projections suggesting an increase to approximately 15% by 2035. This may be due to the small market share of shingled modules which is not expected to significantly increase by 2035 and the competition by lead-free solder.

3 Motivation and Outline

With the exception of the work by Geipel [147], most research regarding ECAs for solar cell interconnection has focused on a specific material property of the ECA such as volume resistivity or shear strength, while module performance is used as the primary metric to evaluate importance or acceptable range of this property. Moreover, the recommendations provided by Geipel are general in nature and mostly derived from ribbon-based interconnection. To the authors knowledge, a comprehensive specification of ECAs for linear solar cell shingling has not yet been reported. However, modifications in the ECA formulation usually affect multiple material properties simultaneously. Therefore, a detailed understanding of application-specific requirements is essential for the targeted formulation and advancement of ECAs.

This thesis aims to define a parameter set for ECAs applied in solar cell interconnection based on the linear-shingled module design. Further, low-silver ECA formulations have been developed that can be used as drop-in alternatives to highly-filled ECA, such that no modifications to existing processing equipment are required and module performance remains uncompromised.

In the previous chapter, ECAs and relevant performance properties have been introduced as well as concepts to tune them. Furthermore, the process steps involved in solar cell shingling and the resulting requirements for ECAs have been outlined.
Chapter 4 summarizes these requirements, based on a literature review and the author's own experimental experience with the objective of defining specifications for the development of a low-filled ECA that still fulfils the functional requirements of shingled cell interconnections. Within this context, the capillary suspension concept is introduced to ECAs and compared with regular two-phase suspensions. An extensive study on material properties is presented in Chapter 4.4, covering aspects ranging from rheological properties in the uncured state, to the curing process and finally to the electrical and mechanical properties and their durability in the cured state in dependence of the silver filler content. The results demonstrate that applying the capillary suspension concept to ECAs can significantly reduce the percolation threshold, which is the second central contribution of the presented work.

Previous attempts to reduce the silver content in ECAs have mainly focused on the (partial) replacement of silver by alternative conductive materials, such as copper or non-conductive core particles coated with silver. However, the filler volume fraction usually remained comparatively high. To improve the mechanical properties of the adhesive system and in terms of sustainability, reducing total filler content is preferable to replacement with other materials. Therefore, Chapter 5 explores the addition of a compatibilizer to the capillary suspension-based ECA formulation with the aim to achieve particle stabilization at very low silver-filler content (≤ 5 vol%) without compromising the promising electrical performance. For the investigated system, such a compatibilizer was found in polyethylene glycol (PEG). PEG dissolves in both the polymer resin and the secondary liquid, allowing for the fine adjustment of interfacial tension between the liquid phases and three-phase contact angle. This compatibilizer phenomenon enables particle stabilization in ECAs at the maximum permissible volume resistivity using a minimal filler content of 4 vol%.

Finally, Chapter 6 presents the application of the concepts developed in Chapters 4 and 5 to ECAs containing silver-reduced particles, namely silver-coated glass and silver-coated copper particles. Particular attention is given to the challenges arising from differences in surface chemistry and particle reactivity, with the objective of minimizing both filler and silver content

while still satisfying the requirements for solar cell shingling applications. A silver content of 1.3-3.5 vol% was realized in the investigated epoxy-based system depending on filler type, which is a significant reduction in silver consumption compared to 20-30 vol% in conventional ECAs.

Overall, ECA specifications for linear solar cell shingling are defined and the formulation of ECAs based on the capillary suspension concept is demonstrated to be feasible to meet these specifications at low silver filler content. Furthermore, the utilization of a compatibilizer in capillary suspensions is investigated. This provides a new formulation method to tune the interfacial properties of the three phases in a capillary suspension allowing for the formation of a stronger particle network. Finally, this formulation concept is demonstrated to be compatible with a variety of filler materials resulting in a significantly reduced silver consumption in solar cell interconnection materials.

4 Capillary suspension-based ECAs

Full title:	*Less is more: Enabling low-filled electrically conductive adhesives for shingled solar cell interconnection using the capillary suspension concept*
Authors:	*Marianne Kronsbein, Leonhard Böck, Katrin Dyhr, Torsten Rößler, Norbert Willenbacher*
Status:	*published*
Bibliographic data:	*Solar Energy Materials and Cells;*
	DOI: https://doi.org/10.1016/j.solmat.2025.113603

Abstract

Lead-free, low temperature materials for solar cell interconnection gain relevance in upcoming cell and module concepts. Electrically Conductive Adhesives (ECAs) are such materials but typically come with a high silver content. We herein give an overview on ECA requirements for shingled cell interconnection. Regular ECAs and stabilized ECAs with varying filler content were characterized regarding their rheological, curing, electrical and mechanical behavior and their performance in modules. It was found that 20 vol% silver is necessary to meet the electrical requirements with a regular epoxy-based ECA containing micron-sized silver flakes. Regarding mechanical properties, as little filler as possible is favorable. To fulfil both the electrical and mechanical requirements, application of the capillary suspension concept to ECAs was found to be suitable. Such an ECA with only 5 vol% silver filler exhibits a volume and contact resistivity of $(4.5 \pm 0.5)\ 10^{-3}\ \Omega\ cm$ and $(0.026 \pm 0.006)\ m\Omega\ cm^2$, resp., and a high lap-shear strength of (17 ± 4) MPa. Testing at both 140°C and 200°C curing temperatures showed that modules with low-filled and highly-filled ECAs achieved comparable initial efficiencies. After damp heat (DH500) testing, modules with capillary suspension ECA showed an efficiency loss of −0.8% ± 0.4%, compared to −2.5% ± 1.1% for highly-filled ECA. After thermal cycling (TC200), losses were −0.6% ± 0.5% versus −1.1% ± 0.5%. Both ECA types maintained efficiency losses below 1% in mechanical load tests. These results demonstrate the potential for silver reduction in shingled solar cell modules through the capillary suspension concept.

4.1 Introduction

First patented in 1956 as conductive cement by Wolfson and Elliott [10] Electrically Conductive Adhesives (ECAs) are now established bonding materials in flip chip, surface mount, advanced packaging and printed circuit board applications [11,30]. In recent years, the solar industry has gained interest in ECAs as cell interconnection material as well [135,182,186,187]. In certain applications, Electrically Conductive Adhesives replace the traditional solder bond. Their main advantage is a lower processing temperature of 110 to 150 °C compared to soldering, which requires temperatures above 200 °C [187]. Additionally, the lead-free adhesives meet the requirements of the RoHS DIR 2011/65/EU directive, which demands lead-free solder [8,188]. Drawbacks of ECAs compared to solder are the need of silver, bleeding, longer processing time and the need of storage at −20 to −40 °C [41]. Concerns regarding lower electrical and thermal conductivity are currently under investigation [189].
Around 95 % of the solar modules produced are connected by tab interconnection [190]. Here, ribbons are used to interconnect the solar cells. The solder bonds joining the ribbon to the cell can be replaced by ECAs without alteration of the module concept [191]. Shingle interconnection is an alternative method to the established tab interconnection of solar cells. In shingle interconnections, solar cells are interconnected by overlapping each other. This allows omitting the ribbons, leading to less shading losses. The principle of shingling is visualized in Figure 7. This technique allows for particularly high shading resilience [192], reduced ohmic losses [125], a high packing density within the module [143,193] and the realization of visually appealing module designs [194].

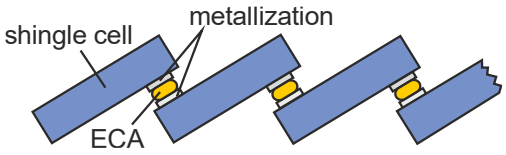


Figure 7. Principle of shingling solar cells. The cells are overlapped and aligned at their busbar metallization, with mechanical and electrical interconnection achieved using an ECA [194]

Temperature cycles during module operation lead to thermomechanical stresses within the solar module. In conventional tab interconnection, these stresses can be mitigated by the displacement of solar cells within the intercell gaps. In shingle interconnection, thermomechanical stresses can only be alleviated at the bonding joint. For this purpose, the interconnection element must be elastically deformable. Due to its higher flexibility, adhesive bonding using ECAs is significantly better suited for shingle interconnection than solder connections [135,138,195].
ECAs consist of a reactive polymer resin and conductive filler, typically silver. The increasing expansion of photovoltaic (PV) manufacturing capacities results in a rising demand for silver [190]. Without optimizing the specific silver consumption, the existing silver reserves could be largely depleted by 2050 [66]. For this reason, there are ongoing efforts to reduce the silver demand in PV manufacturing. In ECAs, decreasing the percolation threshold by conductivity enhancement through surface treatment of the silver particles [51,73,196] or by generation of silver nanoparticles [197] is most common to reduce silver consumption.
The percolation threshold, i.e. the filler content at which a material becomes conductive strongly depends on the shape [15] but even more on the colloidal interactions among the particles. It has been shown, that the capillary suspension phenomenon [80,81] is a powerful tool to reduce the percolation threshold and hence enhance the thermal [76,77] or electrical conductivity in composite materials comprising a polymer matrix and dispersed conductive filler particles [78].

Capillary suspensions (CapS) are ternary solid-liquid-liquid systems in which a second immiscible liquid induces the self-assembly of particles into a percolating network structure [80,81]. The particle network strength is controlled by strong capillary forces acting among the particles due to the added secondary liquid. Thus, the composite material typically exhibits a high yield stress, pronounced shear thinning, and fast structural recovery after strong shear [85]. This results in a high stability against sedimentation and phase separation, but makes it also ideally suited for screen printing or dispensing applications [113]. In this way, composite materials with a high electrical conductivity can be generated at a significantly reduced silver consumption.
In this study, we apply the capillary suspension concept on ECAs and compare them to regular ECAs at different silver filler fractions. For evaluation, we give upper and/or lower limits for rheological, electrical and mechanical parameters for uncured and cured ECA based on literature research and own experience. Finally, this work compares modules build with a low-filled and a high-filled ECA regarding their long-term stability against damp heat, thermal cycling and mechanical load.

4.2 Material and Methods

Material

In this work, epoxy resin and silver flakes (s. Figure 8, $x_{50,3}$ app. 11 µm,) were used as polymer matrix and conductive filler, resp. The filler volume fraction was varied between 5 and 30% (which accounts for 33 to 80 weight-%). For one series of experiments only epoxy and silver filler were used, referred to as “regular”. A second series consists of epoxy and silver and an additional secondary liquid, here referred to as “CapS”.

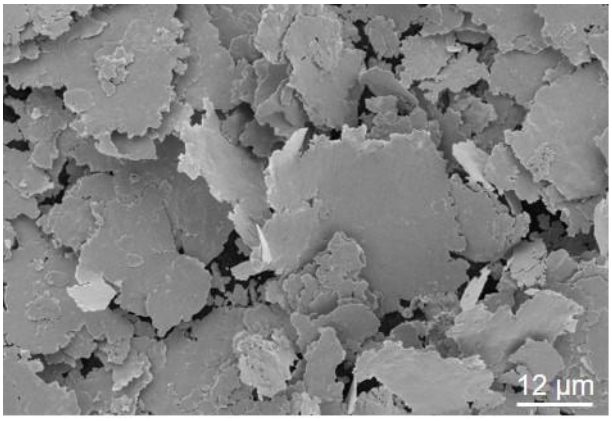


Figure 8. Scanning electron microscopy (SEM) image of silver flakes used in this study

Differential Scanning Calorimetry

Differential Scanning Calorimetry (DSC) was conducted using a DSC Q200 (TA Instruments) to determine peak curing temperature and curing energy of the samples. Samples where heated at a constant rate of 10 K/min from 40 to 210 °C. Curing energy was calculated in the interval from 70 to 200 °C. Deviations of ± 1 K for peak curing temperature and ± 3%$_{rel}$ for curing energy were found for different measurements of one sample.

Rheological characterization

A rotational rheometer (MARS, Haake) with plate-plate geometry was used for yield stress determination. The shear stress was stepwise increased from 0.1 to 1000 Pa in 81 logarithmic steps and deformation was measured. The yield stress was determined from the intersect of the tangents to the elastic and flow region in a double-logarithmic stress-strain diagram [67]. Formulations were measured three times, each. Average and standard deviation were calculated.

Electrical characterization

For determination of volume resistivity three ECA lines of 4 mm width and 0.1 mm thickness were applied by a squeegee through a stencil on a glass slide. They were cured for 2 min at 150 °C on a heat plate. Three measurements per line were taken via four-point-measurement with a 2450 SourceMeter (Keithley) at a current of 100 mA. Contact resistivity was measured similar to [42]. Ten silver fingers on a circuit board were connected with an ECA line and cured for 2 min at 150 °C. The contact resistance ρ_C was calculated from 28 measurements of joint resistance R_J, ECA bulk resistance R_B and finger resistance R_F according to Eq. 10 with contact area A. Average and standard deviation of volume and contact resistivity were calculated.

$$\rho_c = \left(R_J - R_B - R_F\right)/2 \cdot A \tag{10}$$

For volume resistivity measurements during curing the set-up from contact resistivity measurement was taken. Four neighboring silver fingers were connected with the source meter. The circuit board was placed on the heat plate and resistivity was measured over 15 min at 100, 120, 140, 150 and 200 °C, res. via 4-point-measurement.

Long-term storage tests at elevated temperature were conducted with samples containing 10 vol% silver. One regular and one CapS sample was kept for 36 days at 85 °C. Volume and contact resistivity were measured initially and after 18 and 36 days, resp. As reference two samples were stored at room temperature.

Mechanical characterization

Lap-shear strength was determined with a TA.XT plus Texture Analyser (Stable Micro Systems) according to ASTM D1002-10 [158]. Two carbon steel bands were bonded with a joint area of app. 15 mm^2. Samples were cured for 10 min at 150 °C in an oven. Tensile stress was applied to the samples at a speed of 0.2 mm/s. Long-term shear tests samples were prepared by bonding two glass slides with an ECA line of 15 mm length, 0.5 mm width and 0.09 mm thickness. Shear stress was applied up to a deformation of 0.1 mm with a speed of 0.1 mm/s based on [176] and released again. 3600 cycles were conducted. The minimum shear stress amplitude during these cycles was taken for determination of long-term reliability. Three samples per ECA were prepared and measured.

Module building and testing

For module testing, Passivated Emitter and Rear Cell (PERC) host cells in G1 format, produced through a mass production process, were utilized. The shingle cells were separated using a laser scribe and mechanical cleaving (LSMC) process. Only the outer shingles in pseudo-square (PSQ) format, with dimensions of 158.75 x 31.75 mm^2, were used. Test modules comprising six shingle cells were used for Thermal Cycling (TC) and Damp Heat (DH) tests according to IEC 61215-2. TC testing was conducted without current load. For Mechanical Load (ML) tests, full sized modules were built with ten strings of 32 shingles each. Test conditions followed IEC 61215-2: TC between −40 °C and +85 °C, DH at 85 °C/85% relative humidity, and ML with static loads of +5400 Pa and −3600 Pa.

To interconnect the cells, a commercially available capillary suspension ECA with filler content between 5 vol% and 10 vol% and a regular suspension ECA with 20 vol% filler particles and the same polymer matrix were used as a reference. The filler content of the regular suspension was adjusted to match the volume resistivity of the capillary suspension ECA, which was measured at (2.9 ± 0.3) 10^{-3} Ω cm, as confirmed by four-point measurements. To investigate the influence of perovskite-compatible low-temperature processes on long-term stability, a variation of the curing temperature was conducted. A lower temperature of 140 °C was chosen as it is compatible with perovskite materials [198]. The upper temperature of 200 °C was chosen, as it is a commonly used

temperature for interconnecting PERC and heterojunction (HJT) solar cells. This was performed on the modules for TC and DH tests. Full size modules for ML tests were cured at 140 °C.
To interconnect the cells, an prototype shingle stringer from M10 Industries was employed [194]. The ECA was applied using a jet dispensing process. The application of ECA was controlled by adjusting the preheating temperature and the pressure of the dispenser setup. An infrared lamp setup was utilized to cure the ECA. To set the process temperature, the maximum curing temperature was monitored using liquid crystal thermometers affixed to the non-IR-exposed side of the shingle cells. The lamp power was adjusted accordingly.
The modules were laminated in a glass-backsheet configuration using an industrial laminator from Bürkle, model Ypsator M-LAPV 1222-HKV. The peak temperature of the lamination process was 155 °C. The configuration for the produced full-size modules is illustrated in Figure 9. Mini modules were also produced using the same configuration; however, unlike the full-size modules, the mini modules were not framed.

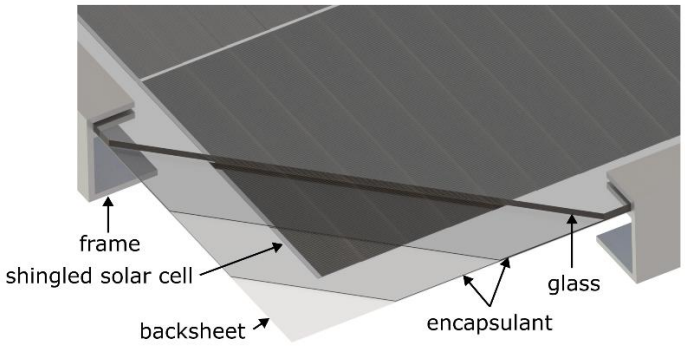


Figure 9. 3D model, illustrating the module setup of the produced full-size modules [13]

After module production, the width of the ECA in the shingle joint was measured using an 2D X-ray inspection system (Dage XD7600NT).
Ageing tests were conducted in accordance with IEC 61215-2 MQT 11 (thermal cycling) and MQT 13 (damp heat). One module with low-filled capillary suspension ECA, cured at 140 °C, was set aside as a reference and was not subjected to ageing tests. The reference module is compared to the aged modules to provide an estimation of calendric ageing and measurement uncertainty. To compare the interconnection quality and resilience against ageing, illuminated *IV* curves were recorded to determine module efficiency. Dark *IV* curves were also measured to assess the pseudo series resistance R_{s^*}, which serves as a representation of interconnection quality. This parameter is less affected by current mismatch due to e.g. inconsistent overlap or different shingle efficiencies than the fill factor *FF* [151]. The value of R_{s^*} was extracted through linear interpolation of the dark *IV* curve within the current range of $(-1.9 > I > -2.1)$ A.

4.3 Theory

4.3.1 Capillary Suspensions

Composite materials consisting of a polymer and a conductive filler follow a typical behavior. At a low filler content, the conductivity of the composite is close to that of the polymer. If a certain filler content, the so-called percolation threshold, is reached, small changes in volume fraction of the filler cause an increase in conductivity over several decades. At higher particle volume fractions, the conductivity approaches that of the filler particles [199].
ECAs are mainly formulated as a mixture of a reactive resin and conductive filler particles, but may also include organic solvents or other additives to adjust processing and application properties. Filler particles typically are coated with an appropriate compatibilizer. This promotes

deagglomeration of the particles during mixing into the matrix as well as long-term stability against recurring thermo-mechanical stresses, but counteracts the formation of conductive pathways. Therefore, state of the art ECAs typically contain 20 vol% filler or more, way beyond the percolation threshold [21,50].

In capillary suspensions [80,81] the conductive particle network is induced by adding small amounts (typically < 1 vol%) of a second liquid, not miscible with the main liquid phase. Capillary suspensions exist either in the pendular state, when the secondary liquid preferentially wets the particles or in the so-called capillary state, when the main fluid preferentially wets the particles. In the pendular state, the secondary liquid forms capillary bridges between the particles. In the capillary state, the particles cluster around secondary liquid droplets, shielding the secondary liquid from the main phase [80,81]. In both cases, sample spanning particle networks self-assemble and may reduce the percolation threshold drastically [77,78]. In ECAs capillary suspensions in the capillary state are favorable as the particles must be compatible with the main phase. A typical characteristic of a capillary suspension is the introduction or significant increase of an existing yield stress in the paste. The particle network strength depends on the interfacial tension, the three-phase contact angle and the coordination number, i.e. the number of liquid bridges. Thus, the yield stress of these systems can be controlled in a wide range by the amount and type of the secondary liquid [80,81]. Due to the, compared to other attractive forces like Van der Waals forces, high capillary forces, the particle network remains stable during drying and curing processes [77,110]. The rupture of the bridges under shear leads to a strong shear thinning behavior and due to its relatively small volume fraction, the second liquid barely affects the high shear viscosity. The high yield stress, shear thinning behavior and a fast structural recovery after cessation of flow are advantageous for the intended screen printing or dispensing application [200,201]. In addition, sedimentation and phase separation, which is a challenge in conductive ECAs due to the high density difference between matrix and filler particles, is prevented because the particles are trapped in the strong network structure, which is beneficial for extended shelf life. Beyond that, additives for particle surface treatment can be directly added to the secondary liquid. These additives are then deposited with the secondary fluid in the contact area between the particles. In ECAs, this can be utilized to remove or replace the compatibilizer at the contact points of the particles only. This results in high conductivity while maintaining the good compatibility between particles and polymer matrix.

Figure 10 shows schematically the two formulation types investigated in this study. The regular ECA consist of a polymer matrix (green) and silver flakes (gray). The flakes are coated with fatty acids (blue) as compatibilizers, which leads to homogenous distribution of the particles in the polymer matrix. By adding a secondary liquid (orange) a capillary suspension is formed. The secondary liquid is chosen to exhibit a three-phase contact angle beyond 90°, meaning the polymer preferentially wets the particles. This leads to an inhomogeneous particle distribution in form of a (three-dimensional) particle network in the capillary state. The formulation is stabilized and exhibits continuous conductive pathways at low filler content.

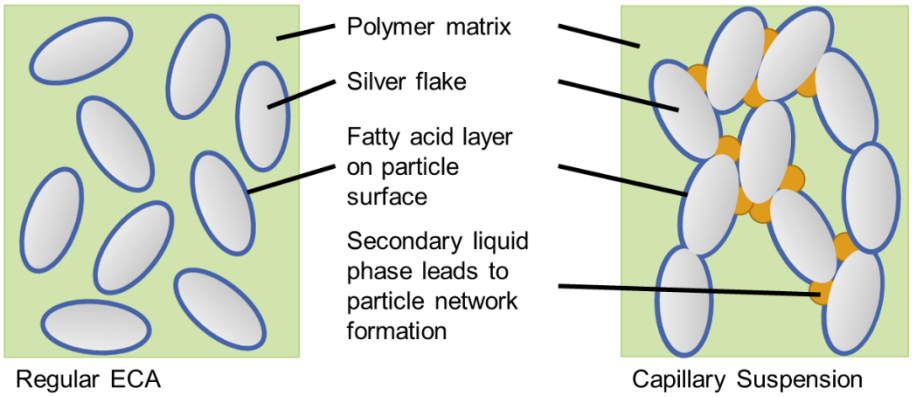


Figure 10. Schematic drawing of the regular and capillary suspension type ECA investigated in this study

4.3.2 Requirements for ECAs in shingled solar cell interconnections

ECAs were initially developed for the electronics industry where they replace the traditional solder bond [10]. Therefore, ECAs are mainly compared with solder and its properties where they often lag behind in conductivity and mechanical reliability [9]. For the application in solar cell interconnection especially in the shingling concept ECAs are valued for their elastic properties [42,135]. Requirements regarding the application process, electrical resistivity or shear strength are still under research [138,176,189]. Thus, solder is often taken as the benchmark. We herein give an overview from own experiments and literature review on requirements regarding the properties of electrically conductive adhesives for application in solar cell shingling.

High-filled ECAs exhibit a stable paste like texture. At low filler content suspensions are prone to sedimentation. For the ECA system given in this paper the introduction of a yield stress greater than 1 Pa was sufficient to prevent sedimentation. According to the well-known Stokes-equation increasing the bulk viscosity would be another means to decrease sedimentation speed, but this would simultaneously affect the application behavior. Depending on the application process, typically dispensing or screen printing [11], rheological properties must be further adjusted. Whereas dispensing requires primarily a homogeneous, air-free and stable paste, screen printing has more specific requirements regarding shear thinning behavior, thixotropy or yield stress [200]. In both cases a controlled flow must be guaranteed. In own experiments, it was found that a yield stress between 10 and 100 Pa yields good results for ECAs.

Lower processing temperatures are one of the main advantages of ECAs. Soldering is typically performed above 200 °C. ECAs can already cure below 140 °C, which is required for temperature sensitive solar cells such as perovskite and tandem cells [7,198]. But the low curing temperature comes often with long curing times. To be competitive to the through-put of soldered module production lines a curing time of maximum 30 s is recommended [147]. Therefore, snap-curing resins are of high interest for ECAs. Post-curing during lamination is also an option to reduce initial curing time [202]. ECAs would need to exhibit sufficient mechanical strength for handling and transportation after the first curing step and could be fully cured during lamination. But as electrical conductivity develops during curing [24] electrical performance tests on string level might not be possible.

The volume resistivity of eutectic solder is app. $2x10^{-5}$ Ω cm [11]. Geipel et al. [189] showed that for ribbon-based interconnections an ECA with a volume resistivity of $1x10^{-3}$ Ω cm did not change the fill factor compared to an ECA with $1x10^{-4}$ Ω cm. Figure 11 shows the absolute efficiency loss of a full-format shingled module with continuous ECA lines depending on the contact and volume resistivity calculated according to [143]. The power output of the module is 310 W. In the given range of volume resistivity of 10^{-4} to 10^{-2} Ω cm the contact resistivity dominates the efficiency loss. It was found that the influence on the efficiency was negligible when contact resistivity is below

$1x10^{-1}$ mΩ cm^2 [13]. Thus, a volume resistivity up to $1x10^{-2}$ Ω cm is sufficient with minor impact on module efficiency. An ECA with volume resistivity of $1x10^{-2}$ Ω cm and contact resistivity of $1x10^{-1}$ mΩ cm^2 accounts for an absolute efficiency loss of 0.028% in the considered module.

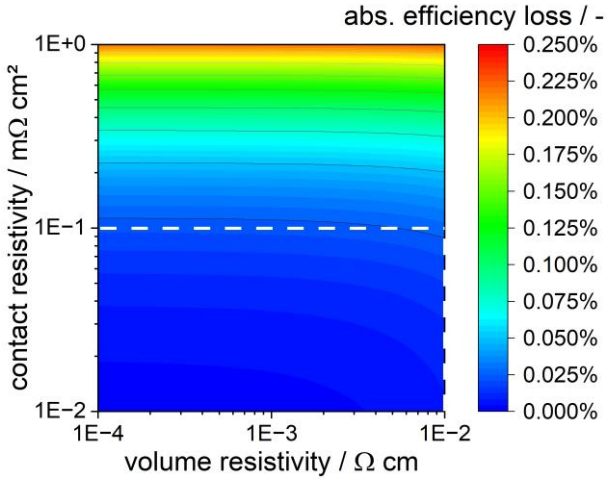


Figure 11. Efficiency loss calculated based on [143] of a full format shingled module bonded with continuous ECA lines of 50 µm thickness and 47.3 mm^2 area in dependence of volume and contact resistivity, module power is 310 W, current is 8.76 A

In shingled modules thermomechanical stress must be compensated within the bond. Beaucarne [138] calculated that the ratio between shear modulus and shear strength should be as low as possible to withstand thermally induced stresses. Therefore, a low shear modulus (< 500 MPa) and high shear strength (> 10 MPa) is recommended. Additionally, experiments have already shown that mechanical properties play a minor role in module performance as long as the bond does not fail [176,203].
In addition to thermomechanical stresses, shingle solar joints are subjected to various loads during operation, including static loads (e.g., snow, hail) and penetrating moisture. IEC 61215-2 outlines methods for assessing the long-term durability of solar modules. Thermal cycling tests (MQT 11), damp heat tests (MQT 13), and static mechanical load tests (MQT 16) are particularly relevant for shingle interconnections. A test is considered failed if the performance loss of the tested solar module is at least 5%.

4.4 Results and Discussion

Regular ECAs based on epoxy resin and silver flakes were prepared with different filler content to determine the percolation threshold for paste stability and electrical conductivity. A capillary suspension based ECAs is shown to decrease both thresholds. The influence of the particle volume fraction as well as the secondary liquid contained in the capillary suspension based ECA on the ECA's properties in the uncured and cured state as well as during curing were investigated. A highly-filled regular ECA is compared to a low-filled capillary suspension based ECA as interconnection material in solar modules.

4.4.1 Uncured ECA

The yield stress was determined as an indicator of the paste's stability against sedimentation and phase separation. Low-filled ECAs formulated as a regular suspension do not exhibit a yield stress. As shown in Figure 12, only pastes with a filler volume fraction of 15 vol% and above possess a yield stress. The sample with 15 vol% silver flakes has a yield stress of (3 ± 1) Pa. The yield stress increases exponentially with increasing filler amount to (136 ± 27) Pa at 30 vol% filler

content. In the given regular ECA, at least 15 vol% silver flakes are necessary to fulfil requirements regarding application by dispensing. To reduce silver content a stabilization mechanism is necessary. The ECA based on the capillary suspension concept possesses a yield stress even at a low filler volume fraction of 5% with (5 ± 3) Pa. This is due to strong attractive interactions induced by the secondary liquid. At higher volume fractions of 10-20%, the yield stress increases to (63 ± 3) Pa, essentially independent of filler content. For the ECA investigated here, a silver content as low as 5 vol% is sufficient to provide sedimentation stability and suitability for dispensing when the capillary suspension concept is applied. Visual inspection did not reveal indications of phase separation even after twelve days of storage at 22 and 8 °C, resp. For screen printing, a yield stress above 10 Pa is required and therefore, higher particle volume fractions are mandatory. A particle volume fraction between 5 and 10 vol% in capillary suspension based ECAs is necessary compared to standard ECAs where at least 20 vol% silver is required to guarantee screen printability.

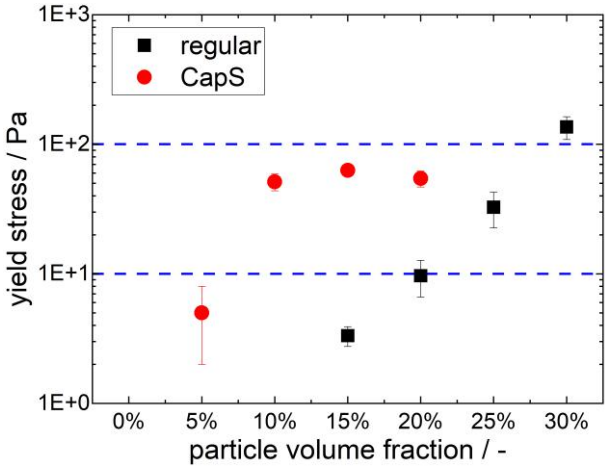


Figure 12. Yield stress of uncured ECAs with 5 to 30 vol% Ag for regular ECAs (black squares) and 5 to 20 vol% Ag for capillary suspension concept ECAs (red circles), regular ECAs with 5 and 10 vol% do not exhibit a yield stress, the dotted lines indicate limits of recommended yield stress

4.4.2 Curing

DSC measurements were carried out to determine whether the secondary liquid in the capillary suspension-based ECA affected the curing reaction. Figure 13a shows the heat flow of ECA samples with 10 vol% silver without and with secondary phase as a function of temperature. Temperature was increased by 10 K per minute. Results are shown for 50 to 205 °C. For a regular ECA, curing initiates at 84 °C and heat flow reaches a peak at 101.7 °C with 2.1 W/g, then up to 108 °C the heat flow decreases symmetrically. At higher temperatures, the decrease in heat flow is lower. Curing occurs up to 200 °C with steadily decreasing heat flow. For the ECA with the secondary liquid phase, the curing reaction starts at 97 °C which is 15 K higher than for the regular ECA. The increase of the heat flow, however, is steeper and reaches a maximum at 108.8 °C and 3.2 W/g, it then deceases symmetrically up to 118 °C where the curve falls onto the curve of the regular ECA. As expected, the total curing energy was the same for both ECAs with 273.1 and 273.7 J/g, resp. The utilized secondary liquid retards the initiation of curing but was selected not to be part of the curing reaction.

Figure 13b shows the peak curing temperature and curing energy per weight of regular ECAs in dependence of the filler volume fraction determined by DSC. The peak curing temperature increases slightly from 94 °C for the pure resin to 111 °C for an ECA filled with 30 vol% particles. This is presumably due to the higher thermal conductivity of the particles compared to the resin. The thermal energy input will preferably lead to a temperature increase of the particles and then

to curing of the resin. The peak curing temperature of ECAs containing a secondary phase is generally 7-9 K higher than the corresponding ECA without secondary phase. All tested ECAs cure at a temperature below 140 °C which is often required for low temperature applications. The curing energy per weight decreases from 535.2 J/g of the pure epoxy by 31, 49, 61, 68, 75 and 79%, resp. with increasing particle volume fraction to 110.8 J/g at 30 vol% Ag. This corresponds well with the weight fraction of particles which account for 33, 51, 62, 70, 76 and 80 wt%, resp. This indicates that the particles have only minor influence on the curing reaction. The difference might be due to the compatibilizers on the particle surface or the value for the pure epoxy was underestimated.

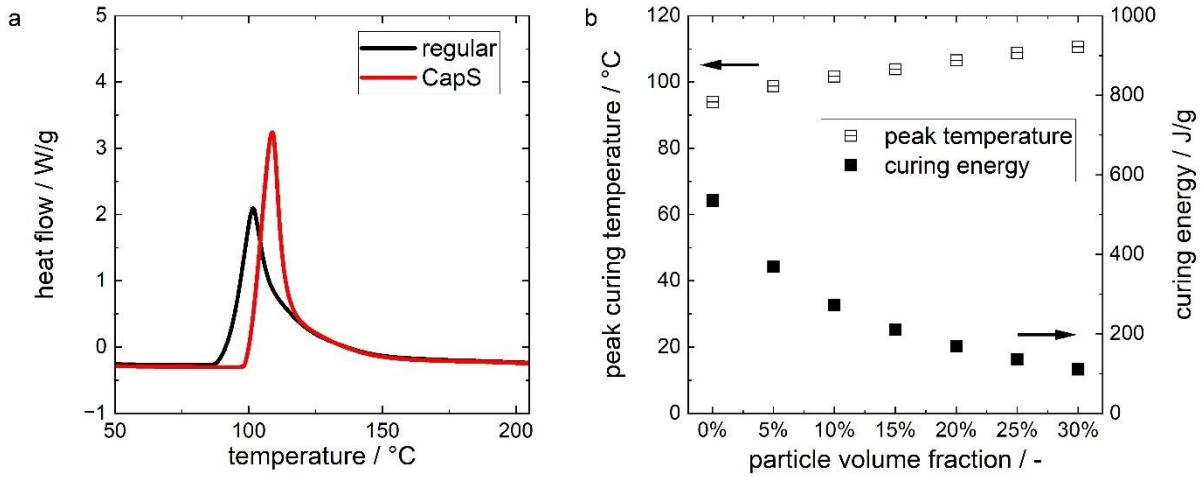


Figure 13. a) DSC curves of a regular ECA (black) and a capillary suspension based ECA (red), both samples contain 10 vol% Ag, b) Peak curing temperature (open squares) and curing energy per weight (filled squares) for regular ECAs with filler content between 0 and 30 vol%

The PV industry requires an ECA with low curing temperature and fast curing to guarantee high throughput. Low-temperature curing was confirmed by DSC. The required curing time mainly depends on the evolution of conductivity during curing. A capillary suspension concept based ECA with 10 vol% silver was cured at 100, 110, 120, 140, 150 and 200 °C, respectively. The volume resistivity was monitored over 15 minutes. Figure 14 shows the resistivity curves for this ECA over curing time. With the first touch on the heat plate, the volume resistivity decreases to $2x10^{-2}$ Ω cm regardless of the temperature. Within 50 s the volume resistivity decreases by at least one order of magnitude irrespective of the curing temperature. The sample cured at 100 °C reaches a volume resistivity of $9.3x10^{-4}$ Ω cm after 400 s which only decreases slightly to $8.9x10^{-4}$ Ω cm after 15 min curing time. A curing temperature of 110 °C leads to an approximately constant resistivity value of $7.8x10^{-4}$ Ω cm after 160 s. With both curing temperatures, 100 and 110 °C, the minimum volume resistivity of $6.4x10^{-4}$ Ω cm measured at higher curing temperatures cannot be reached within 15 minutes. This indicates an incomplete curing of the sample and is in line with DSC measurements. At curing temperatures of 120, 140, 150 and 200 °C, res. the samples exhibit the minimum value of $6.4x10^{-4}$ Ω cm after 140, 30, 26 and 16 s, respectively (Figure 14 inset). We assign the irregular trend between 5 and 10 s to the heat transfer through the circuit board. Therefore, a curing temperature of at least 140 °C is required for the investigated materials to be competitive to soldering when it comes to manufacturing speed. When curing time does not matter a curing temperature of 120 °C is sufficient for full curing. Curing speed will differ on different substrates and with different heat sources.

The results indicate as well that samples should not be kept too long at elevated temperatures above 150 °C. After app. 110 s at 150 °C and 30 s at 200 °C an "over-curing" effect occurs where the volume resistivity increases again. The effect is more pronounced at the higher curing temperature of 200 °C and leads to an increase in resistivity to 10.0×10^{-4} Ω cm after 15 min curing. As cell strings are exposed to elevated temperature during the lamination step an experiment was conducted where an ECA with 10 vol% silver and secondary phase was cured at 150 °C with different curing times. Afterwards, samples were left to cool down to room temperature and then kept on a heat plate for another 10 min at 150 °C. The results of volume resistivity measurements are shown in Table 1. As expected, the volume resistivity is lower after short curing times with approximately 7.0×10^{-4} Ω cm after 60 to 90 s of curing and increases for increasing curing times. When samples are exposed for another 10 min to 150 °C the volume resistivity only alters within the experimental uncertainty. Therefore, the over-curing effect does not occur once the samples have cooled down.

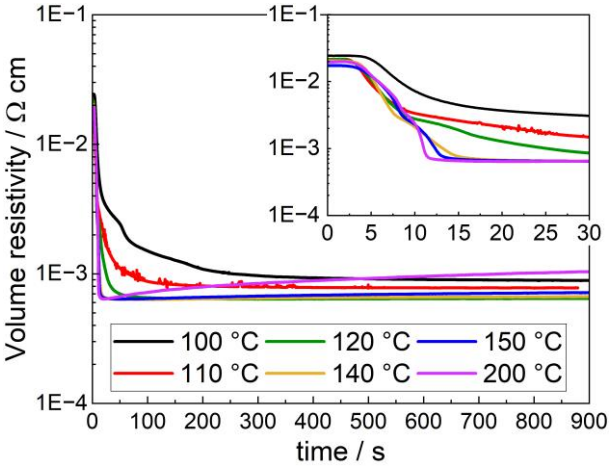


Figure 14. Development of volume resistivity over curing time of a capillary suspension based ECA with 10 vol% Ag filler at curing temperatures of 100, 110, 120, 140, 150 and 200 °C, resp. over 15 min, Inset: over the first 30 s

Table 1. Volume resistivity of a capillary suspension based ECA with 10 vol% Ag filler before and after post-curing at 150 °C for 10 min in dependence of initial curing time at 150 °C

Curing time (150 °C)	**Before post-curing 10^{-4} Ω cm**	**After post-curing (150 °C, 10 min) 10^{-4} Ω cm**
30 s	(6.3 ± 0.2)	(6.1 ± 0.3)
60 s	(7.0 ± 0.6)	(6.8 ± 0.4)
90 s	(6.9 ± 0.3)	(6.8 ± 0.3)
120 s	(7.9 ± 0.9)	(7.7 ± 1.1)
5 min	(8.2 ± 0.2)	(8.4 ± 0.3)
10 min	(9.1 ± 0.7)	(8.6 ± 0.3)

4.4.3 Cured ECA

Once cured, ECAs guarantee the electrical and mechanical interconnection in shingled solar modules. Both properties highly depend on the filler volume fraction. Whereas low resistivity is favored at higher filler content, good mechanical properties require low fill grades. We show that ECAs based on the capillary suspension concept combine low resistivity and low filler content. Furthermore, the long-term stability is investigated.

Electrical properties

For determination of the volume and contact resistivity samples were cured for 2 min at 150 °C. Figure 15a shows the results of the volume resistivity in dependence of the particle volume fraction of ECAs with and without secondary liquid phase. Regular ECAs with 5 and 10 vol%, respectively, exhibit high volume resistivities of 59 and 18 Ω cm. The standard deviation is high as the ECAs exhibit insulating and conductive areas at this low degree of filling. When the silver fraction is increased to 15 vol%, the percolation threshold for electrical conductivity is passed and the volume resistivity drops to (11.6 ± 3.1) 10^{-3} Ω cm. With further increase of particle volume fraction the volume resistivity further decreases to (1.1 ± 0.1) 10^{-3} Ω cm at 30 vol%. The capillary suspension concept reduces the percolation threshold for electrical conductivity below 5 vol%. The secondary liquid distributes between the particles and induces a network structure, wherein the particles come in contact and form conductive pathways. An ECA with secondary liquid phase exhibits a volume resistivity of (4.5 ± 0.5) 10^{-3} Ω cm at 5 vol% silver already, which is lower than that of a regular ECA with three times higher filler content. Above the percolation threshold, the capillary suspension based ECAs investigated here have a one order of magnitude lower resistivity compared to the regular ECAs. The resistivity decreases with increasing particle volume fraction to (0.14 ± 0.01) 10^{-3} Ω cm at 20 vol% silver. Solar cell interconnection by shingling requires a volume resistivity below 1x10^{-2} Ω cm (when low contact resistivity is given). Whereas in regular ECAs more than 15 vol% are necessary to fulfil this requirement, the silver amount can be significantly reduced to 5 vol% silver by addition of a secondary liquid phase.

Contact resistivity against silver was determined for the same ECAs. Results are shown in Figure 15b. When the volume resistivity is higher than 1x10^{-2} Ω cm contact resistivity cannot be calculated as the deviation in volume resistivity becomes the same order of magnitude as the contact resistivity. Therefore, only results for regular ECAs filled with 20 vol% silver and above are shown. The contact resistivity varies in a narrow range between 0.02 and 0.03 mΩ cm^2 for all formulations, regardless of the presence of a secondary liquid phase and volume fraction. This is counter intuitive as one might expect decreasing contact resistivity with increasing filler content. We believe that the silver flakes align parallel to the contact area due to the application using a squeegee. Therefore, very good contact between particles and metallization fingers is always given irrespective of filler volume fraction and contact resistivity is comparably low. The results confirm contact resistivity values below 0.1 mΩ cm^2, which is sufficient for shingling interconnection.

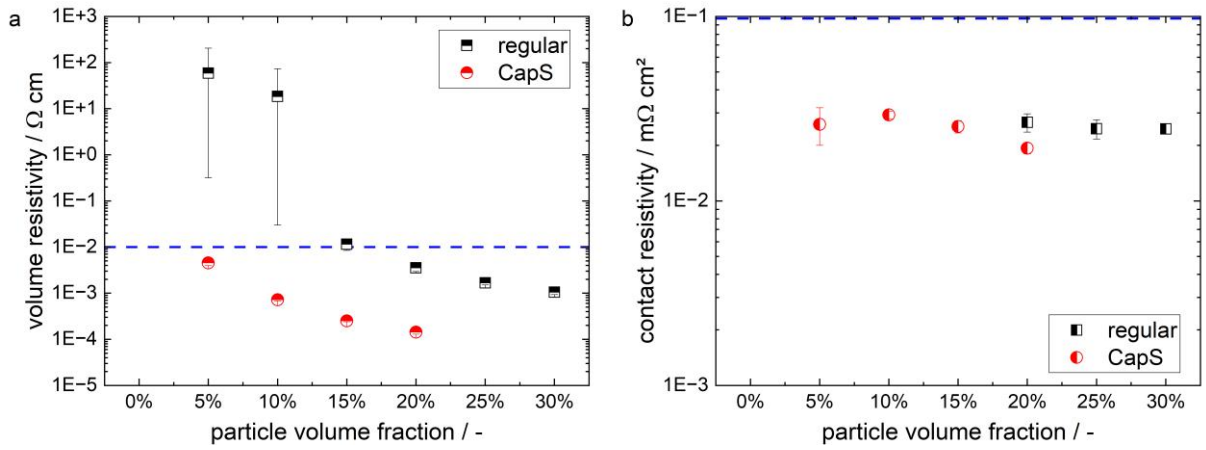


Figure 15. a) Volume resistivity and b) contact resistivity against silver of regular ECAs (black squares) with filler fractions of 5 to 30 vol% and capillary suspension concept ECAs (red circles) with 5-20 vol% silver filler, contact resistivities of regular ECAs with 5-15 vol% Ag were not measurable, dotted lines represent the upper limit of resistivity

The long-term stability of the electrical properties was monitored for 36 days to determine any effects of the uncured secondary liquid. A sample without and one with secondary liquid phase, resp. and 10 vol% silver fraction were kept at 85 °C. Reference samples were stored at room temperature. Measurements were taken on the initial day, day 18 and day 36. Figure 16a shows the volume resistivity of these samples. The initial volume resistivities were (18 ± 3) 10^{-3} Ω cm and (22 ± 2) 10^{-3} Ω cm for the samples without secondary liquid phase and (0.71 ± 0.04) 10^{-3} Ω cm and (0.63 ± 0.04) 10^{-3} Ω cm for capillary suspension based samples. In regular ECAs post-curing occurs which is more pronounced at elevated temperature. It leads to a resistivity drop to (5.5 ± 0.5) 10^{-3} Ω cm at 85 °C and (14 ± 1) 10^{-3} Ω cm at room temperature after 18 days. The volume resistivity of ECAs with secondary phase remains constant both at 85 °C and room temperature over 36 days. The same accounts for the contact resistivity (Figure 16b), which also does not change over storage time and exhibits a value of (0.034 ± 0.003) mΩ cm^2 for the capillary suspension based ECA. The secondary liquid does not deteriorate the long-term stability of the ECA. Contact resistivity for the regular ECA could only be determined for the post-cured samples at 85 °C with similar results to the Capillary Suspension based ECA. These results are promising for a module life-time of more than 30 years regarding the electrical performance.

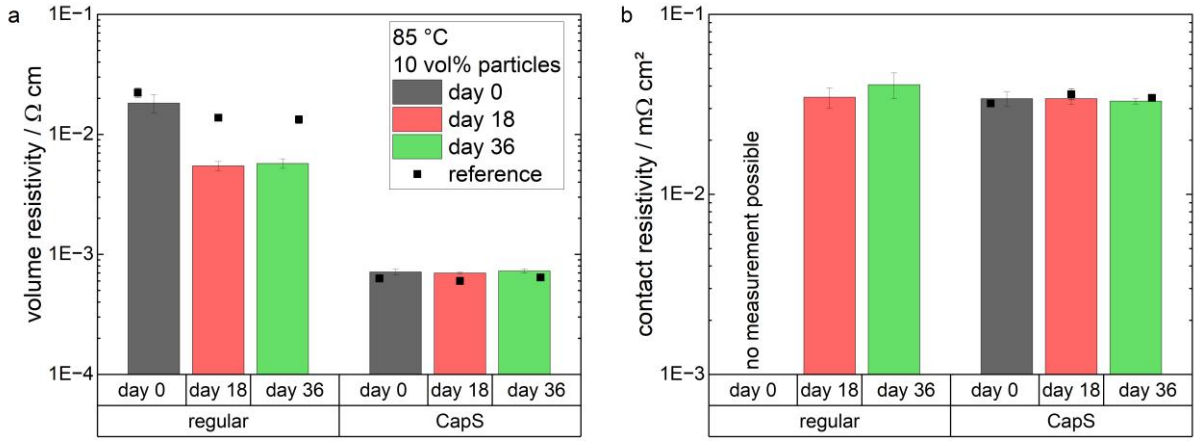


Figure 16. a) Volume resistivity and b) Contact resistivity of regular and capillary suspension based ECAs with 10 vol% particles on day 0, 18 and 36 after storage at 85 °C and room temperature as reference

Mechanical properties

Shingled modules consist of overlapping solar cells which are bonded by an ECA. Therefore, the lap-shear test was performed to characterize the adhesive or cohesive strength of the ECAs. Figure 17a shows the lap-shear strength of ECAs including between 5 and 30 vol% silver with and without secondary liquid. The lap-shear strength decreases approximately linearly with increasing filler volume fraction from (15 ± 2) MPa at 5 vol% to (5 ± 1) MPa at 30 vol%. At 5 vol% filler fraction adhesive and cohesive failure occurs, whereas at higher filler content only cohesive failure is present. As expected, every additional particle weakens the polymer matrix which is responsible for the mechanical strength. A particle network induced by capillary forces does not strengthen the ECA in the cured state. The lap-shear strength of ECAs with secondary liquid phase does not differ from the ones without. The lap-shear strength is independent of the particle distribution and the addition of small amounts of non-curing secondary liquid. For shingling a lap-shear strength of at least 10 MPa is required, and for the polymer matrix given here the filler content should not exceed 15 vol%.

To determine long-term stability under cyclic load two glass slides were bonded with ECA and exposed to 3600 cycles of periodically varying shear with a maximum amplitude of 0.1 mm. Figure 17b shows the lowest stress amplitude of the sample during 3600 cycles normalized with the

initial stress amplitude. All samples retain more than 95% of the initial strength during 3600 cycles irrespective of filler volume fraction or presence of secondary liquid phase, except for one outlier (out of three samples) at a filler content of 25 vol%. These results indicate a high probability, that modules built with the given ECA can operate 30 years or more without mechanical failure.

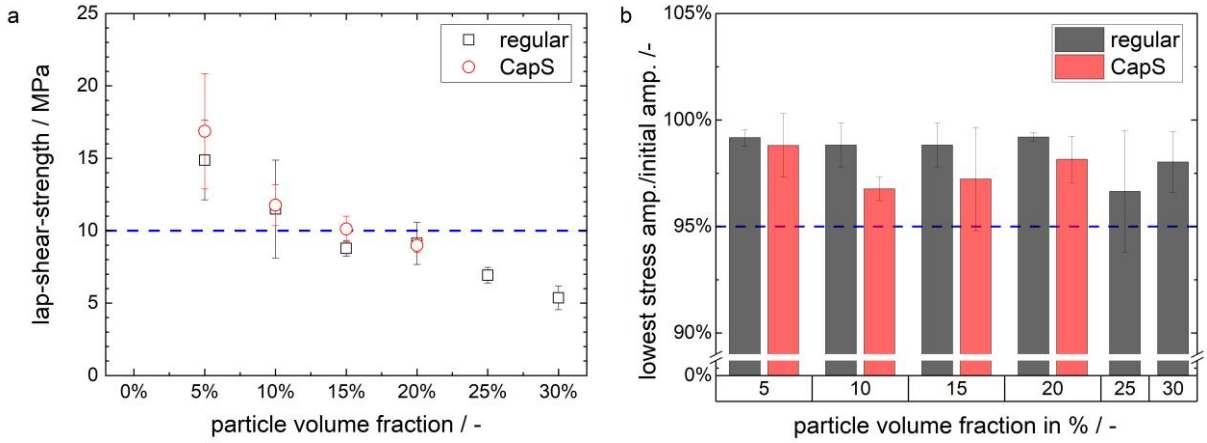


Figure 17. a) Lap-shear strength in dependence of particle volume fraction of regular (black squares) and capillary suspension based (red circles) ECAs, the dotted line indicates the lower limit of recommended lap-shear strength, b) Lowest stress amplitude during 3600 cycles of shear normalized with the initial stress amplitude of regular (black) and capillary suspension based (red) ECAs with filler content between 5 and 30 vol%, the dotted line indicates 95% of initial strength

4.4.4 Module performance

So far, we have shown that regular ECAs with 20 vol% silver exhibit rheological and electrical properties that have been found suitable for shingling applications. On the other hand, for the epoxy/silver system investigated here less than 15 vol% filler is necessary to get an ECA with acceptable bonding strength. The capillary suspension concept enabled a reduction of silver content to 5 vol%, while maintaining electrical and mechanical properties comparable to highly-filled regular suspension ECAs, though showing different rheological behavior. For the module tests, a capillary suspension based ECA with filler content between 5 and 10 vol% was selected, referred to as low-filled ECA. The filler content was chosen to match the volume resistivity of a highly-filled (20 vol%/70 wt% silver) regular ECA based on the same raw materials. Properties of the low-filled ECA are listed in Table 2.

Table 2. Rheological, electrical and mechanical properties of the low-filled ECA

Property	**Value**
Yield Stress	(26 ± 2) Pa
Volume Resistivity (150 °C)	(2.9 ± 0.3) 10^{-3} Ω cm
Contact Resistivity (150 °C)	(0.033 ± 0.003) mΩ cm^2
Lap-Shear Strength (150 °C)	(14.2 ± 1.7) MPa

To assess the impact of curing temperatures at the higher range (200 °C) and a more moderate level (140 °C), which is particularly suitable for temperature-sensitive perovskite solar cells, modules were produced under both conditions. The distinct rheological properties of the two evaluated materials affected the volume of dispensed ECA, leading to differences in the applied material quantity. The width of the ECA in the shingle joint was determined using X-ray microscopy. The width of the jet dispensed ECA lines in modules with highly-filled ECA measured (445 ± 80) µm, while the ECA width in modules with low-filled ECA measured (316 ± 74) µm.

The initial module efficiencies calculated based on aperture area are illustrated in Figure 18a (represented by fully filled boxes). On average, modules interconnected with the highly-filled ECA exhibited slightly higher efficiencies. However, the differences between the groups were within the range of the standard deviation and, therefore, not statistically significant. The groups with low-filled ECA demonstrate lower standard deviations.
The pseudo series resistances are also shown in Figure 18a (hatched boxes). Similar to the module efficiency, only minor differences are observed between the groups, indicating that the interconnection quality remains comparable for both ECAs and curing temperatures [151].
The results of the aging tests are presented in Figure 18b. Notably, the efficiency losses across all groups remain well below the critical threshold of 5% relative loss, indicating that both tests were successfully passed and suggesting good durability of the materials under the tested conditions. However, after DH testing, the group utilizing highly-filled ECA, cured at 140 °C, exhibits significantly higher efficiency losses compared to the other groups. Given the thermal conductivity of the filler particles, enabling efficient heat distribution during curing, it is unlikely that these losses stem from insufficient curing (see Chapter 4.4.2). In both TC and DH testing, modules interconnected with low-filled ECA exhibit, within the range of the standard deviation, lower efficiency losses. This effect is attributed to the lower filler fraction, which reduces the shear modulus and line width, thereby leading to a lower elastic section modulus.

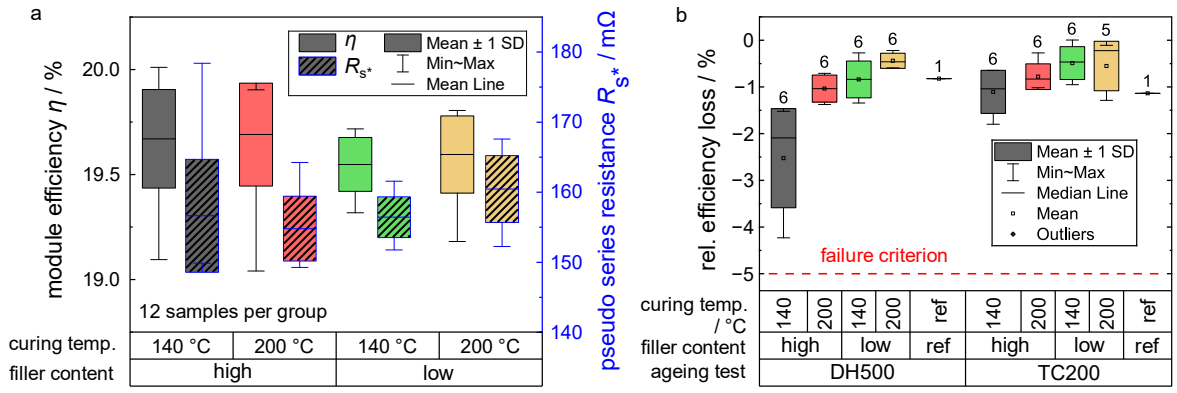


Figure 18. *IV* characteristics of six-cell mini modules. Gray and red bars refer to the regular ECA with 20 vol% silver content, green and yellow bars refer to the capillary suspension based ECA with low silver content. Fully filled boxes denote the efficiency (η), whereas hatched boxes denote the pseudo series resistance R_{s*}. Both ECAs were cured at 140 °C (grey, green) and 200 °C (red, yellow). a) Initial efficiency from illuminated *IV* curves and pseudo series resistance, derived from dark *IV* curves. b) Relative efficiency losses after ageing tests. The group size is shown above the boxes

To evaluate the mechanical load tests, *IV* characteristics were recorded, and the relative losses of short circuit current I_{sc}, open circuit voltage U_{oc}, fill factor *FF*, and efficiency η were determined. The corresponding results are presented in Figure 19.
Efficiency losses were primarily attributed to a decreased fill factor and a reduction in short-circuit current. The module manufactured using the regular suspension ECA exhibited a higher efficiency loss, mainly driven by a more pronounced decline in the fill factor. In both modules, the efficiency losses were below 1%. In a statistical investigation of ML tests with a maximum load of 5400 Pa from the years 2008 to 2019, 16.98% of all modules did not pass the test with a performance loss exceeding 5%. The average performance loss of all modules in this study was 1.76% [172]. Compared to these historical data, the shingle modules produced in this study demonstrate an above-average resilience to mechanical loads.

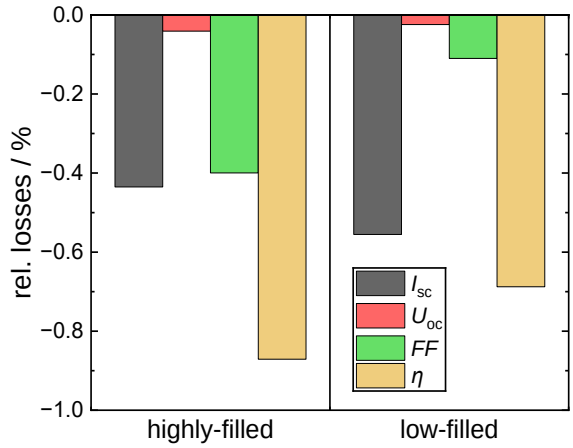


Figure 19. Results of mechanical load tests on two individual solar modules. Relative losses in short circuit current I_{SC} (grey), open circuit voltage U_{OC} (red), fill factor *FF* (green) and efficiency η (yellow) are shown

4.5 Conclusion

This work shows the silver saving potential in Electrically Conductive Adhesives and presents a formulation concept for its implementation. The chosen epoxy resin cures fast (<30 s) and at low temperature (<140 °C). The required yield stress between 10 and 100 Pa as well as a volume resistivity below 10^{-2} Ω cm and contact resistivity below 0.1 mΩ cm^2, once cured, can be achieved by adding 20 vol% of silver flake filler. For a lap-shear strength beyond 10 MPa the filler fraction must be kept below 15 vol% filler. By adding a small amount (< 1 vol%) of a secondary immiscible liquid a sample-spanning particle network can be induced even at 5 vol% silver filler. This capillary suspension type formulation is stable and exhibits sufficient volume and contact resistivity of (4.5 ± 0.5) 10^{-3} Ω cm and (0.026 ± 0.006) mΩ cm^2, resp., as well as superior mechanical strength (lap-shear strength of (17 ± 4) MPa) in the cured state. The secondary liquid does not influence the very good long-term stability of the ECA. By applying the capillary suspension concept a low-filled ECA with good electrical and mechanical properties can be formulated.
The transfer of these material science findings to module level showed promising results: The capillary suspension ECA with a silver content between 5 and 10 vol% achieved the same initial module efficiency and pseudo series resistance as conventional ECAs with 20 vol% filler. Both ECA formulations passed TC200 and DH500 testing in six-shingle mini modules, with the low-filled version cured at 200°C showing the lowest efficiency losses. In mechanical load tests, efficiency losses remained below 1%, with the capillary suspension ECA performing comparably well due to its enhanced flexibility resulting from the lower filler content.
In summary, formulating Electrically Conductive Adhesives as capillary suspensions present significant silver saving potential for the photovoltaic industry. Compared to state-of-the-art silver filled ECAs more than 50% silver can be saved without losses in electrical conductivity or module performance but with gain in mechanical strength.

Acknowledgements

The authors like to thank Vincent Charlot and Frederic Durand of PROTAVIC INTERNATIONAL Laboratory for their professional support.

Funding sources

This work was funded by the German Federal Ministry of Economics and Climate Action (BMWK) as part of the project “Mod30+” with the grant number 03EE1160.

5 Influence of polyethylene glycol on ECAs

Full title:	*Polyethylene glycol-assisted stabilization of low-silver electrically conductive adhesives for solar cell interconnection*
Authors:	*Marianne Kronsbein, Norbert Willenbacher*
Status:	*published*
Bibliographic data:	*Energy Materials;*
	DOI: https://dx.doi.org/10.20517/energymater.2026.15

Abstract

Electrically conductive adhesives (ECAs) represent a low-temperature alternative to solder in electronic and photovoltaic applications. Their electrical performance relies on a conductive filler content typically ranging from 20–30 vol% silver flakes, which ensures percolation and high conductivity but raises cost and sustainability concerns. Here, we demonstrate that an ECA comprising an epoxy resin, a non-miscible polar fluid and silver flakes used in commercial products meets the specifications for shingled solar cell interconnection in terms of volume and contact resistivity as well as mechanical strength at a silver content of only 4 vol%. Such a low-filled ECA, however, suffers from poor stability against de-mixing and its flow properties are not suitable for screen printing or dispensing. This can be remedied by adding a small amount of polyethylene glycol (PEG) 200. PEG 200 partially dissolves in the epoxy resin but also in the polar fluid, thereby reducing the three-phase contact angle of the polar fluid on the silver flake surface. This appears to enable the formation of a “capillary” state capillary suspension with 2-3 vol% added PEG, which provides a high yield stress guaranteeing high stability and good application behavior. The corresponding coarsening of the microstructure does not affect the electrical properties. The application of this concept enables the formulation of an ECA that meets industrial performance criteria even at very low particle content. The transfer to other filler systems, such as silver-coated copper or glass particles, is straightforward and offers a pathway toward robust, cost-effective, and sustainable ECAs for next-generation photovoltaic modules.

5.1 Introduction

Electrically conductive adhesives (ECAs) are composite materials consisting of a polymer matrix and a conductive filler, serving the dual function of mechanical and electrical interconnection. The mechanical properties are primarily determined by the polymer matrix, which is typically based on epoxy resins, although silicone- and acrylate-based systems are also employed [43,131]. The electrical properties, in contrast, are largely determined by the conductive filler, most commonly silver due to its high electrical conductivity and chemical stability [128,134]. Both, mechanical strength and electrical conductivity depend on the filler content. Whereas mechanical properties, such as tensile or lap-shear strength, generally decrease with increasing filler loading, electrical conductivity arises from the formation of sample-spanning conductive pathways [204].

At low filler contents, the electrical conductivity of the composite is dominated by the insulating polymer matrix, typically ranging from 10^{12} to 10^{15} Ω·cm [18]. At a certain filler content, the so-called percolation threshold, the particles form conductive pathways throughout the ECA, and the conductivity increases by several orders of magnitude. The percolation threshold depends on particle size, shape, and surface properties, which influence colloidal interactions. Flake-shaped particles are often preferred over spherical ones due to their higher surface-to-volume ratio and, therefore, lower percolation threshold [181]. Commercially available ECAs typically contain 20 to 30 vol% silver. Increasing the silver volume fraction beyond this range yields only marginal improvements in conductivity while weakening both the cohesive and adhesive strength of the composite [22]. As such, ECAs are widely used in circuit board assembly and die attachment applications, e.g. [22].

In recent years, ECAs have gained considerable attention in the photovoltaic (PV) industry as a replacement for conventional solder bonds, primarily due to their low-temperature processing capability [12,13]. The comparatively low Young's Modulus of ECAs relative to solder materials enables a novel solar module layout. In the shingled interconnection architecture, solar cells overlap like roof tiles and are directly bonded to one another [42,205]. Recent studies have identified key performance requirements for ECAs in shingled solar cell interconnections. These are a volume resistivity below 10^{-2} Ω·cm [13], a contact resistivity below 0.1 mΩ·cm^2 [206], a Young's Modulus below 1,000 MPa, and lap-shear strength exceeding 10 MPa [176]. Furthermore, application techniques such as screen printing or dispensing require a stable formulation characterized by a yield stress in the range of 10-100 Pa.

Considering the growing demand for renewable energy and the associated expansion of PV installations, material supply is becoming an increasing concern. Today, approximately 20% of the annual silver production is demanded by the PV industry [207]. Consequently, silver consumption for solar cell metallization per watt-peak is expected to decrease by 50% over the next decade [190]. Since ECAs represent an additional source of silver in solar modules, reducing the silver content in these adhesives is essential from both economic and resource availability perspectives. Therefore, concepts to lower the silver fraction in ECAs while maintaining low electrical resistivity are of considerable interest.

During the manufacturing process, silver flakes are often coated with lubricants. Chemically, these lubricants are salts formed by the reaction of fatty acids used in the milling process with silver [25]. While such lubricants enhance the dispersibility of the flakes and influence the rheological properties of the adhesive, they deteriorate electrical conductivity [29]. Extensive research has therefore focused on removing these lubricants from the silver particle surface to improve conductivity [208,45,49,209,210,51]. Various approaches have been explored, including pre-treatment with short-chain (di)carboxylic acids [208] or their direct incorporation into the ECA formulation [45], as well as the use of sulfuric acid [49], aldehydes [209], coupling agents [210]

and thermal treatment [51]. As a result, ECAs containing 67-80 wt% silver (app. 20-30 vol%) have achieved volume resistivities in the range of 5 x10^{-4} to 4 x10^{-3} Ω·cm.
By applying the capillary suspension concept to ECAs, the percolation threshold can be significantly reduced [87]. In this approach, a small fraction of secondary, non-miscible liquid phase is added to the ECA, leading to the formation of a particle network stabilized by capillary forces. Furthermore, the secondary liquid can act as a carrier for additives that remove the lubricant layer directly at the particle-particle contact points. In a previous study [206], we demonstrated that this concept enables the formation of a percolated particle network at filler contents between 5 and 10 vol% while still meeting the requirements for solar cell shingling. The high electrical conductivity achieved at such low particle loadings suggests the potential to further reduce the filler content. However, at very low particle loadings (≤5 vol%), the previously employed secondary liquid was insufficient to ensure colloidal stability in the uncured state. Such low-filled ECAs typically exhibit no or only a weak yield stress and low viscosity; thus, they are prone to sedimentation or phase separation, and their flow behavior is not suitable for dispensing or screen printing processes. Although stability and flow behavior may be adjusted by adding established rheology modifiers, this can deteriorate the electrical properties of the cured ECA.
Polyethylene glycol (PEG) with low molecular weight has been reported to enhance the electrical conductivity of ECAs [25]. Lu et al. [25] proposed that PEG facilitates the removal of the fatty acids from the particle surface. However, their study focused on highly-filled ECA with 80 wt% (30 vol%) silver. In the present study, PEG 200 is introduced into low-filled ECAs containing only 5 vol% silver or less. We demonstrate that PEG 200 induces morphological changes within the ECA, enhancing stability and printability in the uncured state, while also improving the cohesive strength of the cured composite. These effects are attributed to the formation or reinforcement of a capillary suspension network, even at low filler contents, enabled by PEG 200. As low electrical resistivity is maintained, this concept offers significant potential for reducing silver consumption in solar cell interconnection technologies.

5.2 Experimental

Materials

The ECA investigated in this study consists of an epoxy resin, a polar liquid and silver flakes ($x_{50,3}$ app. 11 µm in diameter, thickness: 100 nm), which were provided by Protavic International (France). PEG 200 (average molecular weight: 190-210 Da, glass transition temperature (10 K·min^{-1}): -89 °C, viscosity (25 °C): 0.05 Pa·s) was purchased from Sigma-Aldrich (Germany).

ECA preparation

ECAs with silver contents ranging from 1 vol% to 20 vol% were prepared. A low-filled ECA containing 5 vol% silver and modified with PEG 200 was investigated in more detail. These formulations also contain 0.5 vol% of a polar liquid. PEG 200 was added separately at concentrations varying between 0 and 10 vol%, relative to the polymer matrix. For electrical characterization, samples were cured on a hot plate at 150 °C for 2 min. Samples for mechanical testing were cured at 150 °C for 10 min in an oven (vacutherm, Heraeus, Germany). The longer curing time in the oven accounts for the slower heat transfer compared to direct hot-plate curing.

Electrical characterization

Volume resistivity was measured by 4-point-measurement with a 2450 SourceMeter (Keithley, USA). Three ECA lines of 4 mm width and 0.1 mm thickness were applied onto glass substrates using a doctor-blade through a stencil, cured, and measured three times each at a current of 100 mA. Mean values $\bar{x}$ and standard deviations σ were calculated, according to Eqs. 11 and 12, where

x refers to the value, *i* to a single measurement, and *n* to the total number of measurements using Microsoft Excel.

$$\bar{x} = \frac{\sum_i^n x_i}{n} \tag{11}$$

$$\sigma = \sqrt{\frac{\sum_i^n (x_i - \bar{x})^2}{n-1}} \tag{12}$$

Contact resistivity measurements were adapted from [42]. An ECA line was cured on a circuit board featuring ten silver fingers. Joint resistance R_J, ECA bulk resistance R_B, and finger resistance R_F were measured using a 4-point-measurement. Contact resistivity ρ_c was calculated according to Eq. 13 [42]:

$$\rho_c = \left(R_J - R_B - R_F\right)/2 \cdot A \tag{13}$$

where *A* denotes the contact area. Mean values and standard deviations were derived from 28 data points.

Rheological characterization

Yield stress was measured using a rotational rheometer (MARS, ThermoFisher, Germany) equipped with a plate-plate geometry. Shear stress was increased from 0.1 to 1000 Pa in 81 logarithmic steps. The resulting deformation was plotted against shear stress in a double-logarithmic diagram. The yield stress was determined as the intersection point of tangent fits to the regimes of elastic deformation and viscous flow [67]. Each sample was measured three times, and mean values and standard deviations were calculated.

Mechanical characterization

Lap-Shear strength was measured according to [158] using carbon-steel as the substrate. The bonding area was app. 15 mm^2. Three measurements per formulation were performed using a tensile testing machine (TA.XT plus Texture Analyser, Stable Micro Systems, UK) at a crosshead speed of 0.2 $mm \cdot s^{-1}$. For the determination of Young's Modulus, ten specimens per formulation were prepared in accordance with DIN EN ISO 20753, type A22 [160] and pulled at a crosshead speed of 0.01 $mm \cdot s^{-1}$. For both parameters, mean values and standard deviations were calculated.

Long-term stability validation

Moisture uptake

To determine moisture uptake in the uncured state, an ECA formulation without curing agent (5 vol% silver, 3 vol% PEG) was prepared and dried at 120 °C using a moisture analyzer (HX204, Mettler Toledo, Switzerland, resolution: ±0.0001 g). Samples were subsequently stored at -20 °C for one month prior to a second measurement. Each measurement was performed in triplicate. To determine moisture uptake in the cured ECA, three specimens (5 vol% silver, 3 vol% PEG) prepared for volume resistivity measurements were weighed using a precision balance (ME204T/00, Mettler Toledo, Switzerland, resolution: ±0.0001 g). Samples were stored under standard laboratory conditions for one month and re-weighed every seven days, resulting in six measurement points.

Simplified thermal cycling

Four specimens for resistivity characterization were subjected to 35 temperature cycles between 20 and 85 °C, which each cycle lasting 20 min. Electrical performance was determined before and after cycling.

Damp heat exposure

Four specimens for resistivity characterization, of which two were covered with temperature-resistant tape, were placed in an oven at 85 °C above a water bath. Electrical performance was measured before and after 96 h of exposure.

Optical microscopy of ECAs

Microstructural analysis of uncured and cured ECAs was conducted using an optical microscope (Leica DMRX, Leica, Germany) at 100× magnification. To quantify the particle area coverage and the mixing quality, microscope image sections with dimensions of 1000 × 1250 pixels were analyzed. The microscope images were converted to black and white using a threshold value of 125 (greyscale range: 0-255), where white pixels represent silver particles and black pixels correspond to the epoxy resin, polar liquid and PEG. The homogeneity of the particle/polymer mixture was determined using the mixing quality parameter according to Eq. 14 [211]. A total of 100 subsections (100 × 125 pixels) were evaluated. A mixing quality of 1 indicates perfect mixing, whereas a value of 0 corresponds to complete phase separation.

$$mixing\ quality = 1 - \sqrt{\frac{\sum_1^n (p_i - \bar{p})^2}{n-1}} \tag{14}$$

where p_i denotes the fraction of white pixels in subsection i and $\bar{p}$ the average fraction. The characteristic length of the polymer-rich regions (black areas) was determined by placing nine horizontal and nine vertical lines on each image. The number of consecutive black pixels was counted and converted into a physical length (µm) in order to quantify the degree of heterogeneity of the particle/polymer mixture. Thereby, a minimum of 10 consecutive white pixels was classified as a single particle. Smaller clusters were assigned to the polymer phase. For both mixing quality and characteristic length analyses, four images per ECA formulation were analyzed.

Polymer characterization

Differential scanning calorimetry (DSC; DSC 214 Polyma, Netzsch, Germany) was used to determine the glass transition temperature T_g of the components and ECA formulations. Samples were cooled to –130 °C and subsequently heated to –20 °C at a rate of 10 K·min^{-1} for two cycles. T_g was determined from the step-change in the heat flow during the heating cycle as the temperature corresponding to half of the enthalpy change.

Contact angle, interfacial tension, and turbidity determination

For contact angle determination, silver particles were compressed into flat discs. A droplet of secondary liquid (polar liquid and PEG) was set on the particle surface within the surrounding main liquid (polymer and PEG). A shadow image of the drop was recorded and analyzed using the Drop Shape Analyzer (DSA, Krüss, Germany) software. Drop shape analysis was performed five times per liquid combination, and mean values and standard deviations were calculated. Interfacial tension was determined using the pendant drop method. Sample turbidity was characterized by measuring the optical density at app. 600 nm using a photometer (Implen OD600, Implen, Germany). Each sample was measured three-times relative to a reference sample.

5.3 Results and Discussion

5.3.1 PEG 200 enhances the mechanical properties of ECAs

The components of a commercially available ECA, consisting of an epoxy resin, silver flakes, and a small amount of polar liquid, were employed in this study. In a previous study [206], the silver

flake volume fraction was increased from 5 to 20 vol%. Even at a low filler content of only 5 vol%, the cured ECA exhibited a volume resistivity below 10^{-2} Ω·cm (Figure 20a), which is sufficient for application in solar cell shingling. Increasing the filler content led to a further reduction in volume resistivity. At higher filler contents (10-20 vol%), the yield stress of the uncured ECA remained nearly constant at (56 ±8) Pa (Figure 20b). However, the yield stress of the low-filled ECA containing only 5 vol% silver flakes was significantly lower, at (5 ± 3) Pa. Such a low yield stress is insufficient for screen printing or dispensing processes. Moreover, suspensions containing micron-sized, high-density particles with such low yield stresses are prone to sedimentation and phase separation. Nevertheless, the electrical performance at low filler content indicates that ECAs containing 5 vol% filler or less may be accessible, provided that adequate paste stabilization is achieved.

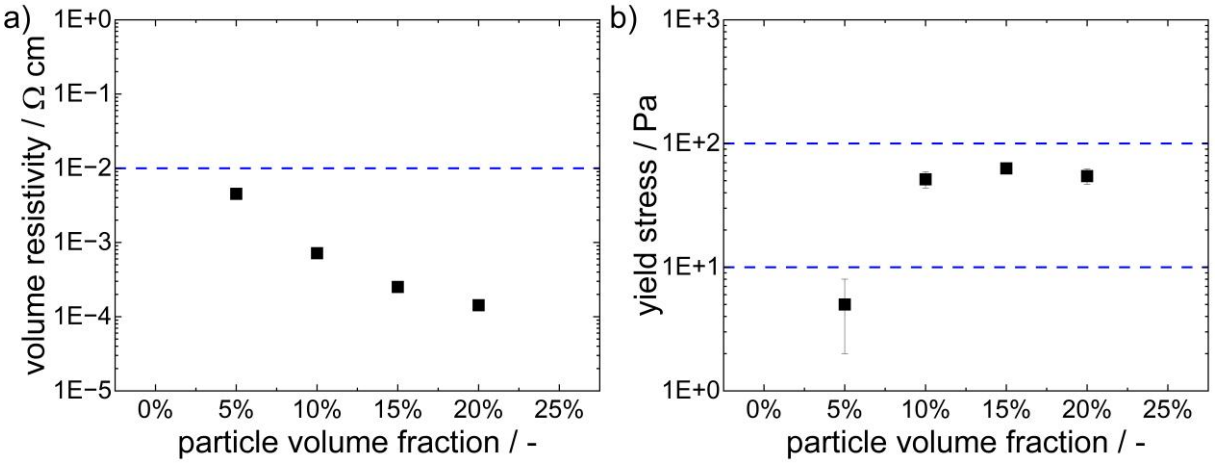


Figure 20. a) Volume resistivity and b) yield stress of ECAs where the silver volume fraction is adjusted between 5 and 20 vol%. The dashed blue lines indicate the maximum allowable volume resistivity and the minimum and maximum yield stress required for solar cell interconnection, respectively. Data was taken from [206]. The squares indicate the mean values, and the error bars denote the standard deviation obtained from 9 (volume resistivity) and 3 (yield stress) measurements, respectively. ECAs: Electrically conductive adhesives.

As shown in Figure 21, the addition of polyethylene glycol with an average molecular weight of 200 Dalton (PEG 200) enhances the yield stress of such a low-filled ECA and its lap-shear strength in the cured state. For an ECA containing 5 vol% silver flakes, the addition of 1 vol% PEG 200 (relative to the epoxy resin) increases the yield stress from (5 ± 3) Pa to (32 ± 1) Pa (Figure 21a). Upon further addition of PEG 200, the yield stress decreases again and vanishes at 10 vol% PEG 200. A similar non-monotonic trend is observed for the lap-shear strength (Figure 21b). In the absence of PEG, the ECA exhibits a lap-shear strength of (17 ± 4) MPa, which increases to a maximum of (28 ± 3) MPa at 3 vol% PEG 200. Even at a high PEG 200 content of 10 vol%, the ECA retains a comparatively high lap-shear strength of (24 ± 2) MPa. Notably, the Young's Modulus of an ECA containing 5 vol% silver is not affected by the addition of PEG and remains constant at an average value of app. 1,380 MPa (Supplementary Figure 1). Low-filled ECAs containing 1-5 vol% PEG 200 thus meet the requirements for yield stress and lap-shear strength for shingled solar cell interconnection.

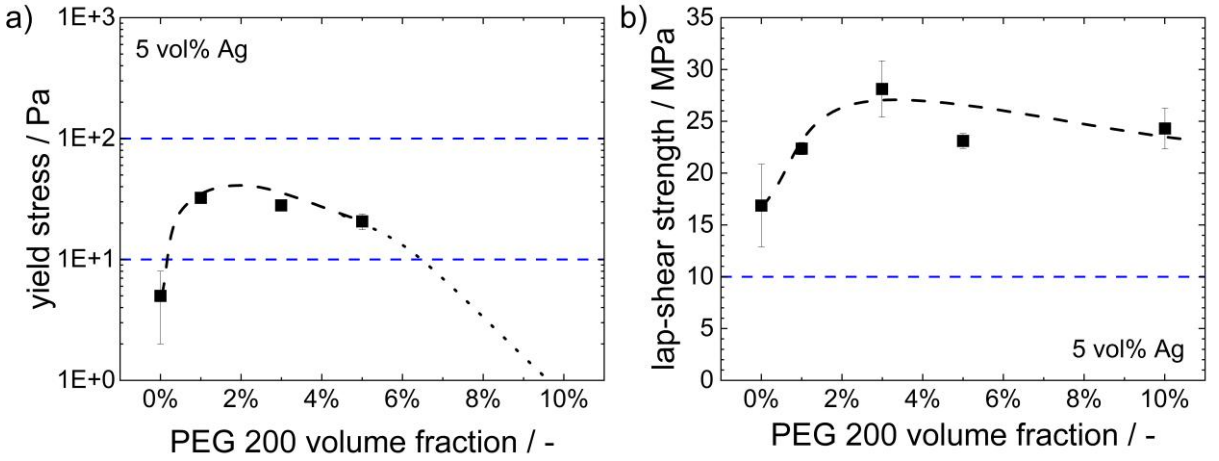


Figure 21. a) Yield stress and b) lap-shear strength of an ECA containing 5 vol% silver as a function of PEG 200 volume fraction (0-10 vol%). Dashed black lines are to guide the eye, while dashed blue lines indicate minimum and maximum yield stress and minimum lap-shear strength required for solar cell interconnection, respectively. The squares indicate the mean values, and the error bars denote the standard deviation obtained from 3 measurements. ECA: Electrically conductive adhesive; PEG: polyethylene glycol.

Remarkably, volume and contact resistivity remain unaffected by the addition of PEG. The volume resistivity remains merely unchanged at app. (0.4 ± 0.04) $x10^{-2}$ Ω·cm (Figure 22a), while the contact resistivity is (0.03 ± 0.004) mΩ·cm^2 across all formulations, independent of PEG 200 content (Figure 22b). Therefore, PEG 200 can be used to tailor yield stress and lap-shear strength without compromising the low electrical resistivity required for the intended application.

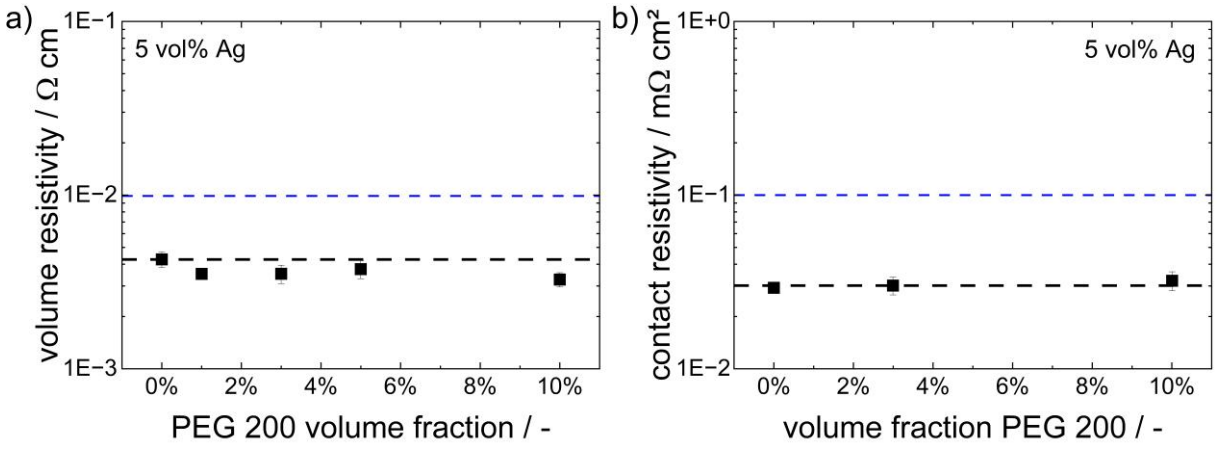


Figure 22. a) Volume resistivity and b) contact resistivity of an ECA containing 5 vol% silver as a function of PEG 200 volume fraction (0-10 vol%). Dashed black lines are to guide the eye, while dashed blue lines indicate the maximum allowable volume and contact resistivity for solar cell interconnection, respectively. The squares indicate the mean values, and the error bars denote the standard deviation obtained from 9 (volume resistivity) and 28 (contact resistivity) measurements, respectively. ECA: Electrically conductive adhesive; PEG: polyethylene glycol.

For the ECA containing 5 vol% silver flakes, the maximum yield stress is observed at 1 vol% PEG 200, whereas the maximum in lap-shear strength occurs at 3 vol% PEG 200. Therefore, a PEG 200 content corresponding to half the particle volume was selected for subsequent experiments. To determine the minimum required silver content, the silver volume fraction was further reduced in steps of 1 percentage points. Formulations containing 3 vol% silver flakes or more exhibit a yield stress. At 4 vol% particles (with 2 vol% PEG 200), the yield stress reaches (12 ± 3) Pa, thereby exceeding the lower limit required for application (Figure 23a). Figure 23b depicts the

corresponding volume resistivity. Formulations without a yield stress are electrically insulating. At 3 vol% silver, the volume resistivity decreases to (2 ± 0.4) x10^{-2} Ω·cm, while at 4 vol% silver flakes it meets the target value for solar cell shingling of 1 x10^{-2} Ω·cm.

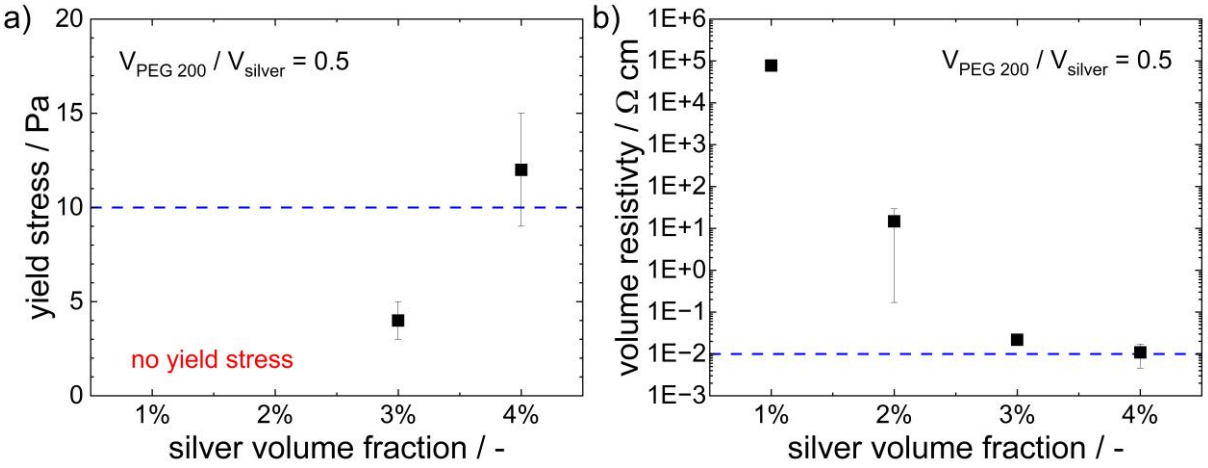


Figure 23. a) Yield stress and b) volume resistivity of ECAs with silver volume fractions between 1 and 4 vol% at a fixed PEG 200-to-silver volume ratio of 0.5. The dashed blue lines indicate the minimum yield stress required for solar cell interconnection and the maximum allowable volume resistivity, respectively. The squares indicate the mean values, and the error bars denote the standard deviation obtained from 3 (yield stress) and 9 (volume resistivity) measurements, respectively. ECAs: Electrically conductive adhesives; PEG: polyethylene glycol.

Since PEG is known to be hygroscopic and moisture plays a critical role in solar cell operation, moisture uptake was evaluated for both uncured and cured ECA samples. No measurable moisture content was detected in the uncured sample, and the mass of the cured samples remained constant over one month during storage under standard laboratory conditions. For all samples, including 3 replicates per formulation, variations were within the measurement uncertainty of the balances. These results indicate that no significant water uptake occurs in the investigated ECAs containing PEG.

Beyond initial performance, ECAs must withstand stresses encountered during work life. In shingled solar modules, these stresses primarily arise from changing environmental conditions, such as temperature fluctuations and therefore, thermomechanical stresses due to mismatched coefficients of thermal expansion of the different materials in the PV module, as well as moisture exposure. On ECA level, four specimens each were subjected to simplified thermal cycling and damp heat testing. After aging, the electrical performance of the ECA containing 4 vol% silver and 2 vol% PEG varied only within the measurement uncertainty compared to the initial values. At module level, stress testing is conducted according to IEC 61215-2. Most common are the thermal cycling test (MQT 11), in which modules are cycled between -40 °C and 80 °C, as well as the damp heat test (MQT 13), involving storage at 85 °C and 85% rel. humidity. Modules produced with ECAs containing the same components as those used in this study, but in different concentration, exhibited a competitive initial module efficiency of (19.6 ± 0.2)% and limited relative efficiency losses of (1.0 ± 1.4)% after 500 h of damp heat exposure and (2.4 ± 1.0)% after 200 accelerated thermal cycles [212]. Therefore, comparable long-term performance can be expected for the ECAs developed in this study.

In comparison with commercially available ECAs dedicated to or suitable for PV applications, the ECA containing 4 vol% silver exhibits comparable or superior electrical and mechanical performance despite its very low silver filler content. Specifically, it achieves a yield stress of (12 ± 3) Pa, a volume resistivity of (1.0 ± 0.6) x10^{-2} Ω·cm, a contact resistivity of (0.04 ± 0.02) mΩ·cm^2,

a lap-shear strength of (20 ± 3) MPa, and a Young's Modulus of (517 ± 70) MPa. Reference data presented in Figure 24 were obtained from product datasheets of commercial silver-based ECAs (e.g. Henkel (Germany), NagaseChemteX (US) and Polytec PT (Germany)) and from literature reports [36]. Recent studies focusing on alternative conductive fillers, such as copper [213–216], were not considered here, as the present work emphasizes filler reduction rather than substitution.

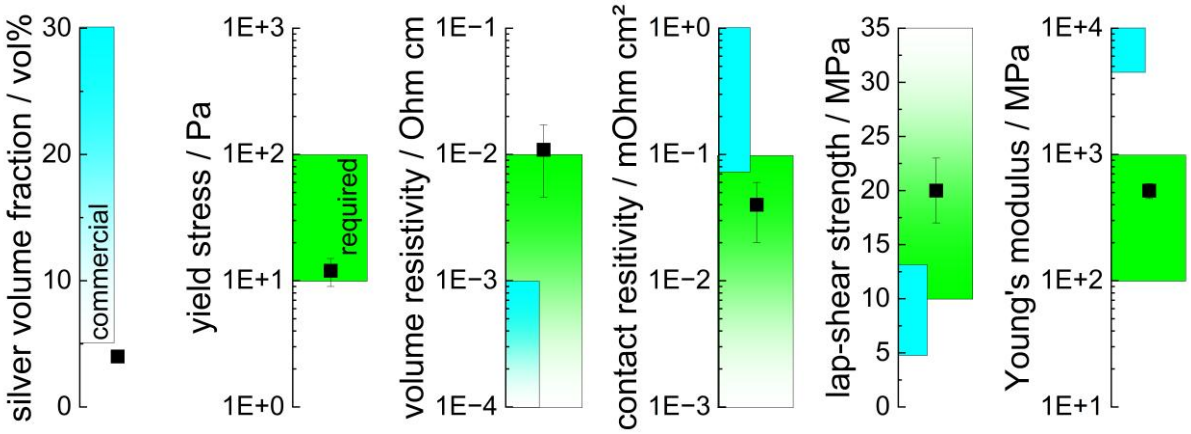


Figure 24. Properties of an ECA containing 4 vol% silver and 2 vol% PEG. Black squares indicate mean values, and error bars represent the standard deviation obtained from 3 (yield stress and lap-shear strength), 9 (volume resistivity), 28 (contact resistivity), and 10 (Young's Modulus) measurements. Results are compared with values reported for commercial products (blue boxes) and the requirements for solar cell shingling (green boxes). ECA: Electrically conductive adhesive; PEG: polyethylene glycol.

In conclusion, PEG 200 effectively stabilizes low-filled ECAs against de-mixing or sedimentation by inducing a yield stress in the range of 10-100 Pa, thereby enabling processing via screen-printing and dispensing. The corresponding cured ECAs meet all relevant electrical and mechanical requirements for solar cell shingling. Thus, PEG 200 enables a significant reduction in silver consumption for solar cell interconnection, allowing the use of ECAs containing as little as 4 vol% silver instead of conventional systems with 20-30 vol% silver.

5.3.2 PEG 200 potentially promotes the formation of a capillary suspension

PEG 200 has previously been reported to partially remove the organic fatty acid layer, which forms on the silver surface during particle processing [25], resulting in a decreased volume resistivity. However, in the present study, no such decrease in resistivity was observed. Instead, thermogravimetric analysis indicates PEG 200 absorbs onto the silver surface (see Supplementary Figure 2), partially replacing rather than removing the fatty acid layer. Notably, the molecular weight of PEG 200 is comparable to that of commonly reported fatty acids typically on the particle surface, such as stearic acid (284 g/mol) or oleic acid (282 g/mol). Consequently, while the chemical composition of the organic surface layer may change, its overall thickness is likely preserved, and a reduction in resistivity is therefore not expected.

PEG 200 primarily enhances the mechanical properties of the ECA in both the uncured and cured states. To further investigate this effect, light microscopy images of the uncured and cured samples were taken. No structural changes were observed upon curing, indicating that the particle arrangement is largely preserved during crosslinking. Representative micrographs of cured samples containing 5 vol% silver flakes and varying PEG 200 content (0-10 vol%) are shown in Figure 25. The original greyscale images were converted into binary images using a threshold value of 125 (greyscale range: 0-255). An overlay of the original and processed images is provided in the Supplementary Materials (Supplementary Figure 3). In the binary images, black pixels

represent the epoxy resin, including the polar liquid and PEG where applicable, while white pixels represent the silver particles. The average area fraction of white pixels of app. 32% exceeds the actual particle content of 5 vol%. This discrepancy can be attributed to the preferential alignment of flake-shaped particles parallel to the sample surface, and to some extent to the optical depth of field of the microscope lens. The two-dimensional images capture features within a depth of several micrometers rather than an infinitesimally thin plane, thereby giving the impression of a higher particle loading. From the images, a morphological evolution in particle distribution is evident with increasing PEG 200 content. The initially homogeneous particle distribution transitions into a progressively heterogeneous microstructure. This change is quantitatively reflected by an increase in the average characteristic length of polymer-rich regions (black areas) from (31 ± 1) µm to (59 ± 4) µm (Figure 26a), indicating a microscale phase separation induced by PEG addition. Consistently, the mixing quality parameter decreases from (67 ± 4)% to (48 ± 3)% (Figure 26b), confirming progressive structural coarsening as the PEG 200 content increases from 0 to 10 vol%.

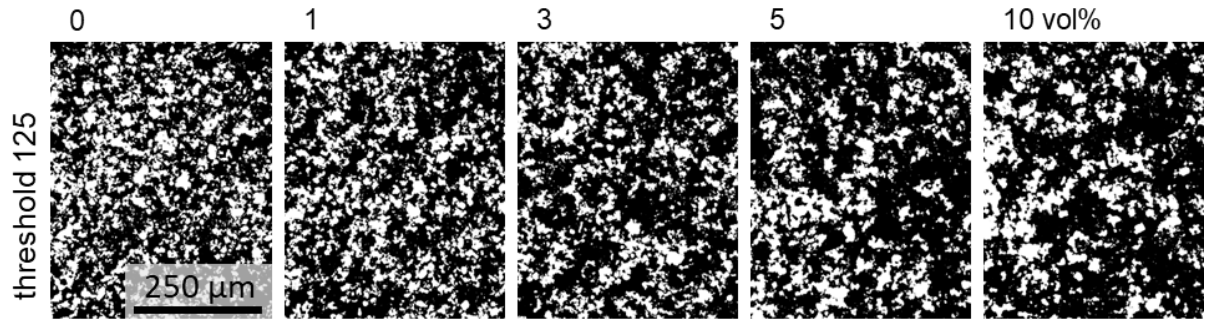


Figure 25. Microstructure of ECAs with varying PEG 200 content, illustrated by light microscopy images of the surface of cured ECA sample which contain 5 vol% silver flakes and 0-10 vol% PEG. ECAs: Electrically conductive adhesives; PEG: polyethylene glycol.

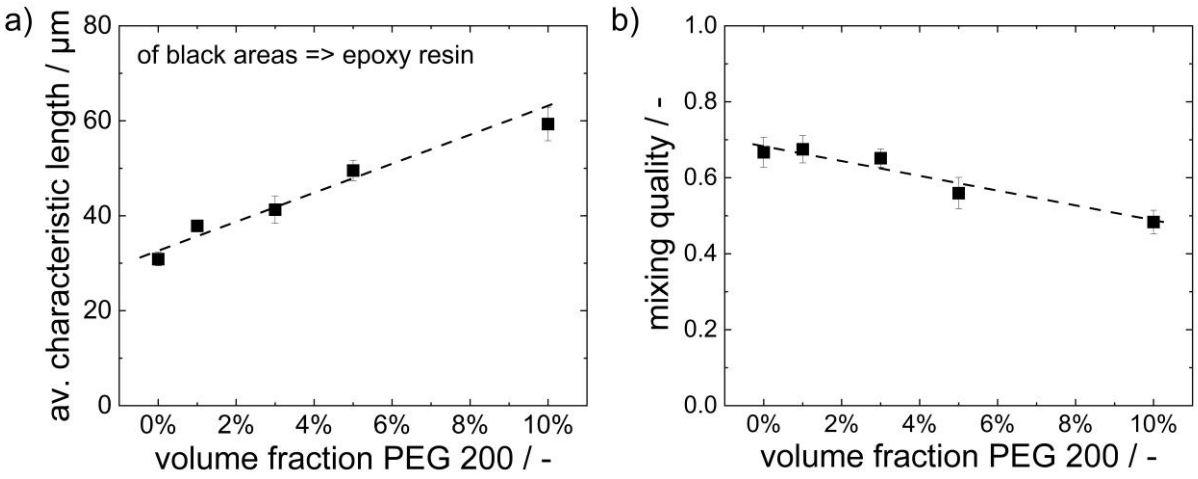


Figure 26. a) Average characteristic length of the polymer-rich regions (black areas which represent the epoxy resin) and b) mixing quality parameter (Eq. 4) as a function of PEG 200 content in ECAs containing 5 vol% silver. Dashed black lines are to guide the eye. The squares indicate the average values, and the error bars denote the standard deviation obtained from 4 images per formulation, as exemplarily shown in Figure 25. ECAs: Electrically conductive adhesives; PEG: polyethylene glycol.

While the morphological analysis reveals a monotonic coarsening of the microstructure with increasing PEG 200 content, both yield stress and lap-shear strength (Figure 21) exhibit non-monotonic behavior. Regarding the mechanical strength of solid composite materials, Gordon et

al. [217] demonstrated that the cohesion of composites strongly depends on particle distribution and orientation. The increasing microheterogeneity with increasing PEG 200 content may lead to an enhancement in lap shear strength. This effect is, however, counteracted by the increasing PEG 200 content itself, which does not participate in the curing reaction. Therefore, PEG 200 does not contribute to the cohesive strength, contrarily, it substitutes up to 10 vol% of the cured polymer matrix. Consequently, the cohesive strength decreases at high PEG contents, resulting in an optimum at 3 vol% added PEG 200.

The increase in yield stress upon addition of PEG (Figure 21a) indicates the formation or reinforcement of a strong, uniform particle network. At higher PEG contents, however, this network appears to transition into a structure of weakly bound particle agglomerates, resulting in a reduction of both strength and yield stress. Such a transition from well-distributed particles to a strongly bound, uniform particle network and subsequently to a network of weakly bound particle agglomerates is typical for capillary suspensions [92] and is consistent with the observed microstructural evolution in the investigated ECAs.

Capillary suspensions [87] are ternary solid-liquid-liquid systems in which a small amount of an immiscible secondary liquid is added to a binary suspension. The secondary liquid induces the formation of a sample-spanning, so-called percolating particle network, resulting in a strong yield stress and pronounced shear thinning behavior. When the secondary liquid preferentially wets the particles (three-phase contact angle < 90°), strong pendular bridges form between the particles and accordingly this is called the “pendular” state. The strength of a “pendular” state suspension is governed by the capillary force acting on each particle bridge, which depends on the interfacial tension between the main and secondary liquid phase and the three-phase contact angle [82]. A large fraction of preferentially wetting secondary liquid may lead to so-called spherical agglomeration, i.e. the formation of large compact agglomerates, which at high enough particle loading self-assemble into a weakly bound percolating network, hence resulting in a decrease of yield stress compared to a uniform pendular network [95]. In systems in which the bulk liquid preferentially wets the particles (three-phase contact angle between 90° and app. 145°), particles assemble around droplets of the secondary liquid, shielding it from the main liquid, forming clusters that reduce the free energy of the system. These particle clusters self-assemble into a percolating particle network, referred to as the “capillary” state, and again result in a strong yield stress and pronounced shear thinning of the suspension. The cluster configuration and hence the yield stress of the suspension primarily depend on the three-phase contact angle and the amount of secondary liquid [87].

A necessary requirement for the formation of a capillary suspension is the presence of a distinct, immiscible secondary liquid phase. However, DSC results (Supplementary Figure 4) show that PEG 200 is miscible with both the epoxy resin and the polar liquid, as evidenced by single glass transition temperatures in their respective mixtures, located between the T_g of the pure components. In contrast, epoxy resin and the polar liquid are non-miscible, as confirmed by a finite interfacial tension of (7.7 ± 0.2) $mN \cdot m^{-1}$ between the phases.

DSC results for ECAs containing 5 vol% silver flakes and varying PEG 200 contents are depicted in Figure 27a. The curves exhibit a glass transition at -56 °C, corresponding to the epoxy resin (lower diagram in Figure 27a). This T_g decreases with increasing PEG 200 content, confirming partial dissolution of PEG 200 in the resin. Additionally, a second glass transition appears for the ECAs containing PEG 200 at app. -85 °C, the glass transition temperature of PEG 200 (upper diagram in Figure 27a). The relatively small step height of this lower T_g reflects the low mass fractions of PEG (0-6.5 wt%) and polar liquid (0.4 wt%). The presence of the glass transition between -80 and -90 °C is further confirmed at higher heating rates, where the signal becomes more pronounced (Supplementary Figure 5). As the fraction of polar liquid remains constant, the

increasing intensity of the low-temperature glass transition must be attributed to PEG 200. It is therefore concluded that PEG partially contributes to the secondary liquid phase volume. Quantitative analysis suggests that app. 17% of the PEG 200 in the ECA containing a total of 5 vol% PEG contributes to the secondary liquid phase. For the ECA with 10 vol% PEG 200, this fraction increases to 26%. This corresponds to secondary liquid volume fractions of 0.8 and 2.6 vol%, resp., in addition to the 0.5 vol% polar liquid. An increase in secondary liquid volume fraction was confirmed by determination of the absorbance at 600 nm of samples containing epoxy resin, polar liquid and different volume fractions of PEG 200. The absorbance is a measure for turbidity and increases slightly with increasing PEG 200 content (Figure 27b), indicating an increase in the number and/or size of dispersed secondary liquid droplets.

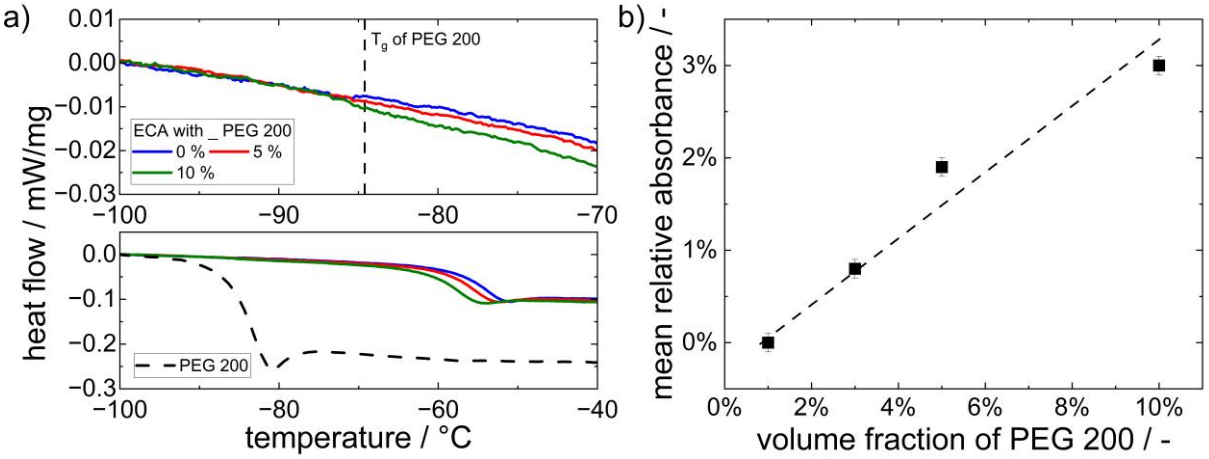


Figure 27. a) DSC analysis of ECAs containing 5 vol% silver and varying of PEG 200 content. The heat flow of pure PEG 200 is shown as reference. The lower diagram depicts the temperature range from -100 to -40 °C, while the upper diagram provides a detailed view of the temperature range between -100 and -70 °C. All measurements were performed at a heating rate of 10 K·min^{-1}. b) Mean relative absorbance of epoxy-polar liquid-PEG 200 mixtures as a function of PEG 200 content, determined at a wavelength of 600 nm using an Implen OD600. The dashed line is to guide the eye. The squares indicate the mean values, and the error bars denote the standard deviation obtained from 3 measurements. ECA: Electrically conductive adhesive; PEG: polyethylene glycol; DSC: differential scanning calorimetry.

To assess whether the formation of a capillary suspension is possible and to identify which state of capillary suspension may form in the ECA, the three-phase contact angle of a PEG/polar liquid mixture including 62 vol% PEG 200 and 38 vol% polar liquid (corresponding to the composition in the ECA with 5 vol% PEG as determined from DSC) in epoxy resin (main phase) against pressed silver flakes was determined. The resulting contact angles which represent mean contact angles expected to be present in the investigated system are shown in Figure 28a. The contact angles of 126° ± 1° and 124° ± 2°, for 0 vol% or 5 vol% PEG 200 in the epoxy resin, respectively, indicate the formation of a capillary suspension in the "capillary" state. For comparison, the three-phase contact angles of drops of pure polar liquid were determined as 145° ± 5° and 140° ± 5°, depending on the PEG 200 content in the epoxy resin. According to [87], a critical upper limit of the contact angle exists beyond which the formation of particle clusters enclosing the immiscible secondary liquid is no longer energetically favorable, i.e. a "capillary" state type capillary suspension cannot form when the contact angle exceeds this critical value depending on cluster geometry and secondary liquid droplet volume. Although the considerations in [87] refer to a system of monodisperse spherical particles, we assume that such a critical contact angle value also exists for the flake-shaped particle suspensions investigated here. The high contact angle of the pure polar liquid may prevent the formation of a capillary suspension, despite the non-miscibility of the epoxy resin and the polar liquid. The combination of polar liquid and PEG 200 therefore

appears to be necessary to obtain a strong capillary suspension in the “capillary” state. Indeed, no comparable morphological changes were observed in systems containing only increased polar liquid content or PEG 200 in the absence of the polar liquid (data not shown).
Figure 28b shows the interfacial tension between different mixtures of polar liquid and PEG 200 and epoxy resin. Obviously, the addition of PEG 200 to the secondary phase leads to a drastic drop in interfacial tension and hence should weaken a capillary suspension network [87]. While a mixture of polar liquid and PEG 200 is needed to reduce the three-phase contact angle and enable the formation of a sample spanning particle network controlled by capillary forces which is characterized by a strong yield stress, the capillary force decreases with decreasing interfacial tension, i.e. increasing PEG 200 fraction in the polar liquid/PEG mixture and accordingly the yield stress decreases (Figure 21a). Finally, the PEG/polar liquid mixture including 84 vol% PEG 200, as calculated for the ECA containing 5 vol% silver and 10 vol% PEG 200, does not form stable droplets in the epoxy resin (with or without PEG 200), as evidenced by pendant drop experiments. The liquid pulls threads and the phase surface is crumply (Supplementary Figure 6), i.e. there is no finite interfacial tension anymore. This explains the disappearance of a yield stress in the ECA containing 10 vol% PEG 200 (Figure 21a).

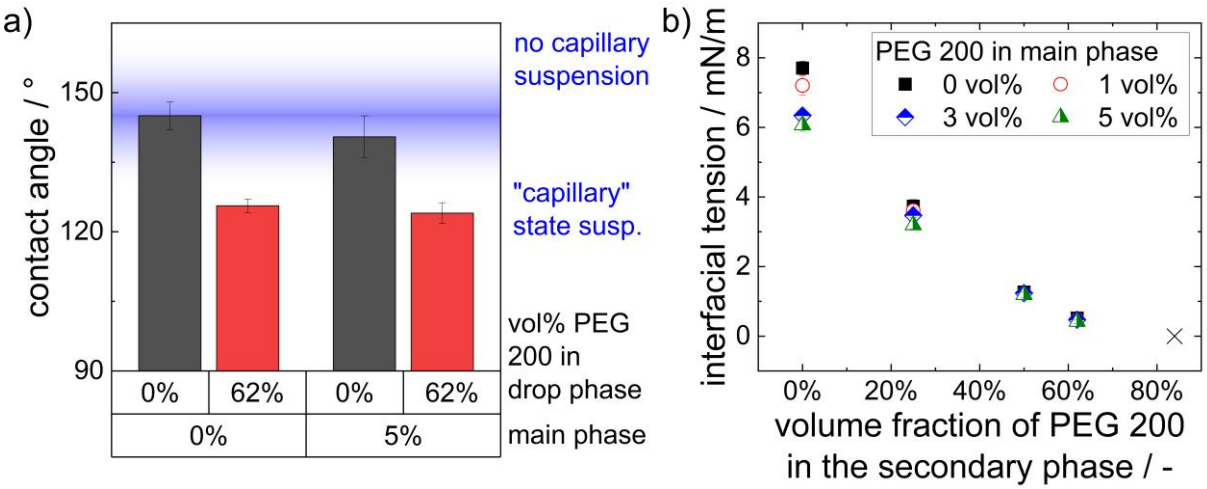


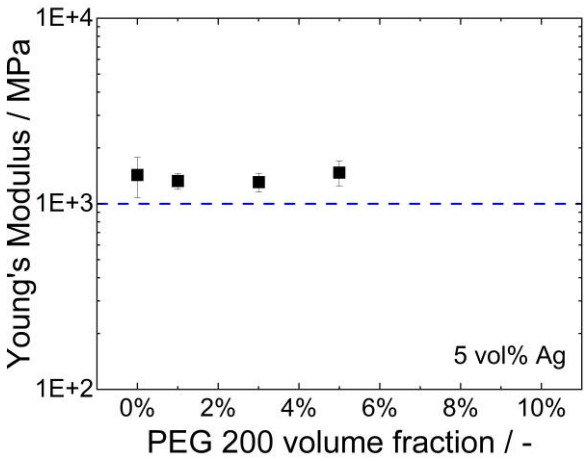
Figure 28. a) Three-phase contact angle of polar liquid and a PEG/polar liquid mixture including a fraction of 62% PEG 200 on silver flakes when covered by epoxy resin or epoxy resin with 5 vol% PEG 200, the blue shaded area indicates the estimated contact angle range above which no more capillary suspension is formed [87]; b) interfacial tension between the epoxy resin with varying PEG 200 content between 0 and 5 vol% (main phase) vs. mixtures of polar liquid and PEG 200 (secondary phase), at 84 vol% PEG 200 in the PEG/polar liquid mixture no finite interfacial tension can be measured. The bar height/symbols indicate the average value and the error bars the standard deviation obtained from 5 (contact angle) and 10 (interfacial tension) measurements, respectively. PEG: Polyethylene glycol.

5.4 Conclusion and Outlook

Electrically conductive adhesives have become highly attractive for applications in the photovoltaic industry. However, their typically high silver content of 20-30 vol% poses both supply and economical challenges. A previous study demonstrated that the application of the capillary suspension concept enables a reduction of the silver content to below 10 vol%. Nevertheless, the selected secondary liquid did not sufficiently stabilize the ECA against sedimentation at filler contents below 5 vol%, although the electrical performance remained promising.
The present study demonstrates that the addition of a small amount of PEG 200 enhances both the yield stress and lap-shear strength of ECAs containing as little as 5 vol% silver, while maintaining low volume and contact resistivity. PEG 200 partially dissolves in both the epoxy resin and the polar liquid acting as a secondary liquid phase. This decreases the three-phase contact

angle of the secondary phase against the used silver flakes and thus appears to enable the formation of a strong capillary suspension in the capillary state, even at low filler contents. As a result, the particle distribution transitions from a homogeneous dispersion to a percolating particle network, thereby preventing particle sedimentation. At the same time, the addition of PEG 200 decreases the interfacial tension between the two liquid phases, which possibly weakens the capillary suspension with increasing PEG 200 volume fraction, as reflected by the observed decrease in yield stress. An optimal PEG-to-particle volume ratio of app. 0.5 was identified.
To fully exploit the requirements for solar cell shingling, the silver volume fraction was further reduced to 4 vol%. The resulting ECA exhibits a yield stress of (12 ± 3) Pa, a volume resistivity of (1.0 ± 0.6) x10^{-2} Ω·cm, a contact resistivity of (0.04 ± 0.02) mΩ·cm^2, a lap-shear strength of (20 ± 3) MPa, and a Young's Modulus of (517 ± 70) MPa. These properties are comparable to, or even surpass, those of commercially available silver-based ECAs suitable for PV applications, despite the substantially reduced silver content. The use of PEG in ECAs based on alternative conductive filler, such as silver-coated glass or copper particles, represents a straightforward strategy to further decrease silver consumption. Overall, this approach offers significant potential to enable more cost-efficient and sustainable solar cell interconnection.

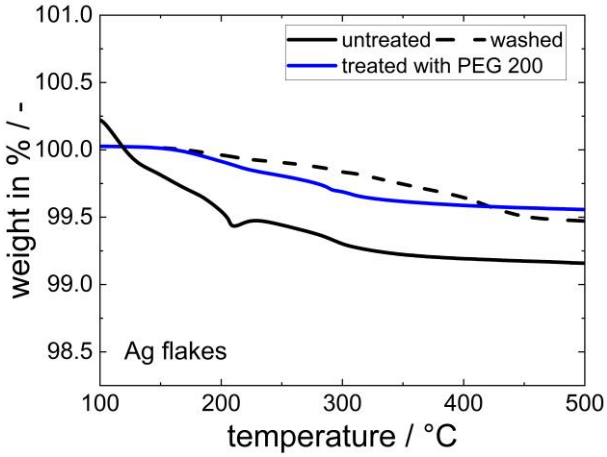
5.5 Supplementary Materials



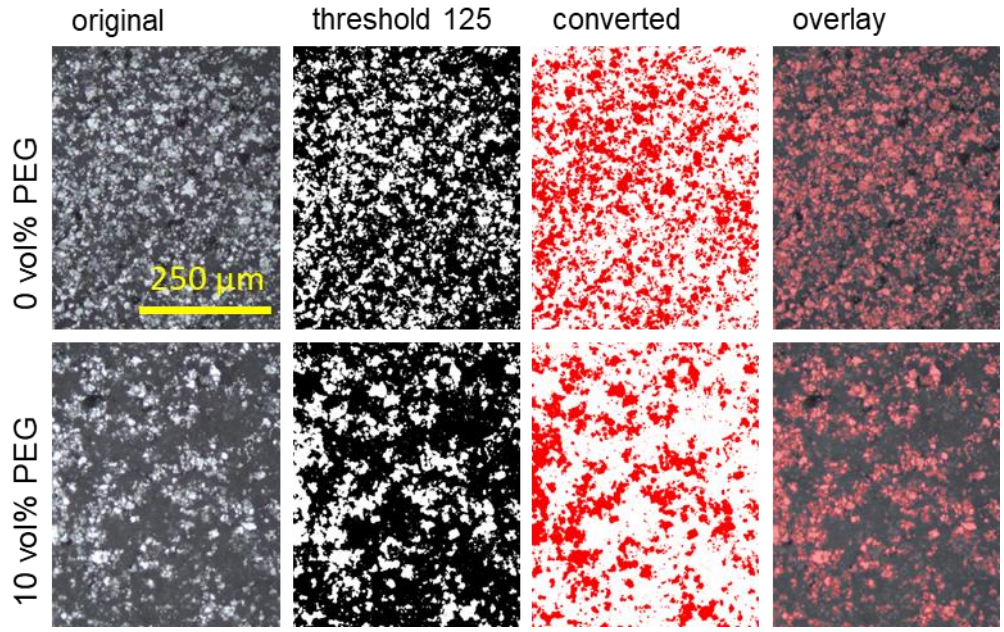
Supplementary Figure 1. Young's Modulus of ECAs containing 5 vol% silver as a function of PEG 200 volume fraction. The modulus is independent of PEG 200 content and slightly exceeds the maximum value required for solar cell interconnection (indicated by the dotted blue line). The squares indicate the mean value, and the error bars denote the standard deviation obtained from 10 replicate test samples.

Characterization of organic compounds on the particle surface

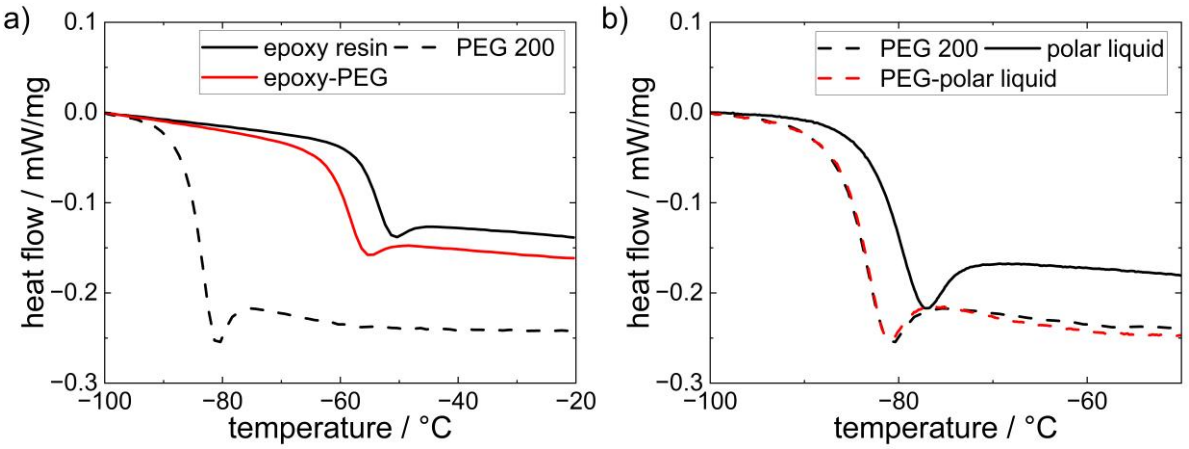
Thermogravimetric analysis (TGA) was conducted using a TGA 5500 (TA Instruments, Germany) under an air atmosphere. The temperature was increased to 600 °C at a heating rate of 10 K·min^{-1}, and the corresponding mass loss was recorded. Silver flakes were analyzed as received. For the preparation of pre-treated particles, 10 g of silver flakes were dispersed in an ethanol-water mixture (50vol%:1vol%). Then, 0.1 g of PEG 200 was added, and the suspension was stirred for 15 h. Afterwards, the particles were rinsed with the ethanol-water mixture and subjected to five centrifugation cycles. The particles were then dried under vacuum and kept overnight at 89.9 °C. One reference sample without PEG was prepared following the same procedure, denoted as "washed".



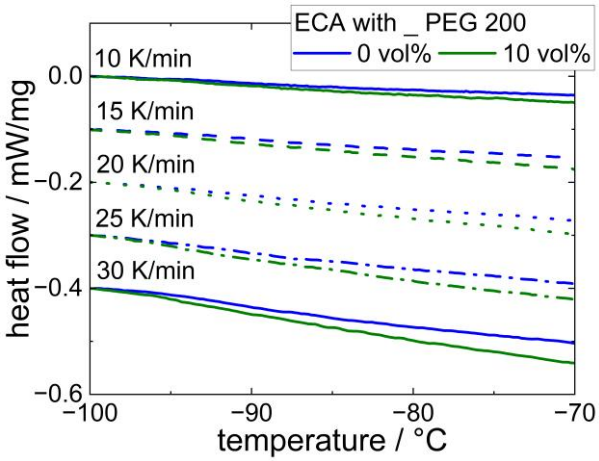
Supplementary Figure 2. TGA of silver flakes: black: as received (untreated), dotted black: washed with ethanol, blue: pre-treated with PEG 200. The mass loss is the highest for untreated particles (1.06%). Washing with ethanol removes app. half of the organic fatty acid layer on the particles surface reducing mass loss to 0.55%. TGA results for PEG-treated particles indicate partial replacement of the original fatty acids by PEG 200, as the primary mass loss occurs around 285 °C, corresponding to the boiling point of PEG 200. Total mass loss is comparable to the mass loss of the washed particles.



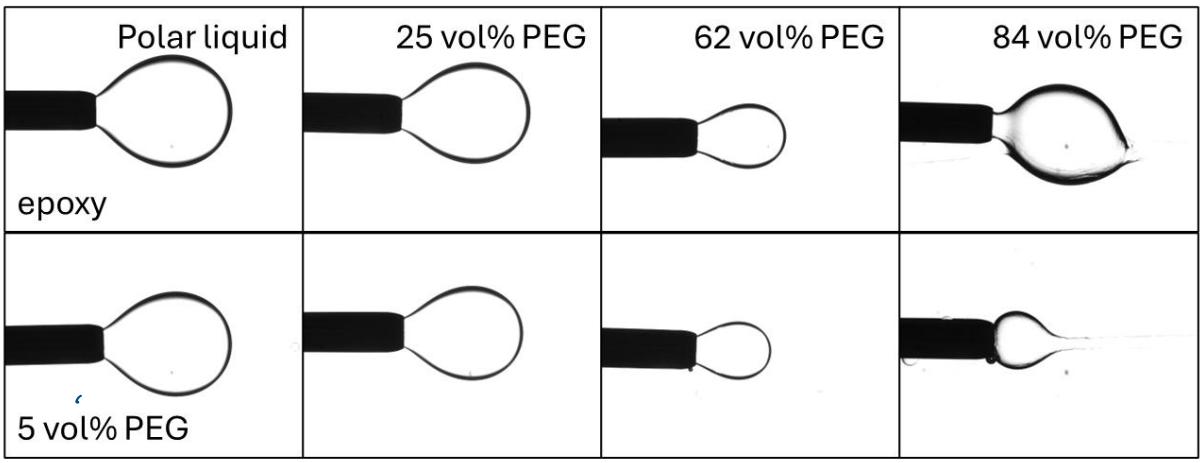
Supplementary Figure 3. Image processing procedure for microstructural analysis. Original light microscopy images of the ECAs were converted to binary (black-and-white) images using a threshold value of 125 (greyscale range: 0-255). The binary images were subsequently converted to white-and-red representations and overlayed onto the original image to verify the suitability of the threshold value: Red areas accurately cover the light grey to white areas of the original images, which correspond to the silver particles.



Supplementary Figure 4. DSC analysis of the individual components included in the ECAs and their mixtures. Heat flow as a function of temperature (heating rate of 10 K·min^{-1}) for a) the epoxy resin, PEG 200, as well as their mixture containing 10 vol% of PEG 200, and b) PEG 200, the polar liquid, and their mixture containing 5 vol% polar liquid.



Supplementary Figure 5. DSC analysis of ECAs containing 5 vol% silver particles and 10 vol% PEG 200. The shoulder associated with the secondary glass transition (compared to the ECA without PEG 200) becomes more pronounced as the heating rate is increased from 10 to 30 K·min^{-1}.



Supplementary Figure 6. Shadow images of droplets containing polar liquid and different volume fractions of PEG 200, enclosed by epoxy resin containing either 0 vol% PEG 200 (upper row) or 5 vol% PEG 200 (lower row), used for interfacial tension determination. At 84 vol% PEG 200 in the secondary liquid, the droplet pulls threads, gradually dissolving into the epoxy resin, exhibiting no finite interfacial tension.

Acknowledgements

The authors would like to thank Vincent Charlot, Frederic Durand and Simon Malandain of PROTAVIC INTERNATIONAL for their professional support and material supply, Klara Urbschat (Institute for Chemical Technology and Polymer Chemistry, KIT) for conducting the TGA measurements and Iliya Stoev (Institute for Biological and Chemical Systems, KIT) for performing the optical density measurements.

Financial support and sponsorship

This work was funded by the German Federal Ministry of Economic Affairs and Energy (BMWE) as part of the project “Mod30+” with grant number 03EE1160.

6 ECAs with silver-coated glass and copper particles

Full title:	*Low-filled electrically conductive adhesives based on silver-coated glass and copper particles*
Authors:	*Marianne Kronsbein, Leonhard Böck, Torsten Rößler, Norbert Willenbacher*
Status:	*published*
Bibliographic data:	*Solar Energy Materials and Cells;*
	DOI: https://doi.org/10.1016/j.solmat.2026.114228

Abstract

Replacing silver in solar module production is the hot topic in metallization and interconnection development. Whereas in metallization mainly silver-coated copper is utilized, the lower electrical requirements for cell interconnection, open up the opportunity to utilize particles with non-conductive cores as well. This study focuses on the development and characterization of an electrically conductive adhesive (ECA) for the shingled cell interconnection based on silver-coated glass and silver-coated copper particles, respectively. The formulated low-filled ECAs were stabilized against sedimentation using a halogen-based additive.

The silver-coated glass particles show good compatibility with the utilized epoxy resin. Employing a mixture of silver-coated glass particles and silver flakes the silver content in the ECA can be reduced to 25 wt% and the mechanical properties can be adjusted by the fraction of glass particles used. In shingled modules such an ECA shows the same stable performance as the reference based on pure silver particles.

An ECA with only 7 wt% silver was formulated using silver-coated copper particles meeting all requirements for solar cell shingling. Shingled modules build from such an ECA show promising initial efficiency. Damp heat 500 was passed comparable to the silver reference, indicating oxidation stability. However, degradation during accelerated thermal cycling 200 is believed to originate from remaining issues with curing.

This study shows, that by carefully adjusting polymer, particles and additives the silver consumption in ECAs can be significantly reduced without any losses in interconnection performance.

6.1 Introduction

The International Technology Roadmap for Photovoltaic (ITRPV) identifies silver as the “most process-critical and most expensive non-silicon material” [4] at cell level. In 2024, the photovoltaic (PV) industry accounted for approximately 19% of global silver demand. Although the average silver consumption per cell is declining—helping to offset rising PV deployment—ongoing large-scale investments in PV infrastructure, primarily driven by climate targets, may continue to place significant strain on the silver supply chain [207]. Consequently, further reductions in silver consumption, particularly in cell metallization pastes, are essential.

Electrically conductive adhesives (ECAs) have emerged as promising alternatives to solder in cell interconnection technologies. These adhesives are thermosetting polymer-based composites filled with conductive particles and are increasingly employed to attach ribbons to busbars on solar cells [187], for contacting back-contact solar cells to conductive backsheets [218], or to directly interconnect the cells in shingled module architectures [135]. Conventional ECAs typically contain silver particles at concentrations above the percolation threshold for electrical conductivity, which depends on filler morphology and generally falls between 15–30 vol% (equivalent to 60–80 wt%) [21]. Therefore, ECAs present an additional source of silver in PV.

To address the high cost and limited availability of silver, research and commercial efforts have explored replacing silver with alternative conductive fillers. Table 3 and Table 4 summarize commercially available and literature-reported ECAs with volume resistivity below 10^{-2} Ω cm. Among the explored alternatives, copper — most commonly used as silver-coated copper particles — has emerged as the predominant substitute due to its favorable electrical properties and significantly lower cost. The ITRPV also anticipates a growing role for copper in future metallization pastes. At present, copper remains an abundant and economically viable alternative to silver [219]. However, long-term availability may become a concern: Nobel laureate and former U.S. Secretary of Energy Steven Chu has projected potential copper shortages by the end of the century, driven by increasing global demand for electrification [220]. Other materials, including nickel, aluminum, and carbon have also been investigated as conductive core particles for use in ECAs.

Some approaches further minimize the use of conductive metals by utilizing non-conductive core particles, such as glass spheres, coated with a thin silver layer. For instance, an ECA based on silver-coated glass microspheres with a volume resistivity of 1.5 x10^{-3} Ω cm has been developed [11]. Nevertheless, nearly all ECAs rely on high filler loadings to achieve sufficient conductivity. While increased filler content enhances electrical pathways, it often compromises the adhesive’s mechanical properties. Moreover, the sustainable approach is to utilize as little valuable materials, both silver and copper, as possible.

This study aims to develop low-filled ECAs with significantly reduced silver and total filler content, while still meeting the stringent electrical and mechanical requirements for shingled solar cell interconnection. These include a yield stress between 10 and 100 Pa in the uncured state, rapid curing within seconds at low temperatures, volume resistivity below 10^{-2} Ω cm, and lap-shear strength exceeding 10 MPa [221]. This study is based on a well characterized low-filled silver-epoxy system [221]. Here, we outline how substantial further silver reduction is achieved by utilizing silver-coated glass and silver-coated copper particles instead of pure silver particles. Halogen-additives stabilize the formulations preventing sedimentation in low-filled, uncured state ECAs and provide low resistivity and high mechanical strength in the cured state. Furthermore, we demonstrate the general suitability of such ECAs for shingled solar cell interconnection.

Table 3. Commercially available ECAs with conductive particles that are not made of pure silver; note: X@Y refers to X coated on Y, for X-Y type fillers structure is not specified by the manufacturer

Manu-facturer	Product	Polymer	Fill grade	Filler	Cure schedule	ρ_v / mΩ cm	Ref
Nagase	CA-260	Epoxy	45-70 wt% Ag	Ag@X (non Cu)	30 s @ 150 °C/ 5 min @ 120 °C	0.15	[222]
Nagase	CA-183	Epoxy	10-30 wt% Ag, 45-70 wt% Cu	Ag@Cu	20 min @ 100 °C/ 1 min @ 150 °C	0.9	[222]
atom adhesives	AA-DUCT GS1	Epoxy	50-70% Ag coated ceramic	Ag@glass spheres	15 min @ 100 °C	1.5	[223]
United Adhesives	Eposolder 6761	Epoxy		Ag-Cu	60 min @ 125 °C	1	[224]
United Adhesives	Eposolder 6763	Epoxy		Ag-Cu	60 min @ 125 °C/ 30 min @ 150 °C	5	[224]
Parker	CHO-BOND 360-20	Epoxy	3-7 wt% Ag, 80-90 wt% Cu	Ag@Cu	25 min @ 115 °C	5	[225]
Master-bond	EP79FL	Epoxy		Ag@Ni	overnight @ RT + 2-3 h @ 110 °C	5	[226]
Holland Shielding	3991 Shieldo-seal	Silicone	50-70 wt% Ni	Ni@ graphite	96-144 h @ RT	7.0	[227]
Soliani	CSA.SPC	Silicone		Ag-Cu	72 h @ RT	8	[228]
Soliani	CSA.SNK	Silicone		Ag-Ni	72 h @ RT	8	[228]
Soliani	CSA.SPA	Silicone		Ag-Al	72 h @ RT	10	[228]

Table 4. ECAs reported in literature with conductive particles that are not made of pure silver

Polymer	Fill grade	Filler	Additive	Cure schedule	ρ_v / mΩ cm	Ref
Epoxy	67 wt%	Cu particles	lactic acid	1 h @ 200 °C under nitrogen	0.12	[229]
Epoxy	70 wt%	Ag@Cu flakes (17.3 wt% Ag)	diisobutyl phthalate, 20 wt%	2 h @ 180 °C	0.127	[230]
Epoxy	75 wt%	Ag@Cu flakes (25 wt% Ag, 74.5 wt% Cu)	terephthalaldehyde and iodine (ratio TPTA/I_2 = 30/1)	1 h @ 150 °C	0.128	[73]
Epoxy	60 wt%	Ag@Cu powder	none	30 min @ 150 °C in vacuum	0.2	[231]
Epoxy	40 wt%	Submicron Ag@Cu particles (15 wt% Ag) and commercial micron Ag@Cu	palmitic acid	2 h @ 160 °C	0.468	[47]
Epoxy	70 wt%	Ag@Cu powder: flake-shaped particles, spherical shaped-particles	none	2 h @ 175 °C	 1.58 3.98	[232]
Epoxy	60 wt%	flaky and spherical Ag@Cu	none	1 h @ 150 °C in vacuum oven	1.95	[213]
Epoxy	70 - 85 wt%	Ag-Cu particles: 20 wt% Ag 50 wt% Ag 30 wt% Ag	 none none graphite	30 min @ 80 °C	 2 1 4	[214]
Epoxy	70 - 85 wt%	flake-shaped, flake- and spherical-shaped: 60:40 Ag@Cu powder (10 - 15 wt% Ag)	none none graphite (8 wt%)	30 min @ 80 °C	3 4.5 8	[215]
Epoxy	55 wt%	Ag@Cu flakes	none	1 h @ 200 °C	6	[216]

6.2 Material and Methods

Material

A two-component thermosetting epoxy resin and silver flakes (Ag flakes) were supplied by PROTAVIC INTERNATIONAL (France). Silver-coated copper particles (AgCu0608-15, 15 wt% Ag, specific surface area (SSA) = 0.63 m^2/g) were provided by AMES Advanced Materials Cop. (US) and are denoted here as Ag@Cu. Silver coated-glass particles (SG05TF40, 40 wt% Ag) were purchased from PI-KEM Hart (UK) and are denoted here as Ag@glass. All particles were used as received.

Particle characterization

Scanning Electron Microscopy (SEM) was performed using a Phenom Pharos G2 (Thermo Fisher Scientific, Germany). Particle size distribution was determined by laser diffraction using a HELOS system equipped with a RODOS dry disperser (SympaTEC, Germany). Thermogravimetric analysis (TGA) was conducted using a TGA 5500 (TA Instruments) under air and nitrogen atmosphere. Differential Scanning Calorimetry (DSC) measurements were carried out using a DSC 214 Polyma (Netzsch, Germany) in closed sample pans. TGA and DSC measurements were performed from room temperature to 400 °C at a heating rate of 10 K/min. For DSC analysis, baseline correction was performed by fitting a 3rd-degree polynomial to the curve while excluding the temperature range of the peaks (100-250 °C); the fitted baseline was subsequently subtracted from the original curve.

ECA preparation

Epoxy resin and particles were mixed for 2 min at 2000 rpm using a SpeedMixer DAC 150.1 FVZ (Hauschild, Germany). Additives were then added and mixed for an additional time of 1 min. In the final step, the catalyst was added and mixed for 1 min. For resistivity measurements, three ECA lines with a thickness of 100 µm and a width of 4 mm were stencil-printed onto glass slides and cured for 2 min at 150 °C on a heat plate. Samples for mechanical testing were cured for 10 min at 150 °C in an oven. A detailed study on the influence of curing time and temperature for silver-filled ECAs based on the epoxy resin and Ag flakes also used here is reported elsewhere [221].

ECA characterization

Rheological measurements were performed using a MARS rotational rheometer (Thermo Fisher Scientific, Germany) equipped with a plate-plate geometry (20 mm diameter) and gap height of 1 mm. For yield stress determination, shear stress was increased stepwise from 0.1 to 1000 Pa in 81 logarithmic steps. The yield stress was defined as the intersection point of the linear fits to the elastic and to the viscous region in a double logarithmic deformation-stress-diagram [69]. Viscosity was determined by increasing the shear rate from 0.1 to 1000 1/s in 41 logarithmic steps. Each rheological measurement was carried out three times per sample.
Volume resistivity was measured using a 4-point probe setup with a 2450 SourceMeter (Keithley, US) and a probe spacing of 15 mm. Nine data points were taken per sample. Contact resistivity was measured according to [42]. Lap-shear strength was determined based on ASTM D1002 [158]. Carbon steel was used as substrate for lap-shear test samples. The bonding area was approximately 15 mm^2. Three specimens per ECA were measured using a universal tensile testing machine TA.XT plus Texture Analyser (Stable Micro Systems, UK) at a crosshead speed of 0.2 mm/s. For Young's Modulus determination, 15 samples were prepared in accordance with DIN EN ISO 20753, type A22 [160], and pulled at a crosshead speed of 0.01 mm/s. Mean values and standard deviation were calculated for all parameters.

Module preparation and testing

For module testing, mass-produced Passivated Emitter and Rear Cell (PERC) cells in G1 5th (158.75 × 31.75 mm^2) format were used. The initial host cell efficiency (before dicing) was 21.8%. Three types of electrically conductive adhesives were evaluated for cell interconnection. The commercially available ECA PROTAVIC® ACE 10720 (PROTAVIC INTERNATIONAL, France) filled with 5-10 vol% Ag flakes was used as the reference material. The Ag@glass ECA contained 3.5 vol% silver at a total filler content of 8 vol%, and the Ag@Cu ECA contained 10 vol% of Ag@Cu particles (1.7 vol% silver).

Cell interconnection was performed using a prototype shingle stringer from M10 Industries. The ECA was dispensed on the cells as continuous lines, covering the entire busbar. ECA curing was performed using an infrared lamp setup with a maximum process temperature of 140 °C. The maximum temperature was monitored by temperature-measuring strips attached to the rear side of dummy cells. Each string consisted of six shingle cells. The modules were laminated in a glass-backsheet configuration using an industrial laminator (Bürkle Ypsator M-LAPV 1222-HKV). The lamination temperature was 155 °C. Ethylene-vinyl acetate foils (F406PS for front side, F806PS for back side, Hangzhou First Applied Material) served as encapsulant material. Module *IV* characteristics were measured on a non-calibrated, xenon-lamp-based sun simulator (halm elektronik GmbH, Germany). *IV* characterization was carried out under STC (AM1.5G spectrum, 1000 W/m^2), and temperature-corrected to 25 °C using the cell temperature coefficients provided by the cell manufacturer.

Each group consisted of 12 samples, where six were intended for thermal cycling and six for temperature-humidity aging. Two additional modules containing reference ECA were set aside without aging treatment to serve as controls for estimating calendar aging effects and measurement uncertainty. To evaluate the interconnection reliability, accelerated Thermal Cycling (aTC) and Damp Heat (DH) tests were selected. The aTC test protocol employed six times faster cycling rates compared to the standard Thermal Cycling (TC) test described in IEC 61215-2 MQT 11. Comparable results between aTC and TC have been demonstrated in [233]. The DH tests followed IEC 61215-2 MQT 13. aTC aging consisted of 200 cycles and DH aging of 500 h.

6.3 Results and Discussion

6.3.1 Particle Characterization

In this study, three different particle types were investigated: silver flakes (Ag flakes), used as reference and additional filler; silver-coated glass flakes (Ag@glass) with a silver content of 40 wt%; and silver-coated copper flakes (Ag@Cu) with a silver content of 15 wt%. SEM images depicting the morphology of the different particles are shown in Figure 29. All investigated particles exhibited a flake-like morphology. The Ag flakes were the thinnest and exhibited an irregular shape. The Ag@Cu particles had a similar shape but with a smoother contour. In contrast, Ag@glass particles had a more angular contour and a rather uniform thickness of app. 2 µm. Figure 30a depicts the particle size distribution determined using laser diffraction. The reported equivalent diameters were calculated assuming spherical particles. As all investigated particles were flake-shaped, they are not characterized by a single diameter value. Nevertheless, the obtained values correlate well with the lateral particle dimensions observed in the SEM images, while the particle thickness is not adequately captured. Overall, all particles fall within a similar size range, with $x_{50,3}$ values ranging from 6.4 µm for the Ag@glass particles to 15.5 µm for the Ag flakes.

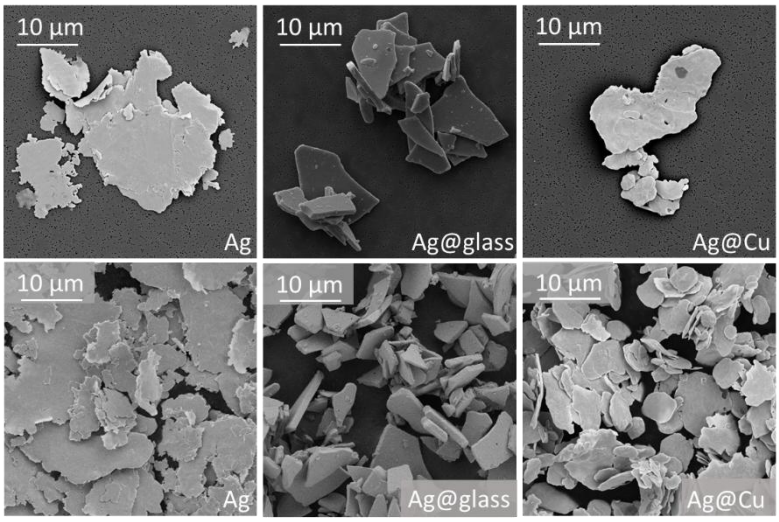


Figure 29. SEM images of Ag, Ag@glass and Ag@Cu as single particles and particle agglomerates for comparison of morphology and particle shape of the different particle types used for ECA formulation.

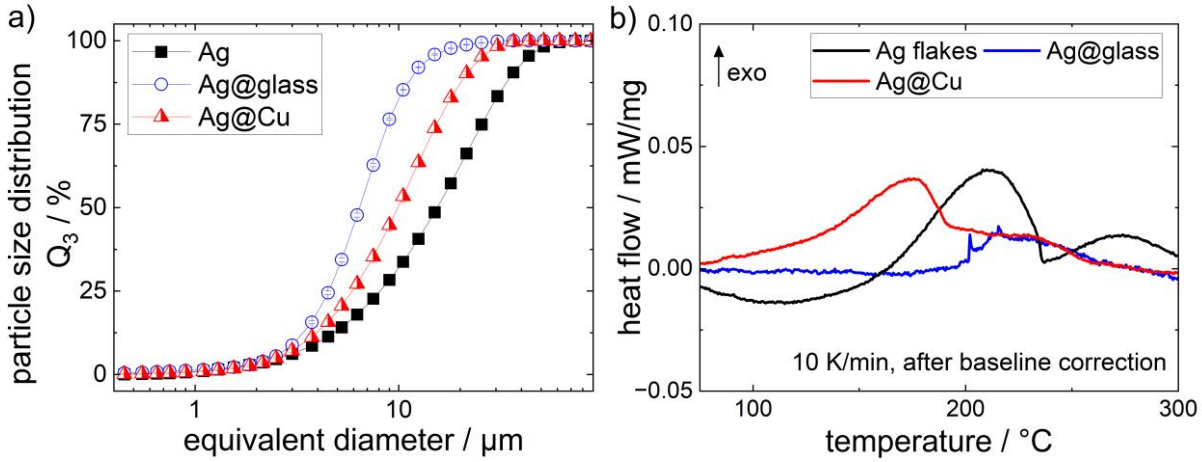


Figure 30. a) particle size distribution Q_3 measured by laser diffraction giving the equivalent sphere diameter and b) DSC analysis in air of Ag (black), Ag@glass (blue) and Ag@Cu (red) flakes for characterization of the surface chemistry of the particles, heating rate: 10 K/min, after baseline correction, exotherm: up.

To characterize the surface chemistry of the particles, DSC and TGA measurements were performed. Figure 30b shows the baseline-corrected heat flow for the particle samples between 75 and 300 °C, determined by DSC at a heating rate of 10 K/min. All particle types exhibited an exothermic peak in the temperature range between 150 and 250 °C. Peak temperatures were app. 180 °C for Ag@Cu and around 220 °C for Ag flakes and Ag@glass particles. In all cases, the observed peaks are relatively broad. In addition, the DSC curve of the Ag flakes exhibited a secondary exothermic peak around 270 °C.

TGA measurements (depicted in Figure S1) confirmed the DSC results. All TGA curves revealed a mass loss in the temperature range corresponding to the exothermic peaks observed in DSC. Furthermore, the Ag@Cu particles exhibited a mass increase above approximately 230 °C, which can be attributed to the oxidation of the copper core. During particle manufacturing, fatty acids are commonly utilized as process aids to prevent cold welding during milling. Residual amounts of these organic compounds typically remain on the particle surface. The observed DSC peak temperatures and the corresponding mass losses in the TGA measurements are in good agreement with literature values reported for the thermal decomposition of such fatty acids

[25,234]. Therefore, DSC and TGA results strongly indicate the presence of a thin fatty-acid-based organic layer on the surface of all investigated particle types.

6.3.2 ECAs based on silver-coated glass particles

In a first set of experiments, silver-coated glass particles were employed as fillers in the epoxy resin. They utilize a non-conductive core, which increases the effective volume of each particle and therefore, the number of potential contact points between the particles.

As a reference, an ECA prepared from the same epoxy resin and pure Ag flakes is reported. This formulation exhibited electrical percolation at a filler content between 10 and 15 vol%, resulting in a decrease in volume resistivity from app. 18 Ω cm at 10 vol% Ag to (1.2 ± 0.3) 10^{-2} Ω cm at 15 vol%, see Figure 31a. Beyond the percolation threshold, such an ECA exhibited a yield stress, providing sedimentation stability. In contrast, Ag@glass-based ECAs without additives did not percolate within the investigated filler content range of 5 to 25 vol%. Increasing the Ag@glass content decreased the volume resistivity from 10^{6} Ω cm at 5 vol% filler to 10^{4} Ω cm at 25 vol%. The standard deviation increased with increasing filler content, indicating the formation of isolated conductive pathways. Simultaneously, the paste exhibited macroscopic inhomogeneities, but no measurable yield stress was observed.

Previous studies have demonstrated that halogens can significantly influence both the yield stress and the electrical conductivity of ECAs [70,77,71]. Yang et al. [70] reported that iodine reacts with the silver particle surface, forming silver-nano islands. Sun et al. [77] observed halogen-induced structural changes resulting in the formation of a particle network, which increased yield stress and decreased volume resistivity. More recently, Marten et al. [71] attributed similar effects to the removal of fatty acids from the particle surface and the formation of silver iodide. This modification of the surface chemistry promotes van der Waals dominated attractive particle–particle interactions and closer particle contact, thereby increasing yield stress and lowering the electrical percolation threshold. Consistent with these findings, the addition of a halogen(h)-based additive to the polymer-particle system investigated here significantly altered both the percolation threshold as well as morphology of ECAs containing Ag@glass particles. The volume resistivity decreased from 10^{5} Ω cm at 5 vol% Ag@glass to (5.1 ± 0.3) 10^{-3} Ω cm at 15 vol% Ag@glass. Further increase in Ag@glass content decreased volume resistivity only marginally. The ECA containing 10 vol% Ag@glass and the halogen-based additive exhibited a yield stress of (51 ± 7) Pa, which increased to (236 ± 173) Pa at 15 vol% Ag@glass. At higher filler contents, the paste became tough and crumbly, rendering it unsuitable for application. The ECA with 15 vol% Ag@glass and halogen-based additive met the requirements for solar cell shingling in terms of volume resistivity and lap-shear strength ((20 ± 2) MPa), while utilizing only 2 vol% (14.4 wt%) silver. However, the yield stress of this formulation was rather high for printing or dispensing processes.

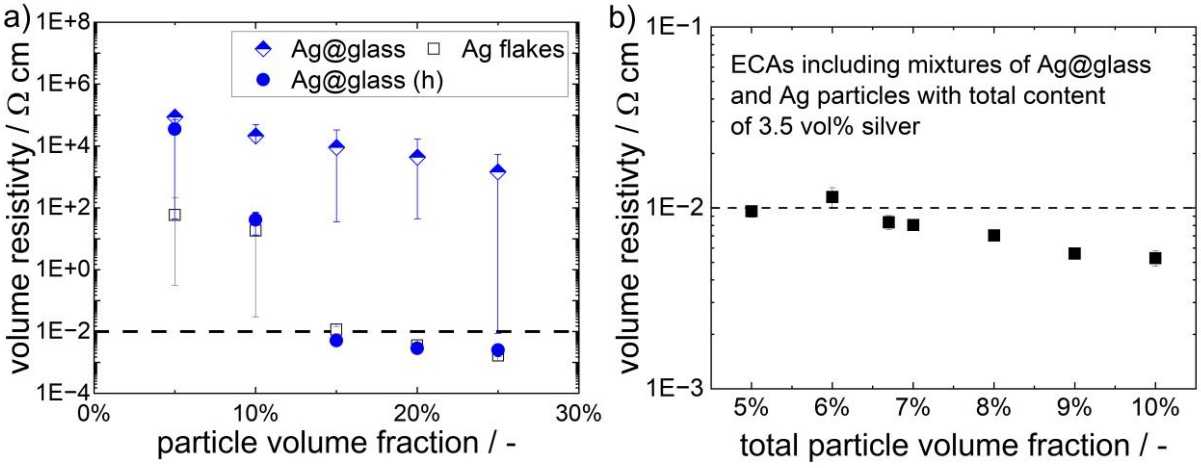


Figure 31. a) volume resisitivity of ECAs with Ag flakes (un-filled black squares) and Ag@glass (blue) without (filled circles) and with (half-filled diamonds) halogen(h)-based additives and filler content between 5 and 25 vol%; b) volume resisitivity of ECAs with varying total filler content between 5 and 10 vol% comprising Ag@glass and Ag particles at different mixing ratios to contain 3.5 vol% silver, higher total particle volume fraction corresponds to a higher fraction of Ag@glass particles in the mixture; dashed lines indicate the maximum volume resistivity required for solar cell shingling.

To overcome this issue, a possible approach to reduce yield stress of the ECA is dilution with a low-boiling solvent. However, solvent evaporation within a shingled joint is unfavorable. Instead, Ag@glass particles were mixed with Ag flakes to reduce the overall particle volume fraction while maintaining low volume resistivity. All formulations in the following experiments contained the halogen-based additive.

In a preliminary study, the total filler volume fraction was fixed at 5.0 and 6.7 vol%, respectively while the mixing ratio of Ag@glass to Ag flakes was varied. To meet the requirements of volume resistivity for a shingled solar cell interconnection of 10^{-2} Ω cm [221], a minimum of 3.5 vol% (app. 25 wt%) silver was required for such a low-filled ECA. The corresponding results are shown in Figure S2.

Figure 31b shows the volume resistivity of ECAs containing Ag@glass and Ag flakes with total particle volume fractions between 5 and 10 vol%. The Ag@glass-to-Ag flakes ratio was adjusted to maintain a constant total silver content of 3.5 vol%. The volume resistivity decreased from (9.6 ± 0.7) 10^{-3} Ω cm at 5 vol% total filler to (5.3 ± 0.5) 10^{-3} Ω cm at 10 vol%. Except for an outlier at 6 vol% with (1.1 ± 0.1) 10^{-2} Ω cm, the volume resistivity of all ECAs was below 10^{-2} Ω cm. The volume resistivity slightly decreases with increasing total particle volume fraction. Accordingly, the total silver fraction could be further reduced at a filler content above 8 vol% due to the higher amount of glass-core particles, that bring the silver shells into closer proximity. Additionally, the ECA with 8 vol% total filler exhibited a sufficiently low contact resistivity of (0.04 ± 0.01) mΩ cm^2.

The yield stress of these ECAs is shown in Figure 32a. The yield stress increased exponentially from (22 ± 1) Pa at 5 vol% total filler to (148 ± 4) Pa at 10 vol%. All ECAs exhibited a superior lap-shear strength ranging from (20 ± 2) MPa at 5 vol% filler to (28 ± 3) MPa at 9 vol% filler (Figure 32b). In all cases, cohesive failure was observed. Despite the increased particle content, which means higher number of potential defects in the polymer matrix, the lap-shear strength remained high. This is attributed to the better adhesion between Ag@glass particles and the epoxy than to Ag flakes. This conclusion is confirmed by lap shear strength measurements of samples containing 15 vol% of only Ag@glass or Ag flakes. The Ag@glass sample had a lap shear strength of (20 ± 2) MPa, which is twice as high as that of the ECA containing only Ag flakes ((10.1 ± 0.9) MPa).

Both volume resistivity and lap-shear strength showed only minor dependence on the glass fraction and remained within the required specifications. Therefore, the total filler fraction,

determined by the additional glass content, can be taken to individually tune the rheological parameters. A yield stress between 10 and 100 Pa is recommended for dispensing and screen-printing application. ECAs containing 3.5 vol% silver and a total filler content of 5 to 8 vol% composed of Ag@glass and Ag flakes meet all requirements regarding rheological, electrical and mechanical properties in the uncured and cured state for shingled solar cell interconnection.

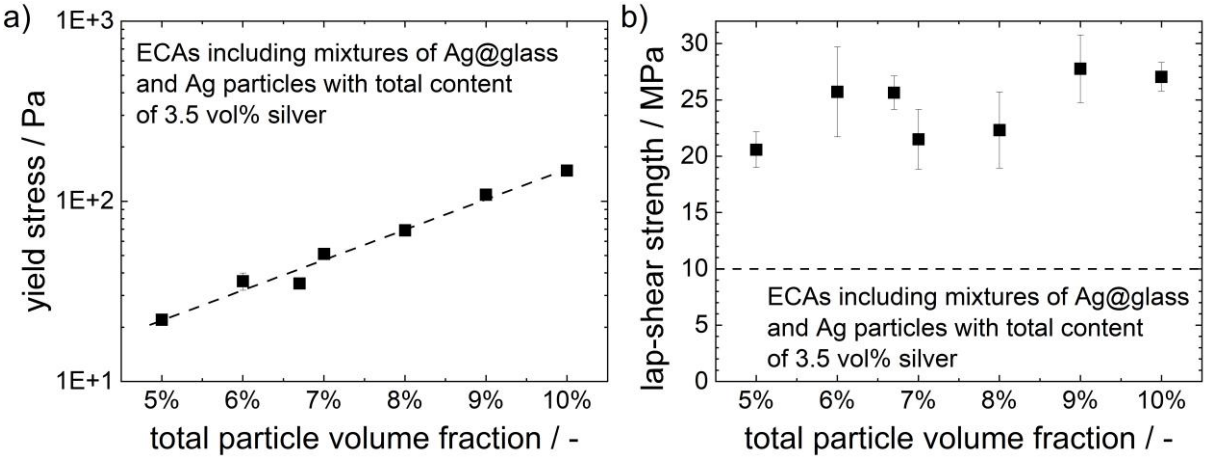


Figure 32. a) yield stress and b) lap-shear strength of ECAs with varying total filler content between 5 and 10 vol% comprising Ag@glass and Ag particles at different mixing ratios to contain 3.5 vol% silver, higher total particle volume fraction corresponds to a higher fraction of Ag@glass particles in the mixture. The standard deviation of the yield stress measurements was too small to be visible in the diagram. Typically, the relative uncertainty of yield stress determination is in the order of 10%. Dashed line in diagram a) is to guide the eye, dashed horizontal line in diagram b) corresponds to the minimum required lap-shear strength for solar cell shingling.

6.3.3 ECAs based on silver-coated copper particles

Further silver reduction was pursued by introducing silver-coated copper particles (Ag@Cu). These allow both shell and core to contribute to electron transport. However, the presence of copper presents challenges, including oxidation sensitivity and interactions with halogen additives, which may result in insulating compounds.

Suspending Ag@Cu particles in the epoxy resin used in this study resulted in ECAs without a yield stress and poor sedimentation stability. Consequently, samples for volume resistivity measurements were applied and cured immediately after mixing. The volume resistivity values shown in Figure 33 thus represent the minimum volume resistivities achievable under proper stabilization. Sedimentation which occurred within minutes after mixing led to insulating samples. As reference, volume resistivities of ECAs containing Ag flakes are also shown in Figure 33. ECAs containing Ag@Cu (15 wt% silver) were already conductive at a filler volume fraction of 5 vol% when cured directly after mixing. The volume resistivity at this filler content was $(3.3 \pm 0.2)\ 10^{-2}\ \Omega$ cm and decreased to $(1.11 \pm 0.05)\ 10^{-3}\ \Omega$ cm with increasing content of Ag@Cu up to 20 vol%. These results show, that ECAs based on silver-coated copper particles can meet the electrical requirements for shingled solar cell interconnection, provided that adequate stabilization against sedimentation is achieved. Obviously, the percolation threshold for the Ag@Cu particles is lower than that for the Ag flakes, this may be attributed to the smaller diameter of the Ag@Cu flakes or different surface chemistry.

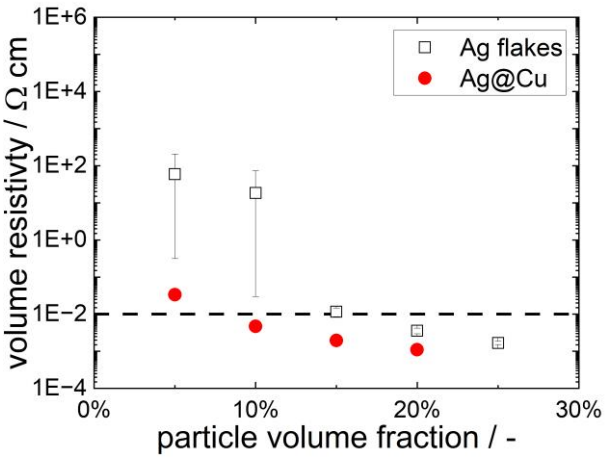


Figure 33. volume resisitivity of ECAs with Ag@Cu (filled red circels) and Ag flakes (un-filled black) with varying particle volume fraction from 5 to 25 vol%, samples were cured directly after mixing to prevent sedimentation, dashed line indicates the maximum volume resisitivty required for solar cell shingling.

Due to the chemical reactivity of copper, several non-reactive thickeners—namely fumed silica, carbon black, and Thixatrol AS 8053—were evaluated to improve particle stabilization. However, the increase in low-shear viscosity induced by these thickeners was not sufficient for particle stabilization. Additionally, the composites became insulating or did not fully cure. Detailed results are provided in the Supplementary Information (Figure S3-S5). Despite copper's reactivity, the suitability of the halogen-based additive was investigated for ECAs containing silver-coated copper particles as well. Halogens can replace the fatty acids on the surface of the particles, leading to enhanced particle-particle interactions, morphological changes and increased electrical conductivity [71]. Careful adjustment of the halogen content resulted in the formation of a yield stress in the ECA based on Ag@Cu particles, effectively suppressing particle sedimentation.

Figure 34 summarizes the properties of this optimized ECA in comparison with commercially available ECAs and the requirements for shingled interconnection. The ECA contained 10 vol% of Ag@Cu particles, corresponding to a silver content of only 1.3 vol%. This is app. one quarter of the silver content of the commercial ECA with the lowest reported silver content (5 vol%) and more than an order of magnitude lower than that of standard highly-filled ECAs, which contain 20 to 30 vol% silver. In terms of weight, the ECA contained 7 wt% silver and 40 wt% copper. This formulation exhibited a volume resistivity of (4.3 ± 0.8) 10^{-3} Ω cm and a contact resistivity of (0.03 ± 0.01) mΩ cm^2, which satisfies the requirements for solar cell shingling. The yield stress of the ECA was (40 ± 11) Pa. The particles were thus stabilized against sedimentation and the ECA is suitable for screen-printing and dispensing. However, the curing kinetics of the ECA were altered, which led to a softer bond and a comparatively low Young's Modulus of (34 ± 13) MPa. DSC analysis revealed a shift of the main curing peak to higher temperature (126 °C instead of 106 °C) and the appearance of an additional shoulder above 150 °C (Figure S3). Nevertheless, flexible bonds are preferred in shingled interconnection and the lap-shear strength of (28 ± 6) MPa was well beyond the required 10 MPa. The uncured ECA remained stable over more than six months when refrigerated at -20°C and showed no degradation in volume resistivity after curing when stored under standard laboratory conditions for the same duration.

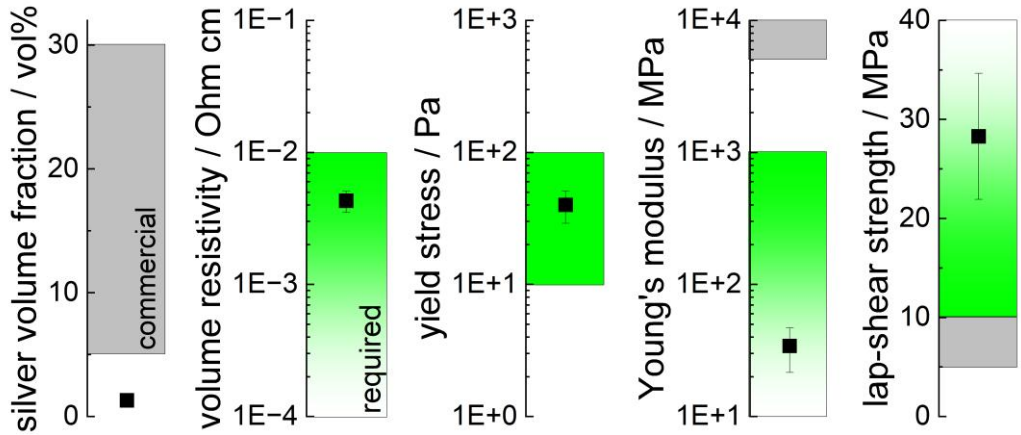


Figure 34. silver content as well as electrical and mechanical properties of the ECA with 10 vol% Ag@Cu and halogen additive indicated as black squares compared to commercial products (grey) and requirements for shingled solar cell interconnection (green).

6.3.4 Application in shingled solar modules

To investigate the suitability of the developed ECAs for application in PV, especially solar cell shingling, mini modules with linear strings of six shingled cells were produced. The ECAs and their silver content as well as dispensed masses and volumes utilized for the three groups of modules are shown in Table 5. Twelve modules per formulations were produced for aging tests, plus two additional modules with the reference ECA serving as unaged reference modules. To obtain similar dispensing volumes with all three ECAs, dispensing parameters (pressure and preheat temperature) were adjusted to achieve dispensed volumes equivalent to the reference system.

Table 5. Applied ECAs in the different module groups with their silver content and masses applied per shingle and calculated dispensed volume per shingle

ECA formulation	Silver volume fraction / -	Silver weight fraction / -	Dispensed mass per shingle / mg	Uncured density / g/mL	Dispensed volume per shingle / µL
Ag (PROTAVIC® ACE 10720), reference	6.5-10%	40-50%	4.2 ± 0.2	1.78	2.4 ± 0.2
Ag@glass	3.5%	25%	3.6 ± 0.2	1.52	2.4 ± 0.2
Ag@Cu	1.7%	7%	4.1 ± 0.3	1.94	2.1 ± 0.2

SEM images of joint cross-sections are shown in Figure 35. It is evident from the images that the particles were arranged in stacks forming conductive pathways. In the case of the Ag@glass ECAs, these stacks comprised Ag@glass and Ag flakes. Joint thickness was between 26 and 38 µm, wider than the average particle diameter. This indicates that current is conducted from particle to particle in all ECA formulations, which is typical for ECAs with a filler content beyond the percolation threshold.

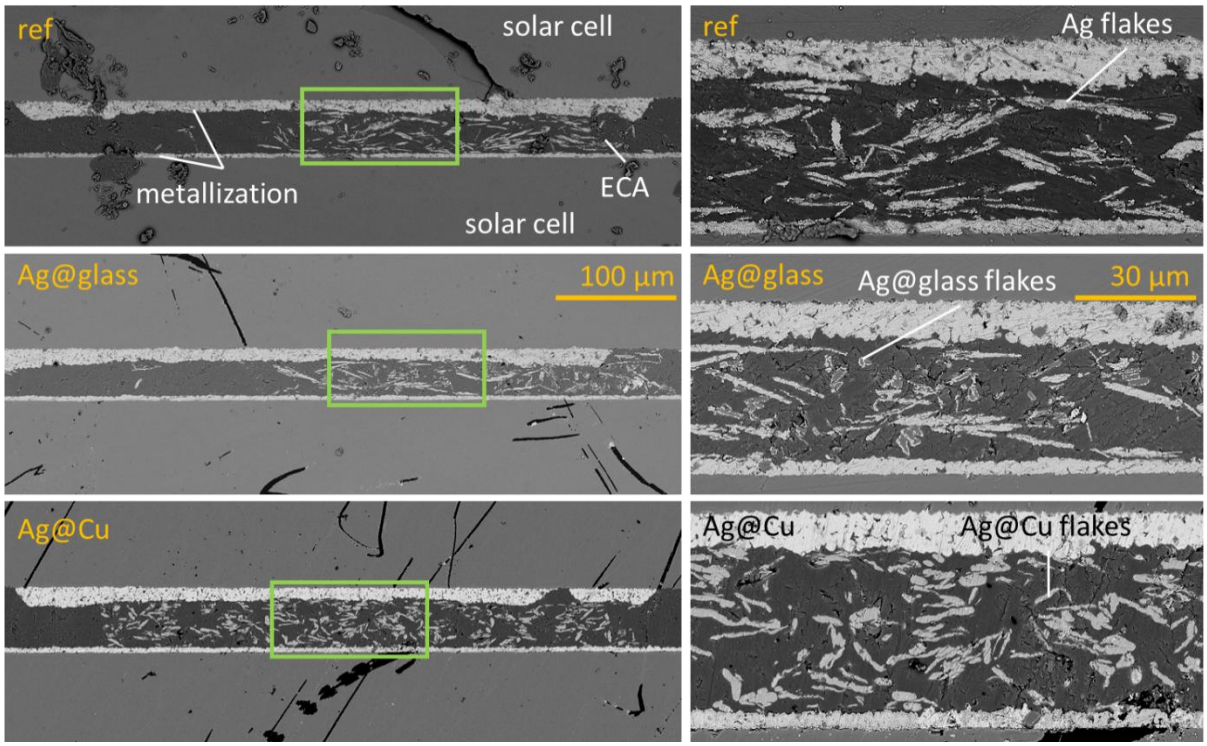


Figure 35. SEM images of shingled solar cell joint cross-sections made from ECAs with Ag flakes, Ag@glass and Ag@Cu flakes, images on the left show the whole metallization, images on the right are magnifications of the left images at the position of the green square.

The initial module performance is visualized in Figure 36. Modules interconnected with Ag and Ag@glass ECAs demonstrated similar efficiencies of app. 19.64%. In contrast, modules with Ag@Cu ECA exhibited a marginally higher efficiency (Figure 36a). Similarly, the module fill factors followed the same trend (Figure 36b). Statistically, the observed differences between all experimental groups fall within one standard deviation of the mean values for both efficiency and fill factor, indicating no statistically significant variance in the initial module performance across the three ECA formulations.

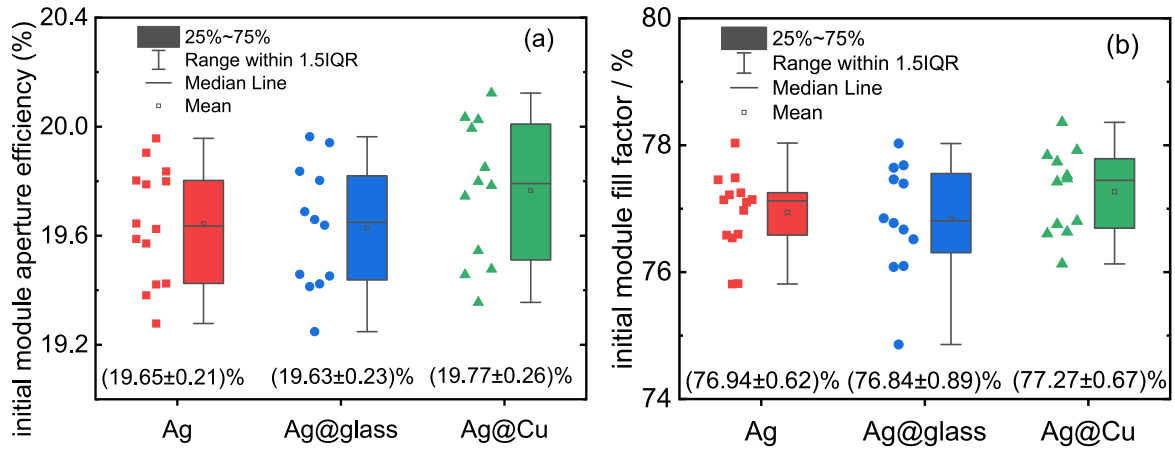


Figure 36. Initial characterization of the produced six-shingle mini modules. (a): aperture efficiency, (b): fill factor. The individual data points are plotted next to bar plots, calculated from the same data. The median value and standard deviation of each group are written below the data.

To compensate calendar aging and the measurement error from the uncalibrated *IV* measurement, the failure criterion for ageing tests was set to a loss of $5\%_{rel.}$ compared to the

unaged reference modules. Figure 37 shows the aging test results along with the criterion derivation (solid red line) and failure threshold (dotted red line). After aTC 200 (Figure 37a), Ag and Ag@glass fillers demonstrated similar relative efficiency changes. In contrast, the Ag@Cu system exhibited significant performance degradation. One module showed no measurable power output after the test and thus is not shown in Figure 37a and was excluded from further analysis. Three modules failed the test due to significant fill factor losses and thus efficiency losses. The fill factor degradation patterns (Figure 37a) mirror those observed for module efficiency. This correlation between efficiency and fill factor degradation strongly indicates that the performance losses are primarily attributed to interconnection degradation. The Young's Modulus of the ECA filled with Ag@Cu ((34 ± 13) MPa) was significantly lower than that of the commercial silver filled ECA (1400 MPa). This could have led to higher strains under thermomechanical stress, which might have interrupted the conductive pathways within the Ag@Cu filler system, leading to progressive deterioration of the electrical connectivity. Additionally, the different curing kinetics of the Ag@Cu ECA may have contributed to the observed stability issues, as insufficient cross-linking density could result in weakened polymer matrix integrity under thermal cycling conditions. Results from DH 500 testing are shown in Figure 37b. All groups showed less than 5% efficiency loss. The stable fill factors after damp heat aging indicate that under these test conditions, oxidative degradation of the filler particles does not represent a limiting factor for any of the studied ECA systems.

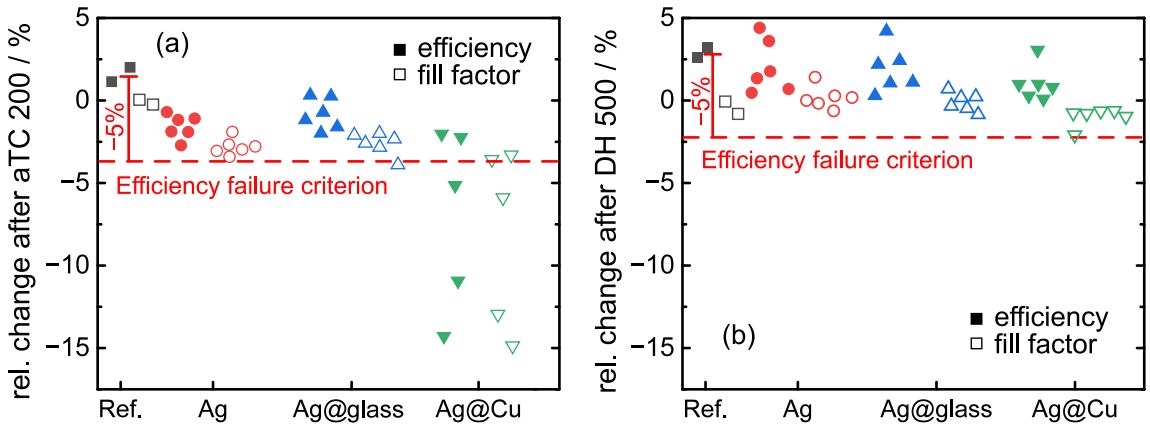


Figure 37. Relative efficiency changes of six-cell mini modules after (a) aTC and (b) DH aging with failure criterion derivation (solid red line) and threshold (dotted red line).

6.4 Conclusion and Outlook

Sustainable energy production requires sustainable material supply. Therefore, the PV industry aims to replace silver in metallization and interconnection of solar cells. However, up to date a full replacement of silver is not possible. Instead, core particles coated with a thin silver layer are utilized. These core particles can be either conductive or non-conductive. In this study, one of each type was evaluated.

Inert glass particles increase particle volume and bring the silver layer in closer contact. However, the particle volume required for conductivity led to a high yield stress, unsuitable for application. This was overcome by replacing only a part of the Ag flakes by Ag@glass. For a volume resistivity of 10^{-2} Ω cm, at least 3.5 vol% silver was necessary in ECAs with a total particle volume fraction below 8%. This led to an ECA containing only 25 wt% silver with lap-shear strength beyond 20 MPa and yield stress between the required 10 and 100 Pa, tunable by the fraction of Ag@glass particles used.

Further reduction in silver content was achieved by utilizing silver-coated copper particles, as example for fillers with conductive cores. However, the formulation with copper is more challenging. The effect of thickeners was retarded in such systems or their application led to high resistivities or incomplete curing. By carefully adjusting the content of a halogen-based additive, an ECA was obtained containing 10 vol% of Ag@Cu, fulfilling all requirements for solar cell shingling at only 1.7 vol% (7 wt%) silver content.
In module evaluation, the formulated ECA systems utilizing Ag@glass or Ag@Cu particles showed similar initial performance as the Ag filled reference system. After aTC 200, while the Ag@glass system passed the test with similar power losses as the Ag system, the Ag@Cu system showed severe degradation. This could be due to insufficient mechanical stability of the conductive pathways under thermomechanical stress, leading to increased series resistance. DH 500 revealed that oxidative degradation is not a limiting factor for all three studied systems (all <5% loss), suggesting that the Ag@Cu degradation mechanism is primarily mechanical, not chemical. Silver-coated glass particles are promising to replace pure silver flakes. With copper containing particles, interaction with the polymer becomes relevant. Other polymer-particle combinations providing better compatibility should be investigated in future studies to formulate a more reliable ECA with silver-coated copper particles. Furthermore, including nano-sized particles in addition to the micron-sized flakes could be addressed in future studies. On module level, it would be interesting to evaluate the ECAs on cells with low-temperature metallization (e.g. SHJ or silicon-perovskite tandem cells) and other encapsulants (e.g. TPO or POE) to study possible interactions between ECA, cell and encapsulant. Extending the aging experiment with the full test series specified in IEC 61215-1 would allow full qualification of the ECA for application in solar modules.

6.5 Supplementary information

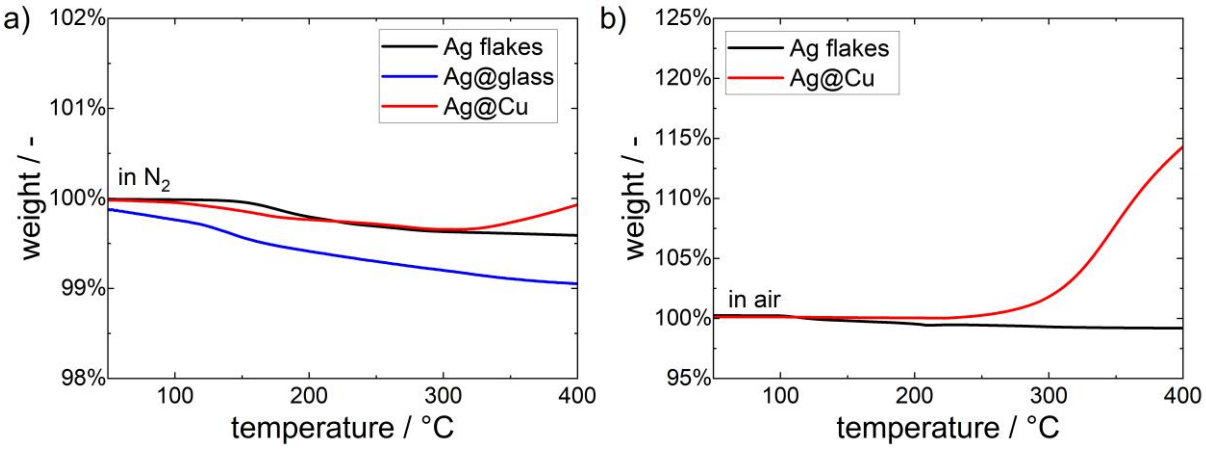


Figure S1. Thermogravimetric analysis of Ag flakes, Ag@glass and Ag@Cu flakes at a heating rate of 10 K/min a) in nitrogen to determine the surface chemistry and b) in air to determine the oxidation behavior of the particles.

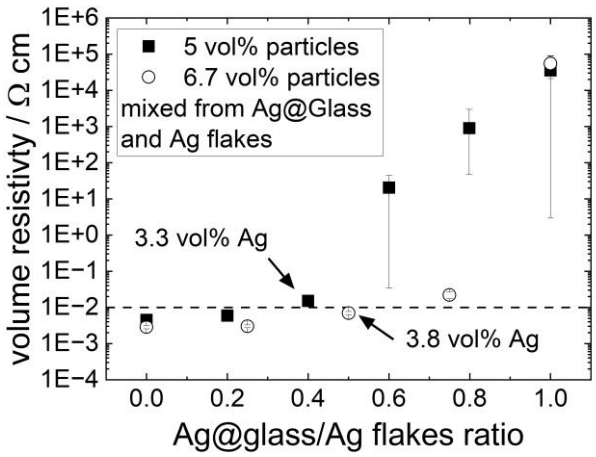


Figure S2. variation of the Ag@glass to Ag flakes ratio at a total particle volume fraction of 5 vol% (square) and 6.7 vol% (circle), respectively, to determine the minimum silver content which is necessary to achieve a volume resistivity of 10^{-2} Ω cm or less, minimum silver content was estimated to lie between 3.3 and 3.8 vol%.

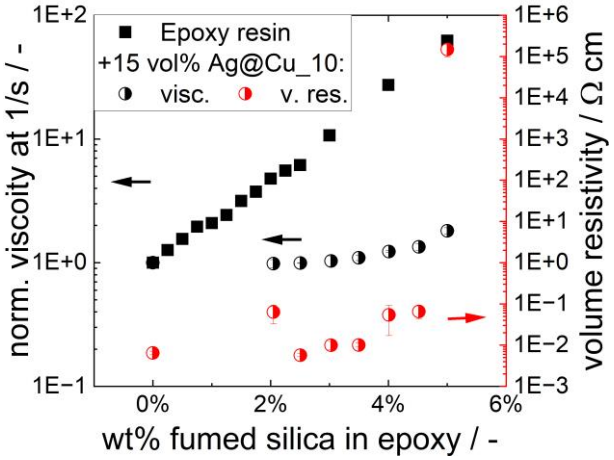


Figure S3. Fumed silica (Silica, fumed S5505; Sigma-Aldrich, US) was utilized to increase the ECAs viscosity and therefore, stabilization against sedimentation. Eventhough, the addition of fumed silica led to an increase in viscosity of the pure epoxy resin (black square), viscosity increase of a composite containing epoxy resin and 15 vol% Ag@Cu_10 (different silver-coated particle type containing 10 wt% silver) was retarded (black circles). With increasing fumed silica content the volume resistivty (red circles) of the composite increased, leading to an insulating composite; similar results were obtained with Ag@Cu.

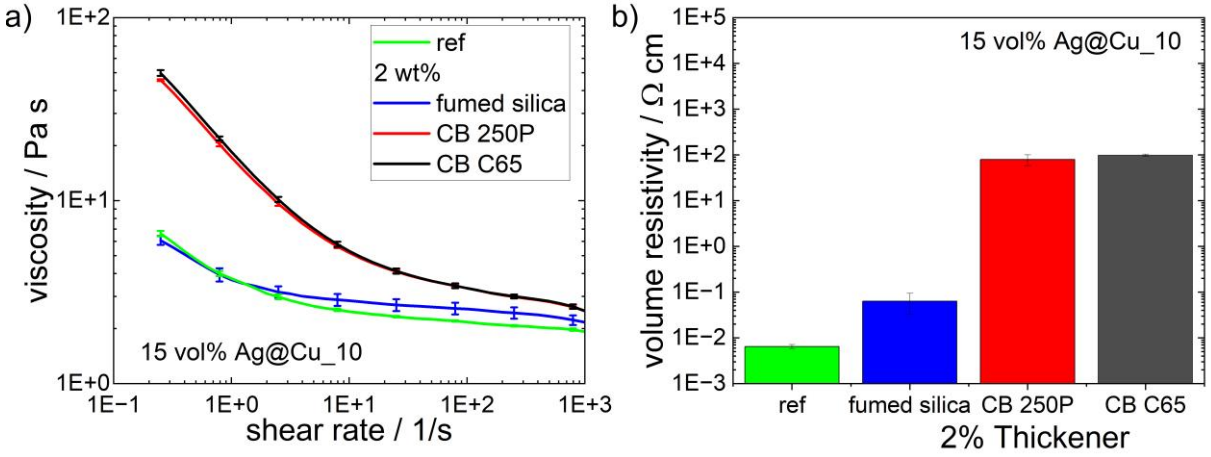


Figure S4. a) viscosity curve and b) volume resistivity of ECAs with epoxy resin, 15 vol% Ag@Cu_10 and 2 wt% of fumed silica, carbon black 250P (Enasco® 250 P; Imerys Graphite & Carbon, Switzerland) or carbon black C65 (C-Nergy Super C65; Imerys Graphite & Carbon, Switzerland) , resp. in the epoxy resin; the increase in low-shear viscosity was not sufficient for particle stabilization and composites became insulating; similar results were obtained with only 10 vol% Ag@Cu_10 or Ag@Cu.

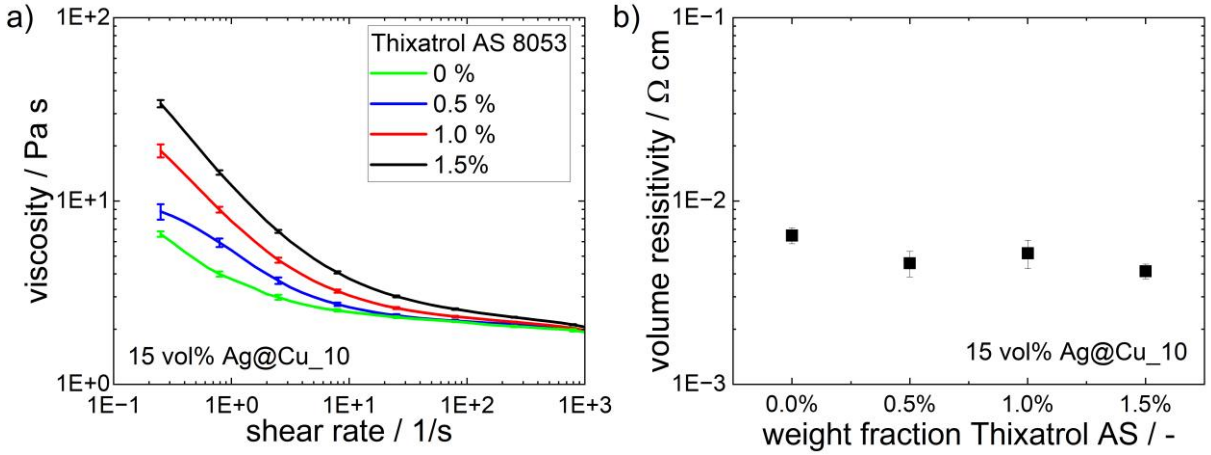


Figure S5. a) viscosity curves and b) volume resistivity of ECAs with epoxy resin, 15 vol% Ag@Cu_10 and up to 1.5 wt% Thixatrol AS 8053 (Thixatrol® AS 8053; Elementis, US) in the epoxy resin; Eventhough, volume resistity stayed low, increase in low-shear viscosity was insufficent for sedimentation stability, higher contents of Thixatrol AS 8053 led to incomplete curing of the ECA.

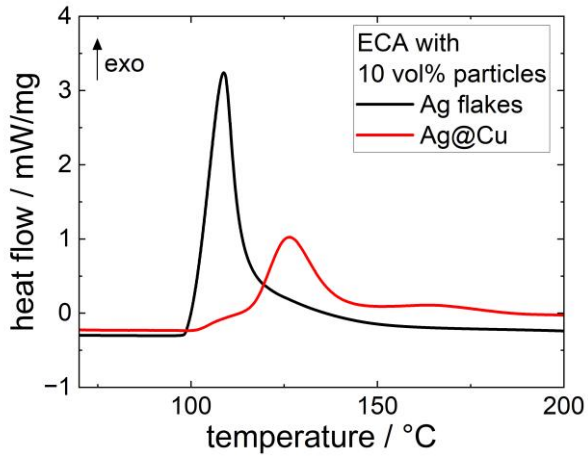


Figure S6. DSC curve of the ECA containing 10 vol% of Ag@Cu and a comparable ECA with 10 vol% of pure silver particles to determine the curing kinetics at a heating rate of 10 K/min, exotherm: up; the curing peak

of the ECA containing Ag@Cu shifted to a higher temperature of 126 °C instead of 106 °C and was generally broader, exhibiting a shoulder above 150 °C.

Acknowledgements

The authors like to thank Simon Malandain and Vincent Charlot and Frederic Durand of PROTAVIC INTERNATIONAL Laboratory for their professional support and material supply and Sofia Franceschini Mayr for conductance of experiments.

Funding sources

This work was funded by the German Federal Ministry for Economic Affairs and Energy (BMWE) as part of the project “Mod30+” with the grant number 03EE1160.

7 Conclusion

Solar cell shingling, in which solar cells are directly bonded to each other, represents a relative new module design concept in PV industry. The corresponding interconnection technology is therefore still under research. Preferentially, ECAs are used as interconnection material due to their higher flexibility compared with solder, which is advantageous as thermomechanical stresses must be accommodated within the joint. Additionally, the low curing temperature of ECA makes it compatible with thin wafers or temperature-sensitive cell materials. However, some challenges remain, most notably the high material cost caused by the high silver content in state-of-the-art ECAs. In order to reduce the silver content and to formulate tailored ECAs for shingled PV interconnection, clearly defined material specifications are required which, so far, have only been reported for individual parameters rather than for a comprehensive property set.

In Chapter 4, an overview of rheological, electrical and mechanical requirements was presented based on literature review and the author's own calculations and experimental evidence. Table 6 summarizes these parameters supplemented by some general requirements. Owing to the overlapping joint geometry, a solvent-free ECA is preferred in order to prevent trapping of the solvent or unwanted interactions with the upper shingle. A sufficient pot and shelf life are general requirements for ECAs independent of the shingling process, whereas life time and operating temperature are application-specific requirements for PV modules. The required rheological properties are mainly determined by the application method, to ensure uniform and reproducible deposition. To maintain throughput comparable to other module interconnection concepts, i.e. soldering, rapid ECA curing preferably at low temperature is required. Regarding the electrical properties, an efficiency loss caused by the interconnection of less than 0.025% is considered acceptable. This loss depends on contact and volume resistivity, but also on the applied volume of ECA. The shear strength has been reported to play a minor role as long as a bond could be obtained, although, a lap-shear strength beyond 10 MPa is generally recommended. In contrast, the required ranges of Young's modulus and shear modulus remain more uncertain and will therefore be discussed in greater detail later.

Table 6. specifications for ECAs applied in the linear-shingled solar cell interconnection

Parameter	Value	Unit	Annotations	Test method
Type			One component, solvent free	
Pot life	>24	h		
Shelf life	>6	month	Stored at -40 °C	
Life time	>30	years		
Operating temperature	40 - 50	°C	Must withstand -45 °C to +80 °C	
Silver content			As little as possible	
Application method			Screen printing, dispensing	
Bleeding	low			
Yield stress	1 10-100	Pa Pa	Sedimentation stability Screen printing	Tangent-intercept method, rotational rheometer
Curing temperature	<140	°C	For perovskite, tandem	
Curing time	<30	s		

Parameter	Value	Unit	Annotations	Test method
Contact resistivity	1 x 10^{-1}	mΩ cm^2	continuous line, vs. silver	Transfer Length Method
Volume resistivity	1 x 10^{-2}	Ω cm	continuous line	4-point measurement ASTM D991
Young's Modulus	<1000 >?*	MPa MPa	 for low-filled ECAs, to be determined	Tensile test ASTM D638
Shear modulus	<500 >?*	MPa MPa	 for low-filled ECAs, to be determined	Lap-shear test ASTM D1002
Shear strength	>10	MPa	Important: initial bonding	Lap-shear test
Module performance	<5%	losses	TC, DH, mechanical load	IEC 61215-2, IEC 61730

The most challenging requirement to meet, is a low silver content. Therefore, the application of the capillary suspension concept to ECAs was investigated as described in Chapter 4. The formulations presented here are all based on a snap-cure epoxy-resin and silver flakes commercially used in die-attach applications and were provided by Protavic Int. These silver flakes are coated with chemically bound fatty acids, which prevent agglomeration and promote dispersibility and particle-polymer integration. However, these surface layers hinder electron transport and particle network formation. In capillary suspensions, the addition of a small amount of a secondary liquid phase leads to the formation of strong percolating particle networks even at low filler content. To maintain the good particle-polymer integration, a "capillary" state capillary suspension is targeted in which the main phase, i.e. the polymer, preferentially wets the particles. In this configuration, a sample-spanning cluster network is formed in which secondary liquid droplets are shielded from the main phase by the particles. An additive which removes the fatty-acid layer selectively at the particle-particle contacts can be incorporated into the secondary liquid. Additionally, the resulting rheological behavior is favorable for ECA application by screen printing or dispensing.

The network structure induces a yield stress in the ECA, which enables particle stabilization at a filler volume content as low as 5 vol% compared to 15 vol% in the conventional binary suspension. However, a sufficient yield stress for screen printing required 10 and 20 vol% particles, respectively, depending on the formulation. The selected secondary liquid shifted the curing peak to slightly higher temperatures, but as intended did not further influence the overall curing kinetics. The investigated polymer system required a minimum curing temperature for complete curing and development of conductivity, which was achieved within seconds. However, too long curing times at elevated temperatures were detrimental for volume conductivity. The shingling requirement of 1 x10^{-2} Ω cm volume resistivity was achieved at 15 vol% silver in the binary suspension and below 5 vol% in the capillary suspension system. The contact resistivity was sufficiently low for all formulations ranging between 0.02 and 0.03 mΩ cm^2. Post-curing, for example during module lamination, was found to reduce the resistivity of ECAs with initially high resistivity, but did not affect ECAs in which conductivity had already fully developed. As expected, the lap-shear strength decreased linearly with increasing filler content as every additional particle acts as a defect in the polymer matrix. A filler volume fraction below 15 vol% is therefore recommended to achieve a lap-shear strength exceeding 10 MPa. This requirement could only be fulfilled by the capillary suspension system as the binary suspension required 20 vol% silver to achieve both processability and conductivity. To guarantee screen printability, between 5 and 10 vol% silver was necessary when applying the capillary suspension concept, potentially reducing silver consumption by more than 50%.

However, the volume resistivity data indicated further potential for reducing the silver content below 5 vol%, provided that sufficient particle stabilization could be achieved. This issue was addressed in Chapter 5 by introducing polyethylene glycol with an average molecular weight of 200 Dalton as a tuning agent into the investigated capillary suspension-based ECA.
The addition of PEG 200 to an ECA containing 5 vol% silver flakes resulted in an increase in both yield stress and lap-shear strength, while the electrical properties remained unaffected. Both parameters exhibit a maximum with increasing PEG 200 content. Simultaneously, the morphology of the ECA changed from uniformly distributed particles to a percolated particle network structure with increasing microheterogeneity. It is believed, that this change in particle distribution enhanced the lap-shear strength, although the effect was counteracted by the increasing proportion of non-curing PEG which replaced the epoxy matrix. PEG was found to be miscible with both the epoxy resin and the secondary polar liquid. Up to a certain volume fraction of PEG, the two-phase configuration was pertained, but the interfacial properties changed. A reduced three-phase contact angle against the particles promoted the formation of a capillary suspension in the "capillary" state. However, with increasing PEG 200 content the interfacial tension between main and secondary liquid decreased, thus weakening the capillary forces between particles. This effect was reflected in a decrease and eventual disappearance of the yield stress. The addition of an additive, such as PEG in the investigated system, that is miscible in both liquid phases, presents a new method to tune the strength of capillary suspensions. Finally, an ECA containing 4 vol% silver stabilized with 2 vol% PEG 200 exhibited a yield stress of (12 ± 3) Pa, at the required volume resistivity for shingling of 1 $x10^{-2}$ Ω cm. In terms of mass fraction, this filler content accounts for 28 wt% silver.

To further reduce the silver consumption, silver-coated core/shell particles were investigated for application in ECAs as discussed in Chapter 6. As example of a non-conductive core material, silver-coated glass particles were chosen. The glass core increases the effective particle volume, thereby bringing the silver shell of neighboring particles in closer proximity. Silver-coated copper particles have also been investigated, in this case both shell and core contribute to the electron transport.
To promote comparability, flake-shaped particles with a size distribution similar to that of the silver flakes used in Chapter 4 and 5 were selected. All particle types possessed a thin fatty-acid-based organic layer on the surface, although the chemical composition differed. Nevertheless, the particles exhibited different behavior in the adhesive formulations. Replacing the silver flakes entirely with silver-coated glass particles in addition with a halogen-based additive, resulted in a sufficient volume resistivity at 15 vol% filler, but produced a tough paste unsuitable for processing. Therefore, the silver flakes could only be partially replaced. To obtain a volume resistivity of 1 $x10^{-2}$ Ω cm, at least 3.5 vol% silver was necessary in ECAs containing 8 vol% total filler or less. By adjusting the proportion of silver-coated glass particles, the yield stress could be tuned without compromising electrical performance or lap-shear strength. The results obtained for ECAs containing pure silver flakes (28 wt% silver) and silver-coated glass/silver particles (25 wt% silver) presented in this work correspond well with the percolation curve reported by Ronayette et al. [204] for ECAs dedicated for PV. Their model predicts a percolation threshold and therefore, minimum silver content of 23.5 wt% for ECAs based on silver as the only conductive component. However, the ECA containing only silver-coated glass particles at a filler content of 15 vol% contained only 2 vol% (14.4 wt%) silver, while still meeting the electrical requirements for shingling. Provided that the rheological properties of the adhesive are properly adjusted, e.g. via exchange of the polymer matrix, the critical silver threshold proposed in [204] may need revision in the future.

For the epoxy system used here, a lower silver content is achievable through partial replacement by copper. An ECA based on silver-coated copper particles containing only 1.3 vol% (7 wt%) silver was demonstrated which exhibited a volume resistivity of (4.3 ± 0.8) 10^{-3} Ω cm, contact resistivity of (0.03 ± 0.01) mΩ cm^2, yield stress of (40 ± 11) Pa and lap-shear strength of (28 ± 6) MPa, a specification set suitable for solar cell shingling. However, the high copper content of 40 wt% is believed to influence the curing kinetics of the polymer resulting in a drastically reduced Young's Modulus of only (34 ± 13) MPa instead of 1000 MPa at identical curing conditions.

A highly-filled reference ECA containing 20 vol% silver was compared with a low-filled ECA containing between 5 and 10 vol% silver, in addition to formulations based on silver-coated glass/silver and silver-coated-copper particles, at module level. The different rheological properties of the ECAs required individual adjustment of preheat temperature and dispensing pressure to obtain the same dispensed volume with all ECAs. All modules exhibited similar good initial performance and stability under damp heat conditions, confirming resistance to oxidation. Under aging conditions, the low-filled silver-based ECA slightly outperformed the highly-filled reference. This was attributed to the lower elastic modulus resulting from the reduced particle content. However, four out of six modules fabricated with the highly elastic silver-coated copper ECA failed the TC 200 test. These results indicate that a reduced shear modulus can facilitate stress relaxation. However, too high strains may disrupt the conductive pathways in low-filled ECAs. It therefore appears necessary to define a lower limit for elastic and shear moduli in low-filled ECAs, as indicated by the marks (*) in Table 6.

All in all, the results demonstrate that silver consumption in ECAs can be significantly reduced through two complementary approaches:

(1) decreasing the percolation threshold, for example by applying the capillary suspension concept, and
(2) replacing the conventional silver filler with silver reduced shell-core particles.

ECAs formulated using these strategies achieved comparable performance to highly-filled ECAs, while reducing silver usage by up to 95%, making them a promising alternative for the shingled PV interconnection.

8 Outlook

In this work, epoxy-based ECA formulations with a silver content as low as 1.7 vol% were developed meeting the limiting requirements for solar cell shingling regarding volume resistivity and mechanical strength in the cured state, but also the requirements for sedimentation stability and processing of the uncured system. A further decrease in filler, i.e. silver, consumption requires proper stabilization. Simultaneously, sufficient electrical conductivity must be retained. In this study, the pursued strategy involved decreasing the percolation threshold as well as removing the organic surface layer on the particles. A second approach frequently reported for conductivity enhancement of ECAs is nanoparticle sintering (Chapter 2). For ceramic materials, Weiß et al. [107] demonstrated that nanoparticles can be incorporated into the secondary liquid of capillary suspensions, enabling the nanoparticles to be deposited directly in the contact regions between the microparticles. However, in their ceramic system, the secondary liquid was removed during the debinding process. For ECAs in shingled PV, evaporation of formulation components is believed to be undesirable. Nevertheless, solvent evaporation from the shingle gap and its influence on the cells has not yet been investigated und should be studied in the future. Up to date, secondary liquid or even polymer remains between the particles hindering nanoparticle sintering. Additionally, the polymer curing reaction competes with the sintering process, partially immobilizing the particles. Nevertheless, an alternative particle stabilization mechanism may allow nanoparticle sintering to become feasible even at low filler content.

All ECAs developed in this work were successfully applied to solar cells by jet dispensing and the resulting modules exhibited promising initial performance. It became apparent that dispensing parameters had to be set for any ECA individually to compensate for the slight differences in rheological behavior. A more detailed study on application behavior of ECAs should be performed, to enable the generation of more consistent deposition patterns, allowing the use of only the minimum required amount of adhesive and therefore silver. Especially, when screen printing is chosen as application technique, special attention should be paid to rheological properties such as viscosity, shear thinning or wall slip [115,200].
Bleeding, where polymer spreads from the printed line, is a frequently reported issue with ECAs [235]. It appears that low-filled ECAs are even more prone to bleeding than highly-filled formulations. In the shingled module technology, bleeding is considered to be non-critical provided that the adhesive does not reach the shingle edge. Contrarily, depletion of the polymer from the bulk may bring particles in closer contact, potentially improving conductivity, while the spreading polymer still contributes to the mechanical strength of the joint. Nevertheless, excessive bleeding may reduce user confidence in the product. Therefore, a study should be performed, in which the influence of the bleeding behavior of ECAs on module performance is investigated. Additionally, other formulation concepts should be explored which alter the bleeding behavior of low-filled ECAs, such as the addition of rheology control agents or utilization of a polymer resin with higher viscosity.

In some cases, particles are protruded along with the polymer during bleeding, which leads to the formation of isolated particle agglomerates. This observation suggests that conductivity in the x-y-plane along the entire printed line may not always be necessary, as was demonstrated by printing discrete pads instead of a continuous line. In the latter case, however, mechanical stability was reduced. In the future, the transition from isotropically conductive adhesives to anisotropically conductive adhesives should be investigated. Anisotropically conductive adhesives potentially combine both sufficient conductivity in z-direction and mechanical strength. In such a design, isolated particle aggregates could be embedded within the polymer

matrix instead of individual, well-distributed particles to avoid the need for external pressure application during curing. However, such an approach requires the presence of a busbar on front- and back-sides of the solar cell. Weber et al. [152,163] reported that pressure contact between the busbars after lamination contributed to the interconnection conductivity, which would not be possible if the non-conductive polymer acted as a spacer between the busbars.
Alternatively, the silver busbars could be omitted as demonstrated by Oh et al. [121]. In this case, a continuous isotropically conductive adhesive line would be required. Otherwise, extremely precise alignment of the metallization fingers would be necessary, which is difficult to obtain due to their small width. In past studies, ECA has primarily been applied onto busbar metallization. Therefore, adhesion between solar cell and adhesive lacks representative examination and requires further investigation. In the end, for the most feasible contact design, i.e. maximum silver reduction in either ECA or busbar, module performance in relation to cost needs to be balanced against each other.

Another design concept is matrix shingling. In contrast to linear shingling, where each cell is connected to a single adjacent cell forming cell strings connected in series, in matrix shingling every second row is shifted by half a cell, resulting in simultaneous series and parallel electrical interconnection of solar cells [205]. In such a configuration, mechanical stresses at a single point within the cell matrix affect the whole composite instead of only one string and the dominant stress direction is no longer confined to a single axis. Experiments indicate that inhomogeneous temperature distribution during curing can already induce significant stresses which could cause bending of the entire assembly. As a result, ECA specifications developed for linear shingling might not be directly transferable to matrix shingling. Especially, the mechanical properties of the ECA, in particular shear and elastic moduli, may require adjustment, and an appropriate specification range should be identified in the future.

To account for modified specifications or further improve the existing formulations, alternative material combinations should be considered. Different epoxy resin systems offer a broad range of material properties, while silicone-based matrices may offer more flexible alternatives. Interaction between polymer matrix and filler particles may also be an important factor, especially when particles containing copper are used. The change in curing kinetics and the resulting low Young's Modulus observed in the epoxy-based ECA containing silver-coated copper particles may be avoided when an alternative polymer or curing agent is employed.
Further silver reduction could potentially be achieved by incorporating carbon-based fillers into the polymer matrix. However, preliminary experiments indicated that only a few vol% of, e.g. carbon black, graphite or carbon nanotubes, are necessary to induce a yield stress and therefore sedimentation stability in carbon-based ECAs. In contrast, achieving sufficient electrical conductivity requires significantly higher particle packing densities, resulting in highly elastic, rubber-like pastes which cannot be processed. Furthermore, substrate adhesion and cohesive strength of the ECA suffer from high particle loading. Future research should investigate solvent-based ECAs as a strategy to temporarily reduce the viscosity of the formulation and enable dispensing or screen printing. After evaporation of the solvent, the close packing required for conductivity would be retained. However, the presence of solvents may be critical in shingled ECA bonds and mechanical strength of the carbon-based ECA should be evaluated.
Alternatively, a thermoplastic polymer could be employed. For application, the polymer could be heated to achieve suitable flow behavior, while forming a stable, conductive interconnect after cooling. Preliminary results regarding thermoplastic ECAs have already been reported [79,236]. Nevertheless, further development is required before such materials reach the level of technological maturity necessary for solar cell shingling application.

References

[1] R. Lindsey, L. Dahlman, Climate Change: Global Temperature, climate.gov, 2025. https://www.climate.gov/news-features/understanding-climate/climate-change-global-temperature (accessed March 9, 2026).

[2] C. Fetting, "The European Green Deal," ESDN Office, Vienna, 2020.

[3] D. Bogdanov, M. Ram, A. Aghahosseini, A. Gulagi, A.S. Oyewo, M. Child, U. Caldera, K. Sadovskaia, J. Farfan, L. De Souza Noel Simas Barbosa, M. Fasihi, S. Khalili, T. Traber, C. Breyer, Low-cost renewable electricity as the key driver of the global energy transition towards sustainability, Energy 227 (2021) 120467. https://doi.org/10.1016/j.energy.2021.120467.

[4] VDMA, International Technology Roadmap for Photovoltaic (ITRPV) 2024 Results, Frankfurt am Main, 2025.

[5] Fraunhofer ISE, Photovoltaics Report, Fraunhofer Institute for Solar Energy Systems ISE, Freiburg, 2025. https://www.ise.fraunhofer.de/de/veroeffentlichungen/studien/photovoltaics-report.html (accessed April 15, 2026).

[6] K.T. VanSant, A.C. Tamboli, E.L. Warren, III-V-on-Si Tandem Solar Cells, Joule 5 (2021) 514–518. https://doi.org/10.1016/j.joule.2021.01.010.

[7] S.F. Ahmed, N. Islam, P.S. Kumar, A.T. Hoang, M. Mofijur, A. Inayat, G.M. Shafiullah, D.-V.N. Vo, I.A. Badruddin, S. Kamangar, Perovskite solar cells: Thermal and chemical stability improvement, and economic analysis, Materials Today Chemistry 27 (2023) 101284. https://doi.org/10.1016/j.mtchem.2022.101284.

[8] DIRECTIVE 2011/65/EU OF THE EUROPEAN PARLIAMENT AND OF THE COUNCIL of 8 June 2011 on the restriction of the use of certain hazardous substances in electrical and electronic equipment, 2011.

[9] R. Aradhana, S. Mohanty, S.K. Nayak, A review on epoxy-based electrically conductive adhesives, International Journal of Adhesion and Adhesives 99 (2020) 102596. https://doi.org/10.1016/j.ijadhadh.2020.102596.

[10] H. Wolfson, G. Elliott, Electrically Conductive Cements Containing Epoxy Resin and Silver, 1956. https://patentimages.storage.googleapis.com/3f/11/41/116238f66323b0/US2774747.pdf.

[11] M.J. Yim, Y. Li, K. Moon, K.W. Paik, C.P. Wong, Review of Recent Advances in Electrically Conductive Adhesive Materials and Technologies in Electronic Packaging, Journal of Adhesion Science and Technology 22 (2008) 1593–1630. https://doi.org/10.1163/156856108X320519.

[12] D. Tune, T. Rößler, G. Oreski, C. Carriere, C. Kaiser, T. Timofte, N. Klasen, J. Weber, B. Jäckel, S. Großer, M. Pander, M. Turek, M. Galiazzo, M.I. Devoto, T. Fischer, I. Ullmann, D. Rudolph, A. Halm, The sun is rising on conductive adhesives, PVI (2022) 57–76.

[13] T. Rößler, D. Von Kutzleben, N. Klasen, V. Nikitina, P. Baliozian, A. Münzer, E. Fokuhl, A. Kraft, Progress in shingle interconnection based on electrically conductive adhesives at Fraunhofer ISE, in: Bhubaneswar, India, 2022: p. 020012. https://doi.org/10.1063/5.0127455.

[14] Li Li, J E Morris, AN INTRODUCTION TO ELECTRICALLY CONDUCTIVE ADHESIVES, International Journal of Microelectronics Packaging (1996).

[15] W. Qiao, H. Bao, X. Li, S. Jin, Z. Gu, Research on electrical conductive adhesives filled with mixed filler, International Journal of Adhesion and Adhesives 48 (2014) 159–163. https://doi.org/10.1016/j.ijadhadh.2013.07.001.

[16] R. Zhang, J.C. Agar, C.P. Wong, Recent advances on Electrically Conductive Adhesives, in: 2010 12th Electronics Packaging Technology Conference, IEEE, 2010: pp. 696–704. https://doi.org/10.1109/EPTC.2010.5702728.

[17] H.J. Lewis, F.M. Coughlan, An Overview of the Use of Electrically Conductive Adhesives (ECAs) as a Solder Replacement, Journal of Adhesion Science and Technology 22 (2008) 801–813. https://doi.org/10.1163/156856108X305543.
[18] M.I. Devoto Acevedo, R. Wells, S. Großer, K. Wienands, D. Rudolph, A. Halm, R. Gottschalg, D. Tune, The effects of increasing filler loading on the contact resistivity of interconnects based on silver–epoxied conductive adhesives and silver metallization pastes, Progress in Photovoltaics (2024) pip.3787. https://doi.org/10.1002/pip.3787.
[19] G. Oreski, S. Pötz, A. Omazic, G. Eder, L. Neumaier, C. Hischl, R. Ebner, J. Scheurer, W. Pranger, Reliability of electrically conductive adhesives, (2019).
[20] S. Khairul Anuar, M. Mariatti, A. Azizan, N. Chee Mang, W.T. Tham, Effect of different types of silver and epoxy systems on the properties of silver/epoxy conductive adhesives, Journal of Materials Science: Materials in Electronics 22 (2011) 757–764. https://doi.org/10.1007/s10854-010-0207-7.
[21] D. Klosterman, L. Li, J.E. Morris, Materials Characterization, Conduction Development, and Curing Effects on Reliability of Isotropically Conductive Adhesives, IEEE TRANSACTIONS ON COMPONENTS, PACKAGING, AND MANUFACTURING TECHNOLOGY—PART A 21 (1998). https://ieeexplore.ieee.org/stamp/stamp.jsp?tp=&arnumber=679028.
[22] F. Zhang, N. Tang, Q. Jiang, K. Qi, X. Zhu, Z. Luo, X. Kong, D. Zang, H. Liu, B. Fang, Progress in polyacrylate-based electrically conductive adhesives: Featured properties, preparation, applications, and perspectives, Polymer Composites (2024) pc.28188. https://doi.org/10.1002/pc.28188.
[23] E. Sancaktar, L. Bai, Electrically Conductive Epoxy Adhesives, Polymers 3 (2011) 427–466. https://doi.org/10.3390/polym3010427.
[24] H.K. Kim, F.G. Shi, Electrical reliability of electrically conductive adhesive joints: dependence on curing condition and current density, Microelectronics Journal 32 (2001) 315–321. https://doi.org/10.1016/S0026-2692(01)00007-6.
[25] D. Lu, Q.K. Tong, C.P. Wong, A study of lubricants on silver flakes for microelectronics conductive adhesives, IEEE Transactions on Components and Packaging Technologies 22 (1999) 365–371. https://doi.org/10.1109/6144.796536.
[26] D. Lu, C.P. Wong, Characterization of Silver Flake Lubricants, Journal of Thermal Analysis and Calorimetry 59 (2000) 729–740. https://doi.org/10.1023/A:1010193402130.
[27] D. Lu, C.P. Wong, Thermal Decomposition of Silver Flake Lubricants, Journal of Thermal Analysis and Calorimetry 61 (2000) 3–12. https://doi.org/10.1023/A:1010112318648.
[28] P. Si, J. Trinidad, L. Chen, B. Lee, A. Chen, J. Persic, R. Lyn, Z. Leonenko, B. Zhao, PEDOT:PSS nano-gels for highly electrically conductive silver/epoxy composite adhesives, Journal of Materials Science: Materials in Electronics 29 (2018) 1837–1846. https://doi.org/10.1007/s10854-017-8093-x.
[29] S. Fukumoto, K. Makimoto, K. Ohta, T. Nakamura, M. Matsushima, K. Fujimoto, Change in electrical conductivity of electrically conductive adhesives during curing process, J Mater Sci 57 (2022) 11189–11201. https://doi.org/10.1007/s10853-022-07305-6.
[30] Y. Li, D. Lu, C.P. Wong, Electrical Conductive Adhesives with Nanotechnologies, Springer US, 2010. https://doi.org/10.1007/978-0-387-88783-8.
[31] M. Springer, N. Bosco, Linear viscoelastic characterization of electrically conductive adhesives used as interconnect in photovoltaic modules, Progress in Photovoltaics 28 (2020) 659–681. https://doi.org/10.1002/pip.3257.
[32] M.I. Devoto Acevedo, K. Wienands, A. Halm, R. Gottschalg, D. Tune, Environmental Stability of the Contact Resistivity of Interconnects Based on Electrically Conductive Adhesives and its Correlation to Photovoltaic Module Power Loss under Accelerated Aging Testing†, IEEJ Transactions Elec Engng (2025) tee.70048. https://doi.org/10.1002/tee.70048.
[33] M. Pander, S. Schulze, M. Ebert, Mechanical Modelling of Electrically Conductive Adhesives for Photovoltaic Applications, 29th European Photovoltaic Solar Energy Conference and

Exhibition; 3399-3405 (2014) 7 pages, 13960 kb. https://doi.org/10.4229/EUPVSEC20142014-5DV.3.39.

[34] D. Lu, C.P. Wong, Effects of shrinkage on conductivity of isotropic conductive adhesives, International Journal of Adhesion and Adhesives 20 (2000) 189–193. https://doi.org/10.1016/S0143-7496(99)00039-1.

[35] Y. Sakaniwa, Y. Tada, M. Inoue, Effect of chemical factors on the evolution of electrical conductivity during curing in Ag-loaded conductive adhesives composed of an epoxy-based binder — A new understanding of electrically conductive adhesives, in: 2014 International Conference on Electronics Packaging (ICEP), IEEE, Toyama, Japan, 2014: pp. 176–180. https://doi.org/10.1109/ICEP.2014.6826684.

[36] M.I. Devoto Acevedo, S. Großer, K. Wienands, T. Timofte, A. Halm, R. Gottschalg, D. Tune, Influence of micro– and macrostructure when determining the contact resistivity of interconnects based on electrically conductive adhesives, Solar Energy Materials and Solar Cells 260 (2023) 112490. https://doi.org/10.1016/j.solmat.2023.112490.

[37] I. Miccoli, F. Edler, H. Pfnür, C. Tegenkamp, The 100th anniversary of the four-point probe technique: the role of probe geometries in isotropic and anisotropic systems, J. Phys.: Condens. Matter 27 (2015) 223201. https://doi.org/10.1088/0953-8984/27/22/223201.

[38] ASTM International, Standard Test Method for Rubber Property—Volume Resistivity Of Electrically Conductive and Antistatic Products, (2020). https://doi.org/10.1520/D0991-89R20.

[39] H.H. Berger, Contact Resistance and Contact Resistivity, J. Electrochem. Soc. 119 (1972) 507. https://doi.org/10.1149/1.2404240.

[40] D.L. Meier, D.K. Schroder, Contact resistance: Its measurement and relative importance to power loss in a solar cell, IEEE Trans. Electron Devices 31 (1984) 647–653. https://doi.org/10.1109/T-ED.1984.21584.

[41] M.I. Devoto, T. Timofte, A. Halm, D. Tune, MEASURING THE CONTACT RESISTIVITY OF ECA-BASED JOINTS, in: 2020. https://doi.org/10.4229/EUPVSEC20202020-4AV.1.26.

[42] M.I. Devoto, T. Timofte, A. Halm, D. Tune, Improved Measurement of the Contact Resistivity of ECA-Based Joints, in: 2021. https://doi.org/10.4229/EUPVSEC20212021-4BO.5.6.

[43] M.I. Devoto, K. Wienands, D. Rudolph, T. Timofte, A. Halm, R. Gottschalg, D. Tune, Validation of methodology to determine the contact resistivity of ECA-based bonds grounded on end–contact resistance measurements using redundant and modified TLM test structures, Solar Energy Materials and Solar Cells 262 (2023) 112518. https://doi.org/10.1016/j.solmat.2023.112518.

[44] C. Yang, C.P. Ching Ping Wong, M.M.F. Yuen, Printed electrically conductive composites: Conductive filler designs and surface engineering, Journal of Materials Chemistry C 1 (2013) 4052–4069. https://doi.org/10.1039/c3tc00572k.

[45] Y. Li, K. Moon, C.P. Wong, Electrical property improvement of electrically conductive adhesives through in-situ replacement by short-chain difunctional acids, IEEE Transactions on Components and Packaging Technologies 29 (2006) 173–178. https://doi.org/10.1109/TCAPT.2006.870388.

[46] Y. Li, K. Moon, A. Whitman, C.P. Wong, Enhancement of Electrical Properties of Electrically Conductive Adhesives (ECAs) by Using Novel Aldehydes, IEEE Transactions on Components and Packaging Technologies 29 (2006) 758–763. https://doi.org/10.1109/TCAPT.2006.885940.

[47] E.B. Choi, J.-H. Lee, Enhancement in electrical conductivity of pastes containing submicron Ag-coated Cu filler with palmitic acid surface modification, Applied Surface Science 415 (2017) 67–74. https://doi.org/10.1016/j.apsusc.2017.01.006.

[48] H.-W. Cui, Q. Fan, D.-S. Li, Surface functionalization of micro silver flakes and their application in electrically conductive adhesives for electronic package, International Journal of Adhesion and Adhesives 48 (2014) 177–182. https://doi.org/10.1016/j.ijadhadh.2013.09.036.

[49] F. Tan, X. Qiao, J. Chen, Removal of chemisorbed lubricant on the surface of silver flakes by chemicals, Applied Surface Science 253 (2006) 703–707. https://doi.org/10.1016/j.apsusc.2005.12.163.
[50] F. Tan, X. Qiao, J. Chen, H. Wang, Effects of coupling agents on the properties of epoxy-based electrically conductive adhesives, International Journal of Adhesion and Adhesives 26 (2006) 406–413. https://doi.org/10.1016/j.ijadhadh.2005.06.005.
[51] C. Li, Q. Li, L. Cheng, T. Li, H. Lu, L. Tang, K. Zhang, S. E, J. Zhang, Z. Li, Y. Yao, Conductivity enhancement of polymer composites using high-temperature short-time treated silver fillers, Composites Part A: Applied Science and Manufacturing 100 (2017) 64–70. https://doi.org/10.1016/j.compositesa.2017.05.007.
[52] B. Meschi Amoli, A. Hu, N.Y. Zhou, B. Zhao, Recent progresses on hybrid micro–nano filler systems for electrically conductive adhesives (ECAs) applications, Journal of Materials Science: Materials in Electronics 26 (2015) 4730–4745. https://doi.org/10.1007/s10854-015-3016-1.
[53] H. Gao, L. Liu, Y. Luo, D. Jia, In-situ preparation of epoxy/silver nanocomposites by thermal decomposition of silver–imidazole complex, Materials Letters 65 (2011) 3529–3532. https://doi.org/10.1016/j.matlet.2011.07.086.
[54] Y.-J. Cheng, D.N. Zeiger, J.A. Howarter, X. Zhang, N.J. Lin, J.M. Antonucci, S. Lin-Gibson, In situ formation of silver nanoparticles in photocrosslinking polymers, Journal of Biomedical Materials Research. Part B, Applied Biomaterials 97 (2011) 124–131. https://doi.org/10.1002/jbm.b.31793.
[55] E. Fantino, A. Chiappone, F. Calignano, M. Fontana, F. Pirri, I. Roppolo, In Situ Thermal Generation of Silver Nanoparticles in 3D Printed Polymeric Structures, Materials 9 (2016) 589. https://doi.org/10.3390/ma9070589.
[56] M.-H. Lee, S.-G. Oh, K.-D. Suh, D.-G. Kim, D. Sohn, Preparation of silver nanoparticles in hexagonal phase formed by nonionic Triton X-100 surfactant, Colloids and Surfaces A: Physicochemical and Engineering Aspects 210 (2002) 49–60. https://doi.org/10.1016/S0927-7757(02)00214-5.
[57] H. Gao, L. Liu, K. Liu, Y. Luo, D. Jia, J. Lu, Preparation of highly conductive adhesives by in situ generated and sintered silver nanoparticles during curing process, Journal of Materials Science: Materials in Electronics 23 (2012) 22–30. https://doi.org/10.1007/s10854-011-0388-8.
[58] C. Luo, Y. Zhang, X. Zeng, Y. Zeng, Y. Wang, The role of poly(ethylene glycol) in the formation of silver nanoparticles, Journal of Colloid and Interface Science 288 (2005) 444–448. https://doi.org/10.1016/j.jcis.2005.03.005.
[59] K. Shameli, M. Bin Ahmad, S.D. Jazayeri, S. Sedaghat, P. Shabanzadeh, H. Jahangirian, M. Mahdavi, Y. Abdollahi, Synthesis and characterization of polyethylene glycol mediated silver nanoparticles by the green method, International Journal of Molecular Sciences 13 (2012) 6639–6650. https://doi.org/10.3390/ijms13066639.
[60] S. Chen, K. Liu, Y. Luo, D. Jia, H. Gao, G. Hu, L. Liu, In situ preparation and sintering of silver nanoparticles for low-cost and highly reliable conductive adhesive, International Journal of Adhesion and Adhesives 45 (2013) 138–143. https://doi.org/10.1016/j.ijadhadh.2013.04.004.
[61] S.-S. Chee, J.-H. Lee, Reduction synthesis of silver nanoparticles anchored on silver micro-flakes and electrical resistivity of isotropic conductive adhesives at percolation threshold, Electronic Materials Letters 8 (2012) 315–320. https://doi.org/10.1007/s13391-012-1105-3.
[62] D.I. Tee, M. Mariatti, A. Azizan, C.H. See, K.F. Chong, Effect of silane-based coupling agent on the properties of silver nanoparticles filled epoxy composites, Composites Science and Technology 67 (2007) 2584–2591. https://doi.org/10.1016/j.compscitech.2006.12.007.
[63] X. Yang, W. He, S. Wang, G. Zhou, Y. Tang, Preparation and properties of a novel electrically conductive adhesive using a composite of silver nanorods, silver nanoparticles, and

modified epoxy resin, Journal of Materials Science: Materials in Electronics 23 (2012) 108–114. https://doi.org/10.1007/s10854-011-0485-8.

[64] D. Chen, X. Qiao, X. Qiu, F. Tan, J. Chen, R. Jiang, Effect of silver nanostructures on the resistivity of electrically conductive adhesives composed of silver flakes, Journal of Materials Science: Materials in Electronics 21 (2010) 486–490. https://doi.org/10.1007/s10854-009-9943-y.

[65] N. Hameed, J.C. Capricho, N. Salim, S. Thomas, eds., Multifunctional Epoxy Resins: Self-Healing, Thermally and Electrically Conductive Resins, 1st ed. 2023, Springer Nature Singapore and Springer, Singapore, 2023. https://doi.org/10.1007/978-981-19-6038-3.

[66] B. Hallam, M. Kim, Y. Zhang, L. Wang, A. Lennon, P. Verlinden, P.P. Altermatt, P.R. Dias, The silver learning curve for photovoltaics and projected silver demand for net-zero emissions by 2050, Progress in Photovoltaics 31 (2023) 598–606. https://doi.org/10.1002/pip.3661.

[67] G. Schramm, Rheology 2 A Practical Approach to Rheology and Rheometry, (2000).

[68] M. Dinkgreve, J. Paredes, M.M. Denn, D. Bonn, On different ways of measuring “the” yield stress, Journal of Non-Newtonian Fluid Mechanics 238 (2016) 233–241. https://doi.org/10.1016/j.jnnfm.2016.11.001.

[69] C. Yüce, N. Willenbacher, Challenges in Rheological Characterization of Highly Concentrated Suspensions - A Case Study for Screen-printing Silver Pastes, JoVE (2017) 55377. https://doi.org/10.3791/55377.

[70] C. Yang, Y.-T. Xie, M.M.-F. Yuen, B. Xu, B. Gao, X. Xiong, C.P. Wong, Silver Surface Iodination for Enhancing the Conductivity of Conductive Composites, Advanced Functional Materials 20 (2010) 2580–2587. https://doi.org/10.1002/adfm.201000673.

[71] J. Marten, J.S. Urallar, T.M. Duong, P. Théato, N. Willenbacher, Iodine-Induced Microphase Separation Controls the Flow Behavior and Electrical Conductivity of Silver-Filled Polymer Composites, ACS Appl. Mater. Interfaces (2025). https://doi.org/10.1021/acsami.5c09040.

[72] H. Wu, S. Chiang, W. Han, Y. Tang, F. Kang, C. Yang, Surface iodination: A simple and efficient protocol to improve the isotropically thermal conductivity of silver-epoxy pastes, Composites Science and Technology 99 (2014) 109–116. https://doi.org/10.1016/j.compscitech.2014.04.021.

[73] C. Li, X. Gong, L. Tang, K. Zhang, J. Luo, L. Ling, J. Pu, T. Li, M. Li, Y. Yao, Electrical property enhancement of electrically conductive adhesives through Ag-coated-Cu surface treatment by terephthalaldehyde and iodine, Journal of Materials Chemistry C 3 (2015) 6178–6184. https://doi.org/10.1039/C5TC00593K.

[74] C. Li, Q. Li, X. Long, T. Li, J. Zhao, K. Zhang, E. Songfeng, J. Zhang, Z. Li, Y. Yao, In Situ Generation of Photosensitive Silver Halide for Improving the Conductivity of Electrically Conductive Adhesives, ACS Applied Materials and Interfaces 9 (2017) 29047–29054. https://doi.org/10.1021/acsami.7b07045.

[75] P. Zheng, H. Zhuo, Y. Zou, W. Guo, H. Wu, Z. Li, Highly-Conductive Stretchable Electrically Conductive Composites by Halogenation Treatment and Its Application in Stretchable Electronics, in: 2018 IEEE 68th Electronic Components and Technology Conference (ECTC), IEEE, San Diego, CA, USA, 2018: pp. 1744–1750. https://doi.org/10.1109/ECTC.2018.00262.

[76] H. Sun, M.M.F. Yuen, Conductivity Enhancement of Thermal Interface Material via Capillary Attraction, in: 2016 IEEE 66th Electronic Components and Technology Conference (ECTC), IEEE, 2016: pp. 1409–1414. https://doi.org/10.1109/ECTC.2016.94.

[77] H. Sun, X. Zhang, M.M.F. Yuen, Enhanced conductivity induced by attractive capillary force in ternary conductive adhesive, Composites Science and Technology 137 (2016) 109–117. https://doi.org/10.1016/j.compscitech.2016.10.028.

[78] H. Sun, Z. Han, N. Willenbacher, Ultrastretchable Conductive Elastomers with a Low Percolation Threshold for Printed Soft Electronics, ACS Applied Materials & Interfaces 11 (2019) 38092–38102. https://doi.org/10.1021/acsami.9b11071.

[79] J. Marten, M. Schnaiter, Y. Zemen, L. Podlowski, S. Ricken, N. Willenbacher, Highly conductive coated wires for interconnection of solar cells with TECC-wire technology, Solar

Energy Materials and Solar Cells 273 (2024) 112966. https://doi.org/10.1016/j.solmat.2024.112966.
[80] E. Koos, N. Willenbacher, Capillary Forces in Suspension Rheology, Science 331 (2011) 897–900. https://doi.org/10.1126/science.1199243.
[81] E. Koos, N. Willenbacher, Particle configurations and gelation in capillary suspensions, Soft Matter 8 (2012) 3988. https://doi.org/10.1039/c2sm07347a.
[82] F. Bossler, E. Koos, Structure of Particle Networks in Capillary Suspensions with Wetting and Nonwetting Fluids, Langmuir 32 (2016) 1489–1501. https://doi.org/10.1021/acs.langmuir.5b04246.
[83] B. Bitsch, B. Braunschweig, N. Willenbacher, Interaction between Polymeric Additives and Secondary Fluids in Capillary Suspensions, Langmuir 32 (2016) 1440–1449. https://doi.org/10.1021/acs.langmuir.5b03861.
[84] J. Maurath, B. Bitsch, Y. Schwegler, N. Willenbacher, Influence of particle shape on the rheological behavior of three-phase non-brownian suspensions, Colloids and Surfaces A: Physicochemical and Engineering Aspects 497 (2016) 316–326. https://doi.org/10.1016/j.colsurfa.2016.03.006.
[85] S. Bindgen, J. Allard, E. Koos, The behavior of capillary suspensions at diverse length scales: From single capillary bridges to bulk, Current Opinion in Colloid & Interface Science 58 (2022) 101557. https://doi.org/10.1016/j.cocis.2021.101557.
[86] C. Haessig, J. Landman, E. Scholten, A. Jarray, How bulk liquid viscosity shapes capillary suspensions, Journal of Colloid and Interface Science 678 (2025) 400–409. https://doi.org/10.1016/j.jcis.2024.09.021.
[87] E. Koos, Capillary suspensions: Particle networks formed through the capillary force, Current Opinion in Colloid & Interface Science 19 (2014) 575–584. https://doi.org/10.1016/j.cocis.2014.10.004.
[88] J. Dittmann, N. Willenbacher, Micro Structural Investigations and Mechanical Properties of Macro Porous Ceramic Materials from Capillary Suspensions, J. Am. Ceram. Soc. 97 (2014) 3787–3792. https://doi.org/10.1111/jace.13184.
[89] T. Domenech, S.S. Velankar, On the rheology of pendular gels and morphological developments in paste-like ternary systems based on capillary attraction, Soft Matter 11 (2015) 1500–1516. https://doi.org/10.1039/C4SM02053G.
[90] F. Bossler, J. Maurath, K. Dyhr, N. Willenbacher, E. Koos, Fractal approaches to characterize the structure of capillary suspensions using rheology and confocal microscopy, Journal of Rheology 62 (2018) 183–196. https://doi.org/10.1122/1.4997889.
[91] E. Koos, J. Johannsmeier, L. Schwebler, N. Willenbacher, Tuning suspension rheology using capillary forces, Soft Matter 8 (2012) 6620. https://doi.org/10.1039/c2sm25681a.
[92] A. Jarray, A. Feichtinger, E. Scholten, Linking intermolecular interactions and rheological behaviour in capillary suspensions, Journal of Colloid and Interface Science 627 (2022) 415–426. https://doi.org/10.1016/j.jcis.2022.07.067.
[93] G. Meng, N. Arkus, M.P. Brenner, V.N. Manoharan, The Free-Energy Landscape of Clusters of Attractive Hard Spheres, Science 327 (2010) 560–563. https://doi.org/10.1126/science.1181263.
[94] K. Hauf, E. Koos, Structure of capillary suspensions and their versatile applications in the creation of smart materials, MRS Communications 8 (2018) 332–342. https://doi.org/10.1557/mrc.2018.28.
[95] F. Bossler, L. Weyrauch, R. Schmidt, E. Koos, Influence of mixing conditions on the rheological properties and structure of capillary suspensions, Colloids and Surfaces A: Physicochemical and Engineering Aspects 518 (2017) 85–97. https://doi.org/10.1016/j.colsurfa.2017.01.026.
[96] T. Domenech, S. Velankar, Capillary-driven percolating networks in ternary blends of immiscible polymers and silica particles, Rheologica Acta 53 (2014) 593–605. https://doi.org/10.1007/s00397-014-0776-0.

[97] S. Hoffmann, E. Koos, N. Willenbacher, Using capillary bridges to tune stability and flow behavior of food suspensions, Food Hydrocolloids 40 (2014) 44–52. https://doi.org/10.1016/j.foodhyd.2014.01.027.
[98] O. Ranquet, C. Duce, E. Bramanti, P. Dietemann, I. Bonaduce, N. Willenbacher, A holistic view on the role of egg yolk in Old Masters' oil paints, Nat Commun 14 (2023) 1534. https://doi.org/10.1038/s41467-023-36859-5.
[99] S.S. Velankar, A non-equilibrium state diagram for liquid/fluid/particle mixtures, Soft Matter 11 (2015) 8393–8403. https://doi.org/10.1039/C5SM01901J.
[100] J. Allard, S. Burgers, M.C. Rodríguez González, Y. Zhu, S. De Feyter, E. Koos, Effects of particle roughness on the rheology and structure of capillary suspensions, Colloids and Surfaces A: Physicochemical and Engineering Aspects 648 (2022) 129224. https://doi.org/10.1016/j.colsurfa.2022.129224.
[101] T.S. Dunstan, A.A.K. Das, P. Starck, S.D. Stoyanov, V.N. Paunov, Capillary Structured Suspensions from *In Situ* Hydrophobized Calcium Carbonate Particles Suspended in a Polar Liquid Media, Langmuir 34 (2018) 442–452. https://doi.org/10.1021/acs.langmuir.7b03589.
[102] L. Ruiz-Martínez, F. Leermakers, S. Stoyanov, J. Van Der Gucht, Tunable Capillary Suspensions from Aqueous Two-Phase Systems, Langmuir 41 (2025) 11604–11613. https://doi.org/10.1021/acs.langmuir.5c00749.
[103] R. Kazama, Y. Murakami, A. Shono, Microstructure and rheological behavior of capillary suspension prepared with plate-shaped particles, Colloids and Surfaces A: Physicochemical and Engineering Aspects 637 (2022) 128254. https://doi.org/10.1016/j.colsurfa.2022.128254.
[104] K. Kulkarni, M. Tiwari, H. Lama, C. Clasen, V.R. Dugyala, Capillary bridging and microstructural evolution in suspensions of cube-shaped particles: The role of wettability and structural ordering, Journal of Colloid and Interface Science 706 (2026) 139694. https://doi.org/10.1016/j.jcis.2025.139694.
[105] B. Bitsch, J. Dittmann, M. Schmitt, P. Scharfer, W. Schabel, N. Willenbacher, A novel slurry concept for the fabrication of lithium-ion battery electrodes with beneficial properties, Journal of Power Sources 265 (2014) 81–90. https://doi.org/10.1016/j.jpowsour.2014.04.115.
[106] B. Bitsch, T. Gallasch, M. Schroeder, M. Börner, M. Winter, N. Willenbacher, Capillary suspensions as beneficial formulation concept for high energy density Li-ion battery electrodes, Journal of Power Sources 328 (2016) 114–123. https://doi.org/10.1016/j.jpowsour.2016.07.102.
[107] M. Weiß, P. Sälzler, N. Willenbacher, E. Koos, 3D-Printed lightweight ceramics using capillary suspensions with incorporated nanoparticles, Journal of the European Ceramic Society 40 (2020) 3140–3147. https://doi.org/10.1016/j.jeurceramsoc.2020.02.055.
[108] D. Menne, L. Lemos Da Silva, M. Rotan, J. Glaum, M. Hinterstein, N. Willenbacher, Giant Functional Properties in Porous Electroceramics through Additive Manufacturing of Capillary Suspensions, ACS Appl. Mater. Interfaces 14 (2022) 3027–3037. https://doi.org/10.1021/acsami.1c19297.
[109] J. Maurath, J. Dittmann, N. Schultz, N. Willenbacher, Fabrication of highly porous glass filters using capillary suspension processing, Separation and Purification Technology 149 (2015) 470–478. https://doi.org/10.1016/j.seppur.2015.06.022.
[110] K. Tedjokusuma, W. Lauth, N. Willenbacher, Manufacture and filtration performance of glass filters made from capillary suspensions, Separation and Purification Technology 329 (2024) 125097. https://doi.org/10.1016/j.seppur.2023.125097.
[111] S. Nider, F. De Ceulaer, B. Göksel, A. Braem, E. Koos, Hierarchical materials with interconnected pores from capillary suspensions for bone tissue engineering, J Am Ceram Soc. 108 (2025) e20179. https://doi.org/10.1111/jace.20179.
[112] M. Schneider, E. Koos, N. Willenbacher, Highly conductive, printable pastes from capillary suspensions, Scientific Reports 6 (2016) 31367. https://doi.org/10.1038/srep31367.

[113] R. Xing, J. Yang, D. Zhang, W. Gong, T.V. Neumann, M. Wang, R. Huang, J. Kong, W. Qi, M.D. Dickey, Metallic gels for conductive 3D and 4D printing, Matter 6 (2023) 2248–2262. https://doi.org/10.1016/j.matt.2023.06.015.
[114] S. Zhao, K. Hu, M. Huang, J. Hong, H. Wu, D. Zou, P. Zhu, Y. Chen, Optimization of capillary suspension silver pastes for enhanced metallization in silicon solar Cells: A comparative analysis of Screen-Printing and pattern transfer printing, Solar Energy 277 (2024) 112746. https://doi.org/10.1016/j.solener.2024.112746.
[115] M. Ailinger, K. Abdel Aal, N. Willenbacher, Rheology and fine-line screen printing of solar cell front-side metallization pastes – What really matters, Solar Energy Materials and Solar Cells 292 (2025) 113763. https://doi.org/10.1016/j.solmat.2025.113763.
[116] C. Zhang, J. Zhang, X. Ma, Q. Feng, Semiconductor Photovoltaic Cells, Springer Singapore, Singapore, 2021. https://doi.org/10.1007/978-981-15-9480-9.
[117] Y. Abou Jieb, E. Hossain, Photovoltaic Systems: Fundamentals and Applications, Springer International Publishing, Cham, 2022. https://doi.org/10.1007/978-3-030-89780-2.
[118] A. Rachid, A. Goren, V. Becerra, J. Radulovic, S. Khanna, Solar Energy Engineering and Applications, Springer International Publishing, Cham, 2023. https://doi.org/10.1007/978-3-031-20830-0.
[119] VDMA, International Technology Roadmap for Photovoltaic (ITRPV) 2022 Results, Frankfurt am Main, 2023.
[120] D.K. Ghosh, S. Bose, G. Das, S. Acharyya, A. Nandi, S. Mukhopadhyay, A. Sengupta, Fundamentals, present status and future perspective of TOPCon solar cells: A comprehensive review, Surfaces and Interfaces 30 (2022) 101917. https://doi.org/10.1016/j.surfin.2022.101917.
[121] W. Oh, H. Jee, J. Bae, J. Lee, Busbar-free electrode patterns of crystalline silicon solar cells for high density shingled photovoltaic module, SOLAR ENERGY MATERIALS AND SOLAR CELLS 243 (2022). https://doi.org/10.1016/j.solmat.2022.111802.
[122] D. Tune, K. Wienands, I. Ullmann, M.I. Devoto, T. Timofte, A. Halm, ELECTRICALLY CONDUCTIVE ADHESIVE INTERCONNECTS: HOW LOW CAN YOU GO?, in: 2021: pp. 735–738.
[123] D.C. Dickson, Photo-voltaic semiconductor apparatus or the like, U.S. Patent No. 2938938A, 1960.
[124] M.A. Green, Event Report. Brain Sport: The 1996 World Solar Challenge Solar Car Race Across Australia, Prog. Photovolt: Res. Appl. 5 (1997) 69–76. https://doi.org/10.1002/(SICI)1099-159X(199701/02)5:1<69::AID-PIP157>3.0.CO;2-N.
[125] D. Tonini, G. Cellere, M. Bertazzo, A. Fecchio, L. Cerasti, M. Galiazzo, Shingling Technology For Cell Interconnection: Technological Aspects And Process Integration, Energy Procedia 150 (2018) 36–43. https://doi.org/10.1016/j.egypro.2018.09.010.
[126] N. Klasen, D. Weisser, T. Roessler, D.H. Neuhaus, A. Kraft, Performance of shingled solar modules under partial shading, PROGRESS IN PHOTOVOLTAICS 30 (2022) 325–338. https://doi.org/10.1002/pip.3486.
[127] A.X. Chen, N.A. Azpiroz, S.E. Brew, A.M. Valdez, G.L. Esparza, Y. Qie, N.J. Valdez, R. Blau, J.A. Bunch, T.J. Perry, T. Rafeedi, A. Abdal, I. Simon, D.W. Harwood, D.J. Lipomi, D.P. Fenning, Silver-free intrinsically conductive adhesives for shingled solar cells, Cell Reports Physical Science 5 (2024) 101967. https://doi.org/10.1016/j.xcrp.2024.101967.
[128] H. Son, H. Lim, J. Moon, D. Jun, B.-K. Ju, S. Kim, Investigating the reliability of electrically conductive adhesives for shingled photovoltaic Si modules, Solar Energy Materials and Solar Cells 236 (2022) 111403. https://doi.org/10.1016/j.solmat.2021.111403.
[129] The Silver Institute, Word Silver Survey 2025, The Silver Institute, Washington, 2025. https://silverinstitute.org/wp-content/uploads/2025/04/World_Silver_Survey-2025.pdf.
[130] V. Cattaneo, J. Mast, I. Hackenhaar, S. Nardone, S. Scheerlinck, J. Mertens, J. Dewulf, Forecasting silver demand and supply by 2030: Impact of silver-intensive photovoltaic cells

and sectoral competition, Resources, Conservation and Recycling 224 (2026) 108562. https://doi.org/10.1016/j.resconrec.2025.108562.

[131] B. Hartweg, K. Fisher, S. Niverty, N. Chawla, Z. Holman, Analysis of electrically conductive adhesives in shingled solar modules by X-ray imaging techniques, Microelectronics Reliability 136 (2022) 114627. https://doi.org/10.1016/j.microrel.2022.114627.

[132] M. Pudas, J. Hagberg, S. Leppävuori, Gravure offset printing of polymer inks for conductors, Progress in Organic Coatings 49 (2004) 324–335. https://doi.org/10.1016/j.porgcoat.2003.09.013.

[133] A. Reithe, M. Münch, K.-J. Wolter, Effect of surface treatment on the conductive adhesive interconnection of flexible solar cells, in: 2012: pp. 117–122. https://doi.org/10.1109/ISSE.2012.6273120.

[134] M.I. Devoto, T. Timofte, A. Halm, D. Tune, Contact resistivity of ECA bonded joints, in: 2021 AIP Conference Proceedings 2367, 2021: p. 020011. https://doi.org/10.1063/5.0055980.

[135] L. Theunissen, B. Willems, J. Burke, D. Tonini, M. Galiazzo, A. Henckens, Electrically conductive adhesives as cell interconnection material in shingled module technology, in: 2018 AIP Conference Proceedings 1999, 2018: p. 080003. https://doi.org/10.1063/1.5049305.

[136] J. Weber, S. Hoffmann, K. Kaufmann, A. de Rose, Magnetic Field Imaging (MFI) of Shingle Solar Modules, in: 2022: pp. 1424–1427. https://doi.org/10.1109/PVSC48317.2022.9938644.

[137] S. Chowdhury, E.-C. Cho, Y. Cho, Y. Kim, J. Yi, Analysis of Cell to Module Loss Factor for Shingled PV Module, New & Renewable Energy 16 (2020). https://doi.org/10.7849/ksnre.2020.0009.

[138] G. Beaucarne, Materials Challenge for Shingled Cells Interconnection, Energy Procedia 98 (2016) 115–124. https://doi.org/10.1016/j.egypro.2016.10.087.

[139] S. Harrison, C. Carriere, V. Barth, A. Bettinelli, P. Bertrand, B. Portaluppi, 400W in Shingle SHJ configuration: promising optimization path for high power modules, in: 2021 IEEE 48th Photovoltaic Specialists Conference (PVSC), 2021: pp. 0331–0334. https://doi.org/10.1109/PVSC43889.2021.9518854.

[140] V. Nikitina, C. Reichel, D. Erath, S. Kirner, A. Richter, T. Roessler, A. De Rose, A. Kraft, H. Neuhaus, Shingling meets perovskite-silicon heterojunction tandem solar cells, SOLAR ENERGY MATERIALS AND SOLAR CELLS 263 (2023). https://doi.org/10.1016/j.solmat.2023.112590.

[141] A. Louwen, W. van Sark, R. Schropp, A. Faaij, A cost roadmap for silicon heterojunction solar cells, SOLAR ENERGY MATERIALS AND SOLAR CELLS 147 (2016) 295–314. https://doi.org/10.1016/j.solmat.2015.12.026.

[142] S.R. Pettersen, K. Redford, J. Njagi, H. Kristiansen, S. Helland, E. Kalland, D.V. Goia, Z. Zhang, J. He, Room-Temperature Curing and Grain Growth at High Humidity in Conductive Adhesives with Ultra-Low Silver Content, Journal of Electronic Materials 46 (2017) 4256–4266. https://doi.org/10.1007/s11664-017-5376-1.

[143] M. Mittag, T. Zech, M. Wiese, D. Blasi, M. Ebert, H. Wirth, Cell-to-Module (CTM) Analysis for Photovoltaic Modules with Shingled Solar Cells, in: 2017 IEEE 44th Photovoltaic Specialist Conference (PVSC), IEEE, 2017: pp. 1531–1536. https://doi.org/10.1109/PVSC.2017.8366260.

[144] B. Hartweg, K. Fisher, Z. Holman, Electrically conductive adhesive (ECA) processing for shingled modules analyzed by x-ray imaging, in: 2020: pp. 0340–0341. https://doi.org/10.1109/PVSC45281.2020.9300776.

[145] T. Geipel, U. Eitner, Cure Kinetics of Electrically Conductive Adhesives for Solar Cell Interconnection, IEEE Journal of Photovoltaics 3 (2013) 1208–1214. https://doi.org/10.1109/JPHOTOV.2013.2270356.

[146] A. De Rose, D. Erath, V. Nikitina, J. Schube, D. Güldali, Ä. Minat, T. Rößler, A. Richter, S. Kirner, A. Kraft, A. Lorenz, Low-temperature metallization & interconnection for silicon

heterojunction and perovskite silicon tandem solar cells, Solar Energy Materials and Solar Cells 261 (2023) 112515. https://doi.org/10.1016/j.solmat.2023.112515.
[147] T. Geipel, Electrically Conductive Adhesives for Photovoltaic Modules, PhD Thesis, Fraunhofer ISE, 2018.
[148] H. Jee, S. Lee, C. Jeong, J. Lee, Electrically Conductive Adhesives and the Shingled Array Cell for High Density Modules, JOURNAL OF NANOSCIENCE AND NANOTECHNOLOGY 19 (2019) 1360–1363. https://doi.org/10.1166/jnn.2019.16200.
[149] H. Jee, J. Song, D. Moon, J. Lee, C. Jeong, Improvement in Power of Shingled Solar Cells for Photo-Voltaic Module, JOURNAL OF NANOSCIENCE AND NANOTECHNOLOGY 20 (2020) 7096–7099. https://doi.org/10.1166/jnn.2020.18830.
[150] J. Park, W. Oh, H. Park, C. Jeong, B. Choi, J. Lee, Analysis of solar cells interconnected by electrically conductive adhesives for high-density photovoltaic modules, Applied Surface Science 484 (2019) 732–739. https://doi.org/10.1016/j.apsusc.2019.03.307.
[151] J. Weber, T. Roessler, How to assess the electrical quality of solar cell interconnection in shingle solar modules, PROGRESS IN PHOTOVOLTAICS 31 (2023) 949–959. https://doi.org/10.1002/pip.3699.
[152] J. Weber, A. Krieg, T. Roessler, Applying and evaluating a new method to determine the interconnection-induced resistance in shingle solar modules, SOLAR ENERGY MATERIALS AND SOLAR CELLS 269 (2024). https://doi.org/10.1016/j.solmat.2024.112788.
[153] V. Ivanov, B. Boehme, K.-J. Wolter, Resistance of conductive adhesive joints on non-noble surface finishes, in: 2012: pp. 254–259. https://doi.org/10.1109/ISSE.2012.6273082.
[154] D. Ren, M. Mills, M. DeGroot, L. Clark, S. Brown, J. Curphy, Glass transition temperature as an in situ cure index of electrically conductive adhesives in solar photovoltaic module interconnect assemblies, SOLAR ENERGY MATERIALS AND SOLAR CELLS 107 (2012) 403–406. https://doi.org/10.1016/j.solmat.2012.07.028.
[155] N. Klasen, F. Heinz, A. De Rose, T. Roessler, A. Kraft, M. Kamlah, Root cause analysis of solar cell cracks at shingle joints, SOLAR ENERGY MATERIALS AND SOLAR CELLS 238 (2022). https://doi.org/10.1016/j.solmat.2022.111590.
[156] M. Lang, G. Oreski, E. Helfer, P. Fuchs, A. Halm, M. Klenk, FEM simulation of influence of different polymeric module materials and layouts on thermomechanical deformations in strings of shingled solar cells, in: 2023. https://doi.org/10.1109/EuroSimE56861.2023.10100805.
[157] M. Lang, G. Oreski, E. Helfer, A. Halm, M. Klenk, P. Fuchs, FEM simulation of deformations and stresses in strings of shingled solar cells under mechanical and thermal loading., in: AIP Conference Proceedings, 2022: pp. 1–15. https://research.ebsco.com/linkprocessor/plink?id=0cede921-6925-39d8-8a62-6af2cadbb339.
[158] ASTM International, Standard Test Method for Apparent Shear Strength of Single-Lap-Joint Adhesively Bonded Metal Specimens by Tension Loading (Metal-to- Metal), (2010). https://doi.org/10.1520/D1002-10R19.
[159] ASTM International, Standard Test Method for Tensile Properties of Plastics, (2022). https://doi.org/10.1520/D0638-22.
[160] DIN-Normenausschuss Kunststoffe (FNK), Plastics Standards Committee, DIN EN ISO 20753 Kunststoffe - Probekörper, (2024). https://www.dinmedia.de/de/norm/din-en-iso-20753/376084817.
[161] M. Springer, N. Bosco, Environmental influence on cracking and debonding of electrically conductive adhesives., Engineering Fracture Mechanics 241 (2021) N.PAG-N.PAG.
[162] N. Klasen, P. Romer, A. Beinert, A. Kraft, FEM Simulation of Deformations in Strings of Shingled Solar Cells Subjected to Mechanical Reliability Testing., in: AIP Conference Proceedings, 2019: pp. 020016-1-020016–11. https://research.ebsco.com/linkprocessor/plink?id=d54eaa8c-3837-36e9-96fb-f2291aff06db.

[163] J. Weber, T. Roessler, Electrically conductive adhesive-free interconnection of shingle solar cells, SOLAR ENERGY MATERIALS AND SOLAR CELLS 261 (2023). https://doi.org/10.1016/j.solmat.2023.112517.
[164] NOCT - Standardtemperatur unter Normalbedingungen, (n.d.). https://photovoltaiksolarstrom.com/photovoltaiklexikon/noct/.
[165] DKE Deutsche Komission Elektrotechnik Elektronik Informationstechnik in DIN und VDE, DIN EN IEC 61730 Photovoltaik(PV)-Module – Sicherheitsqualifikation, (2018).
[166] DKE Deutsche Komission Elektrotechnik Elektronik Informationstechnik in DIN und VDE, DIN EN IEC 61215 Terrestrische Photovoltaik(PV)-Module – Bauarteignung und Bauartzulassung, (2022).
[167] T. Potthoff, K. Bothe, U. Eitner, D. Hinken, M. Köntges, Detection of the voltage distribution in photovoltaic modules by electroluminescence imaging, Progress in Photovoltaics 18 (2010) 100–106. https://doi.org/10.1002/pip.941.
[168] L. Veríssimo Mesquita, N. Klasen, E. Fokuhl, D. Philipp, L.P. Bauermann, Analysis of Shingle Interconnections in Solar Modules by Scanning Acoustic Microscopy., in: AIP Conference Proceedings, 2019: pp. 090003-1-090003–8. https://research.ebsco.com/linkprocessor/plink?id=56b454e3-8d93-39ed-9c15-bae8307641d4.
[169] E. Aranda, J. Gomez Galan, M. De Cardona, J. Andujar Marquez, Measuring the I-V curve of PV generators, EEE Ind. Electron. Mag. 3 (2009) 4–14. https://doi.org/10.1109/MIE.2009.933882.
[170] K.C. Fong, K.R. McIntosh, A.W. Blakers, Accurate series resistance measurement of solar cells, Progress in Photovoltaics 21 (2013) 490–499. https://doi.org/10.1002/pip.1216.
[171] J. Weber, L. Kniffki, L. Gutmann, J. Huyeng, E. Lohmueller, T. Roessler, Investigating the impact of edge passivation on shingle solar modules, SOLAR ENERGY MATERIALS AND SOLAR CELLS 271 (2024). https://doi.org/10.1016/j.solmat.2024.112876.
[172] P. Gebhardt, G. Mülhöfer, A. Roth, D. Philipp, Statistical analysis of 12 years of standardized accelerated aging in photovoltaic-module certification tests, Progress in Photovoltaics 29 (2021) 1252–1261. https://doi.org/10.1002/pip.3450.
[173] M.-J. Park, S. Youn, K. Jeon, S.H. Lee, C. Jeong, Optimization of Shingled-Type Lightweight Glass-Free Solar Modules for Building Integrated Photovoltaics, APPLIED SCIENCES-BASEL 12 (2022). https://doi.org/10.3390/app12105011.
[174] N. Abdel Latif, D. Von Kutzleben, J. Weber, T. Rößler, J. Markert, J.D. Huyeng, E. Lohmüller, S. Birnkammer, L.E. Alanis, A. Kraft, H. Neuhaus, Advancements in Shingle Matrix Technology for High Volume Production, in: 2024 IEEE 52nd Photovoltaic Specialist Conference (PVSC), IEEE, Seattle, WA, USA, 2024: pp. 0605–0611. https://doi.org/10.1109/PVSC57443.2024.10748959.
[175] N. Abdel Latif, J. Markert, D. von Kutzleben, S. Birnkammer, T. Rößler, J. Weber, A. Kraft, H. Neuhaus, Design, Manufacturing and Reliability of Shingle Matrix Modules, 40th European Photovoltaic Solar Energy Conference and Exhibition (2023) 020261-001-020261–006. https://doi.org/10.4229/EUPVSEC2023/3DO.18.1.
[176] N. Abdel Latif, R. Lamsairhri, T. Rößler, Characterization of Mechanical Strength of Shingle Joints Using Die Shear Tests, SiliconPV Conf Proc 1 (2024). https://doi.org/10.52825/siliconpv.v1i.944.
[177] S. Hoffmann, T. Geipel, M. Meinert, A. Kraft, Analysis of Peel and Shear Forces after Temperature Cycle Tests for Electrical Conductive Adhesives: 4 pages / 33rd European Photovoltaic Solar Energy Conference and Exhibition; 183-186, (2017). https://doi.org/10.4229/EUPVSEC20172017-1CV.3.91.
[178] M. Springer, J. Hartley, N. Bosco, Multiscale Modeling of Shingled Cell Photovoltaic Modules for Reliability Assessment of Electrically Conductive Adhesive Cell Interconnects, IEEE Journal of Photovoltaics 11 (2021) 1040–1047. https://doi.org/10.1109/JPHOTOV.2021.3066302.

[179] J.-N. Jaubert, S.V. Nair, J. Cai, R. Lv, B. Marteau, T. Xu, G. Zhang, H.E. Ruda, Conductive adhesive based shingled solar cells: Electrical degradation under cyclic loading, Solar Energy Materials and Solar Cells 245 (2022) 111823. https://doi.org/10.1016/j.solmat.2022.111823.
[180] M.-J. Park, J. Song, D. Moon, C. Jeong, H. Jee, Improvement in the Power of Shingled-Type Photovoltaic Module by Control of the Overlapped Width, JOURNAL OF THE KOREAN PHYSICAL SOCIETY 77 (2020) 1040–1043. https://doi.org/10.3938/jkps.77.1040.
[181] H.U. Kayaci, G.U. Ozdemir, M.E. Karahalli, A.H. Aksoy, S. Guler, D. Doganay, S. Coskun, T. Ozden, S.C. Aygun, R. Turan, H.E. Unalan, Waterbased electrically conductive adhesive for PERC-type shingled solar cells, SOLAR ENERGY MATERIALS AND SOLAR CELLS 285 (2025). https://doi.org/10.1016/j.solmat.2025.113525.
[182] J.-N. Jaubert, J. Cai, B.X.J. Yu, R. Lv, Y. Lu, T. Xu, G. Zhang, Service Lifetime Prediction of Electrically Conductive Adhesives-Based Shingled PV Module, IEEE Journal of Photovoltaics 12 (2022). https://doi.org/10.1109/JPHOTOV.2022.3141343.
[183] M.I. Devoto Acevedo, M. Helbig, K. Wienands, A. Halm, D. Tune, Effect of carbon nanotubes in conductive adhesives for photovoltaics., Solar Energy Materials & Solar Cells 292 (2025) N.PAG-N.PAG.
[184] P. Hacke, D.C. Miller, D. Pierpont, T. Wu, Performance and durability of electrically conductive tape for shingled Si heterojunction technology cells, PROGRESS IN PHOTOVOLTAICS 33 (2025) 16–26. https://doi.org/10.1002/pip.3749.
[185] N. Roosloot, J. Zhu, S.E. Foss, G. Otnes, Extended Thermal Cycling of Shingled Cell Interconnects, in: 2021: pp. 2328–2331. https://doi.org/10.1109/PVSC43889.2021.9518892.
[186] J.J. Jang, J.E. Park, D.S. Kim, W.S. Choi, D. Lim, A Comparison Analysis on the Efficiency of Solar Cells of Shingled Structure with Various ECA Materials, Kses 39 (2019) 1–9. https://doi.org/10.7836/kses.2019.39.4.001.
[187] S. Schwertheim, M. Scherff, T. Mueller, W.R. Fahrner, H.C. Neitzert, Lead-free electrical conductive adhesives for solar cell interconnectors, in: 2008 33rd IEEE Photovolatic Specialists Conference, PVSC 2008. Proceedings. Vol.3, IEEE, 2008: pp. 1–6. https://doi.org/10.1109/PVSC.2008.4922588.
[188] S. Maranghi, M.L. Parisi, R. Basosi, A. Sinicropi, The critical issue of using lead for sustainable massive production of perovskite solar cells: a review of relevant literature, Open Res Europe 1 (2021) 44. https://doi.org/10.12688/openreseurope.13428.2.
[189] T. Geipel, M. Meinert, A. Kraft, U. Eitner, Optimization of Electrically Conductive Adhesive Bonds in Photovoltaic Modules, IEEE Journal of Photovoltaics 8 (2018) 1074–1081. https://doi.org/10.1109/JPHOTOV.2018.2828829.
[190] VDMA, International Technology Roadmap for Photovoltaic (ITRPV) 2023 Results, Frankfurt am Main, 2024.
[191] K. Hartman, P. Hacke, M. Owen-Bellini, Y. Jin, M. Cummings, A. Taylor, J. Pretorius, L. Fritzemeier, Validation of Advanced Photovoltaic Module Materials and Processes by Combined-Accelerated Stress Testing (C-AST), in: 2019 IEEE 46th Photovoltaic Specialists Conference, PVSC 2019, IEEE, 2019: pp. 2243–2248. https://doi.org/10.1109/PVSC40753.2019.8980545.
[192] N. Klasen, F. Lux, J. Weber, T. Roessler, A. Kraft, A Comprehensive Study of Module Layouts for Silicon Solar Cells Under Partial Shading, IEEE J. Photovoltaics 12 (2022) 546–556. https://doi.org/10.1109/JPHOTOV.2022.3144635.
[193] N. Klasen, A. Mondon, A. Kraft, U. Eitner, Shingled Cell Interconnection: A New Generation of Bifacial PV-Modules, SSRN Journal (2018). https://doi.org/10.2139/ssrn.3152478.
[194] D. Von Kutzleben, T. Rößler, M. Mittag, J. Weber, S. Sigdel, N. Klasen, P. Zahn, A. Kraft, H. Neuhaus, DEVELOPMENT OF SHINGLE MATRIX TECHNOLOGY FOR INTEGRATED PV APPLICATIONS, in: 2022 8th World Conference on Photovoltaic Energy Conversion, 2022.

[195] N. Klasen, Schindelfügestellen in photovoltaischen Solarmodulen, Dissertation, Karlsruher Institut für Technologie, 2023.
[196] Q. Fan, H. Cui, C. Fu, D. Li, X. Tang, Z. Yuan, L. Ye, J. Liu, The Effect of Functionalized Silver on Rheological and Electrical Properties of Conductive Adhesives, ECS Trans. 34 (2011) 811–816. https://doi.org/10.1149/1.3567678.
[197] N. Matsuhisa, D. Inoue, P. Zalar, H. Jin, Y. Matsuba, A. Itoh, T. Yokota, D. Hashizume, T. Someya, Printable elastic conductors by in situ formation of silver nanoparticles from silver flakes, Nature Materials 16 (2017) 834–840. https://doi.org/10.1038/nmat4904.
[198] G. Divitini, S. Cacovich, F. Matteocci, L. Cinà, A. Di Carlo, C. Ducati, In situ observation of heat-induced degradation of perovskite solar cells, Nat Energy 1 (2016) 15012. https://doi.org/10.1038/nenergy.2015.12.
[199] M.L. Clingerman, J.A. King, K.H. Schulz, J.D. Meyers, Evaluation of electrical conductivity models for conductive polymer composites, J of Applied Polymer Sci 83 (2002) 1341–1356. https://doi.org/10.1002/app.10014.
[200] C. Xu, N. Willenbacher, How rheological properties affect fine-line screen printing of pastes: a combined rheological and high-speed video imaging study, J Coat Technol Res 15 (2018) 1401–1412. https://doi.org/10.1007/s11998-018-0091-2.
[201] S. Roh, D.P. Parekh, B. Bharti, S.D. Stoyanov, O.D. Velev, 3D Printing by Multiphase Silicone/Water Capillary Inks, Advanced Materials 29 (2017) 1701554. https://doi.org/10.1002/adma.201701554.
[202] T.R. Klein, M.S. Young, A.C. Tamboli, E.L. Warren, Lamination of transparent conductive adhesives for tandem solar cell applications, Journal of Physics D: Applied Physics 54 (2021) 184002. https://doi.org/10.1088/1361-6463/abe2c4.
[203] D. Jun, H. Son, J. Moon, S. Cho, S. hyun Kim, A Study on Correlation Peel Strength and the Efficiency of Shingled Modules According to Curing Condition of Electrically Conductive Adhesives, Current Photovoltaic Research 9 (2021) 31–35. https://doi.org/10.21218/CPR.2021.9.2.031.
[204] N. Ronayette, O. Poncelet, S. Sousa Nobre, S. Barthélémy, D. Bellet, R. Monna, Reduction of silver content in Electrically Conductive Adhesives for low-temperature interconnection of solar cells, Solar Energy Materials and Solar Cells 292 (2025) 113762. https://doi.org/10.1016/j.solmat.2025.113762.
[205] N. Klasen, D. Weisser, T. Rößler, D.H. Neuhaus, A. Kraft, Performance of shingled solar modules under partial shading, Progress in Photovoltaics 30 (2022) 325–338. https://doi.org/10.1002/pip.3486.
[206] M. Kronsbein, L. Böck, K. Dyhr, T. Rößler, N. Willenbacher, Less is More: Enabling Low-Filled Electrically Conductive Adhesives for Shingled Solar Cell Interconnection Using the Capillary Suspension Concept, (2025). https://doi.org/10.2139/ssrn.5123528.
[207] The silver institute, The silver survey 2025, The silver institute, Washington, 2025. https://silverinstitute.org/wp-content/uploads/2025/04/World_Silver_Survey-2025.pdf.
[208] W. Zhang, J. Liu, H. Liu, J. Wang, L. Zhang, J. Wang, H. Wang, F. Wang, X. Wang, F. Yu, Z. Lv, Z. Zhang, C. Hang, M. Li, H. Chen, Surface Functionalization of Micrometer Silver Flakes for Fabricating High-Performance Electrically Conductive Adhesives, ACS Appl. Electron. Mater. 4 (2022) 5387–5396. https://doi.org/10.1021/acsaelm.2c01055.
[209] H. Liu, H. Lai, J. Chen, X. Zhang, Enhancing conductivity of silver-based conductive adhesives via biomass-derived aldehydes: Interfacial modification and network densification, International Journal of Adhesion and Adhesives 147 (2026) 104259. https://doi.org/10.1016/j.ijadhadh.2026.104259.
[210] W. Zhang, J. Wang, H. Liu, Z. Zhang, J. Wang, L. Zhang, H. Wang, F. Wang, F. Duan, J. Liu, M. Li, C. Hang, H. Chen, Surface treatment of micron silver flakes with coupling agents for high-performance electrically conductive adhesives, International Journal of Adhesion and Adhesives 122 (2023) 103300. https://doi.org/10.1016/J.IJADHADH.2022.103300.

[211] L. Von Damnitz, D. Anders, A Review on the Mixing Quality of Static Mixers, ChemEngineering 9 (2025) 128. https://doi.org/10.3390/chemengineering9060128.
[212] M. Kronsbein, L. Böck, T. Rößler, N. Willenbacher, Low-filled electrically conductive adhesives based on silver-coated glass and copper particles, Solar Energy Materials and Solar Cells 299 (2026) 114228. https://doi.org/10.1016/j.solmat.2026.114228.
[213] W. Zhang, J. Liu, L. Zhang, J. Wang, Z. Zhang, J. Wang, H. Liu, H. Chen, M. Li, The synergistic effect of micron spherical and flaky silver-coated copper for conductive adhesives to achieve high electrical conductivity with low percolation threshold, International Journal of Adhesion and Adhesives 114 (2022) 102988. https://doi.org/10.1016/j.ijadhadh.2021.102988.
[214] Z.S. Hamrah, M. Pourabdoli, V.A. Lashgari, M.H.D. Mohammadi, Effect of time, temperature and composition on the performance of conductive adhesives made of silver-coated copper powder, International Journal of Adhesion and Adhesives 114 (2022) 103114. https://doi.org/10.1016/j.ijadhadh.2022.103114.
[215] Z.S. Hamrah, V.A. Lashgari, M.H.D. Mohammadi, D. Uner, M. Pourabdoli, Microstructure, resistivity, and shear strength of electrically conductive adhesives made of silver-coated copper powder, Microelectronics Reliability 127 (2021) 114400. https://doi.org/10.1016/j.microrel.2021.114400.
[216] N. Cheng, Z. Sun, X. Yu, Q. Yu, J. Zhao, Effect of flake silver-plated copper particles on the property enhancement of electrically conductive adhesives, Phys. Chem. Chem. Phys. 25 (2023) 10022–10032. https://doi.org/10.1039/D3CP00209H.
[217] R. Gordon, R. Orias, N. Willenbacher, Effect of carboxymethyl cellulose on the flow behavior of lithium-ion battery anode slurries and the electrical as well as mechanical properties of corresponding dry layers, J Mater Sci 55 (2020) 15867–15881. https://doi.org/10.1007/s10853-020-05122-3.
[218] K.M. Broek, I.J. Bennett, M.J.H. Kloos, W. Eerenstein, Cross Testing Electrically Conductive Adhesives and Conductive Back-sheets for the ECN Back-contact Cell and Module Technology, Energy Procedia 67 (2015) 175–184. https://doi.org/10.1016/j.egypro.2015.03.301.
[219] U.S. Geological Survey, U.S. Geological Survey, Mineral Commodity Summaries, January 2025, U.S. Geological Survey, 2025.
[220] S. Chu, Materials as an enabling technology in getting to net-zero GHG Emissions, (2024).
[221] M. Kronsbein, L. Böck, K. Dyhr, T. Rößler, N. Willenbacher, Less is more: Enabling low-filled electrically conductive adhesives for shingled solar cell interconnection using the capillary suspension concept, Solar Energy Materials and Solar Cells 287 (2025) 113603. https://doi.org/10.1016/j.solmat.2025.113603.
[222] Nagase ChemteX America, Nagase CA, (2025). https://nagasechemtex.com/wp-content/uploads/2024/07/Solar-Stringing-and-Shingling-Solar-Back-Contact.pdf.
[223] atom adhesives, atom adhesives AA-DUCT GS1, (2025). https://atomadhesives.com/aa-duct-gs1-silver-glass-sphere-coated-electrically-conductive-epoxy-adhesive/.
[224] United Adhesives, Inc., United Adhesives Eposolder, (2025). https://unitedadhesives.com/epoxy_eca.html.
[225] Parker Hannifin Corp, Parker Electrically Conductive Sealants, (2025). https://ph.parker.com/us/en/series/electrically-conductive-sealants-and-rtv-silicone.
[226] Master Bond Inc., Masterbond EP79FL, (2025).
[227] Holland Shielding Systems B.V., Holland Shielding Shieldoseal, (2025). https://hollandshielding.com/en/shieldoseal-130-g-plastic-cartridge.
[228] Soliani Emc s.r.l., Soliani CSA, (2025). https://www.solianiemc.com/wp-content/uploads/2024/03/SOL-08-Conductive-silicone-adhesives-r9.pdf.
[229] W. Chen, D. Deng, F. Xiao, Electrically conductive adhesives filled with surface modified copper particles, in: 2013 14th International Conference on Electronic Packaging

Technology, IEEE, Dalian, China, 2013: pp. 288–291. https://doi.org/10.1109/ICEPT.2013.6756473.
[230] H.-M. Ren, K. Zhang, Y.M. Matthew, X.-Z. Fu, R. Sun, C.-P. Wong, Preparation and performance of Ag-coated Cu flakes filled epoxy as electrically conductive adhesives, J Sol State Light 1 (2014) 10. https://doi.org/10.1186/s40539-014-0010-9.
[231] X.M. Zhang, X.-L. Yang, B. Wang, Electrical properties of electrically conductive adhesives from epoxy and silver-coated copper powders after sintering and thermal aging, International Journal of Adhesion and Adhesives 105 (2021) 102785. https://doi.org/10.1016/j.ijadhadh.2020.102785.
[232] Y. Lin, S. Chiu, Electrical properties of conductive adhesives as affected by particle compositions, particle shapes, and oxidizing temperatures of copper powders in a polymer matrix, J of Applied Polymer Sci 93 (2004) 2045–2053. https://doi.org/10.1002/app.20670.
[233] C.H. Schiller, L.C. Rendler, D. Eberlein, G. Mülhöfer, A. Kraft, D.-H. Neuhaus, Accelerated TC Test in Comparison with Standard TC Test for PV Modules with Ribbon, Wire and Shingle Interconnection, 36th European Photovoltaic Solar Energy Conference and Exhibition; 995-999 (2019) 5 pages, 4421 kb. https://doi.org/10.4229/EUPVSEC20192019-4AV.1.8.
[234] C.P. Wong, D. Lu, Q.K. Tong, Lubricants of silver fillers for conductive adhesive applications, (1998). https://doi.org/10.1109/adhes.1998.742025.
[235] U. Eitner, T. Geipel, S.-N. Holtschke, M. Tranitz, Characterization of Electrically Conductive Adhesives, Energy Procedia 27 (2012) 676–679. https://doi.org/10.1016/j.egypro.2012.07.128.
[236] T. Finger, F. Glaum, L. Böck, N. Willenbacher, T-ECA – Thermoplastic Adhesives for Solar Cell Interconnection, in: Presentations and Posters of 13th MIW Workshop, Berlin, 2025.

Verification of the contribution from the co-authors

Title: **Less is more: Enabling low-filled electrically conductive adhesives for shingled solar cell interconnection using the capillary suspension concept**
Journal: Solar Energy Materials and Solar Cells
Authors: M. Kronsbein, L. Böck, K. Dyhr, T. Rößler, N. Willenbacher

Position in the dissertation: The content of this paper has been included in Chapter 4.

Contribution of "Marianne Kronsbein"
Writing – review & editing, Writing – original draft, Visualization, Investigation: Characterization of ECAs - uncured, during curing and cured.
Contribution of "Leonhard Böck"
Writing – review & editing, Writing – original draft, Investigation: Module performance.
Contribution of "Katrin Dyhr"
Writing review & editing, Writing – original draft, Methodology: ECA formulation based on a Capillary Suspension.
Contribution of "Torsten Rößler"
Writing – review & editing, Supervision.
Contribution of "Norbert Willenbacher"
Writing – review & editing, Supervision, Funding acquisition.

Title: **Polyethylene Glycol-assisted Stabilization of Low-Silver Electrically Conductive Adhesives for Solar Cell Interconnection**
Journal: Energy Materials
Authors: M. Kronsbein and N. Willenbacher

Position in the dissertation: The content of this paper has been included in Chapter 5.

Contribution of "Marianne Kronsbein"
Conceptualization, Methodology, Investigation, Writing – Original draft, Writing – Review & Editing, Visualization.
Contribution of "Norbert Willenbacher"
Writing – Review & Editing, Supervision, Funding acquisition.

Title: **Low-filled Electrically Conductive Adhesives based on Silver-coated Glass and Copper Particles**
Journal: Solar Energy Materials and Solar Cells
Authors: M. Kronsbein, L. Böck, T. Rößler, N. Willenbacher

Position in the dissertation: The content of this paper has been included in Chapter 6.

Contribution of "Marianne Kronsbein"
Writing – review & editing, Writing – original draft, Visualization, Investigation: ECA formulation and characterization.
Contribution of "Leonhard Böck"
Writing – review & editing, Writing – original draft, Investigation: Module performance.
Contribution of "Torsten Rößler"
Writing – review & editing, Supervision.
Contribution of "Norbert Willenbacher"
Writing – review & editing, Supervision, Funding acquisition.